Aggregated Author Response Documents with Tracked Manuscript Changes

All *Editor and Reviewer comments are included below in italic black font* and the Author responses are in blue font.

Summary of Manuscript Revisions:

- We revised the manuscript to mainly present the relative abundance weighted values of the identified molecular formulas in the main paper and moved the non-weighted values to the Supplement.
- We substantially revised the discussion in section 3.5 regarding the observed organic aerosol and its glass transition temperatures (T_g). This aspect of the paper is one that is especially unique because we pulled out the GFS ambient conditions along the FLEXPART retroplume to consider the role of the ambient conditions on the observed chemistry. We paired this with a discussion of the markers of aqueous phase chemistry.
- We carefully evaluated the significance of limitations associated with the method preparation with respect to the average O/C and average T_g values.
- The manuscript has been edited for grammar corrections and clarity.

Co-Editor Initial Decision: Start review and discussion (22 Feb 2018) by Neil M. Donahue

Comments to the Author:

A few things to consider during the review process:

1. Some paragraphs are long and tend to wander. The paragraph starting on line 205 is an example. There are several points in that, which would do well to be called out with separate short paragraphs.

Thank you for the suggestion. We agree that the paragraph starting on line 205 was somewhat unfocused. To correct it, we split the paragraph into multiple shorter paragraphs more focused on one particular component or implication of the ion chromatography results. We also removed a sentence that was off topic in order to keep the section more focused.

2. In the main text (on a quick scan) it is hard to tell whether you are relying more on the relative abundance of individual compounds or simply on their presence in a sample. It seems to me that relative abundance should be used exclusively, or in the vary least predominantly. The discussion has lots of "such and such was present". This seems like "George Washington slept here" to me. I want to know how much (or how often in the example case...).

Thank you for the suggestion. The reason why we originally discussed the presence or absence is because of the nature of electrospray ionization. The abundance of any one peak is not solely dependent on the compound abundance in the sample, but also reflects its ionization efficiency. However, in light of your and the reviewers comments we decided to present the normalized relative abundances of the species in the main paper and moved the non-weighted values to the Supplement. We also changed Figure 4 to contain a histogram of the sum of normalized relative abundances as opposed to the sum of the number of molecular formulas. In some places using presence or absence makes more sense, such as when comparing whether or not formulas are common or unique between two or more samples and so those comparisons are retained as they were. We also added a sentence within the main paper to address the fact

that abundance in ESI is not solely dependent on abundance in order to head off any potential confusion or misinterpretation. Lines 324-326: **"We note that the relative abundance of compounds in ESI mass spectra is not directly proportional to their solution concentration, other factors including surface activity and polarity impact the ionization efficiency (Cech & Enke, 2001)."**

3. You seem to be attributing glassy character to individual compounds, whereas that is definitely an extensive attribute of the whole phase and/or particle.

We agree that the glassy character of the aerosol is dependent on the whole particle and the interactions within and outside it. It was not our intention to attribute glassy character to individual compounds. To clarify, we rewrote Section 3.5 of the paper and changed the Figures 7 and S12 (now S17). Now, we show the boxplot distributions of the estimated glass transition temperatures for each of the components with the GFS extracted ambient temperature as reference to imply the particle viscosity during transport. We also included Boyer-Kauzemann rule (Koop et al., 2011; Shiraiwa et al., 2017; DeRieux et al., 2018) estimated T_g values for the acid forms of the three most abundant organic ions along with their measured concentrations to provide some insight as to their potential impact on the overall T_g of a particle containing the identified species.

4. The aerosol mixing studies of Ellis Robinson and Qing Ye might be relevant to the discussion of diffusivity.

Thank you for the suggestion. After reading through the papers, we agreed that the Ye et al. (2016) in particular provided additional insight regarding diffusivity of the aerosol species in our study, as such the following sentence was added to Section 3.5 of the paper: **"Similarly, lower volatility is expected to lead to lower diffusivity in aerosol even at elevated relative humidity as demonstrated by Ye et al. (2016)."**

Author Responses to Reviewer #1

The *Reviewer comments are black italic font* and the Author responses are blue font.

The authors describe the analysis of three selected filter samples that were collected within a more comprehensive sampling campaign (a total of 127 filters) at the Pico Mountain Observatory (PMO) on Pico Island / Azores. The samples were chosen because of the high organic carbon (OC) concentration. While major small ions and OC of the three filter samples were measured as well, the focus of the manuscript certainly lies on the analysis using direct infusion electrospray ionization ultra-high resolution mass spectrometry in the negative ion mode ((−)ESI/UHRMS). Differences in the mass spectra are discussed with regard to a back-trajectory analysis. The authors observe signals in one sample (out of three) that exhibits higher O/C ratios compared to the other two samples that likely have undergone a longer atmospheric transport time (and thus aging). The authors argue that the two samples with the lower O/C ratio were transported in the free troposphere (FT) to PMO, and thus the particle phase state during transport was likely solid. They conclude that "biomass burning emissions", which are directly injected by pyro-convection into the FT, "are longer-lived than emissions in the boundary layer".

We thank the reviewer for his comments. We made several changes to both the main paper and the supplemental information. In particular, we made major revisions to section 3.5.

General comments:
Overall, the manuscript presents results from an atmospheric measurement station that is certainly very well suited for studying aerosol transformation processes during long-range transport. Furthermore, the authors demonstrate the need for ultra-high resolution mass spectrometry techniques when it comes to ambient measurements of particulate matter. However, I have major concerns regarding a weak reasoning that is used as a basis for their conclusions and implications for atmospheric aging (see my point (1) below). Also, the authors remain too speculative in many cases, or even state arguments that are not supported by their figures (see (2)). Furthermore, I have serious technical concerns that might have an effect on the outcome of the ESI/UHRMS analysis (see (3)).

My major remarks concerning the above mentioned points:
(1) The authors argue that particle phase state is affected by the conditions during atmospheric transport. Their observation of a low O/C in the biomass burning samples (PMO-1 and PMO-3) is reasoned by the phase state of the particles during transport. Although, the authors mention that the PMO-2 sample is originating from another source (from the Eastern United States – dominated by a mix of biogenic and anthropogenic emissions), they argue that the high O/C ratio of this sample is caused by the semi-solid phase state, which allows faster aging during atmospheric transport to PMO. Assuming that the back-trajectory analysis is getting the sources right, the authors don't present a convincing argument why we can use the two different sources (biomass burning organic aerosol (BBOA) vs. anthropogenic/biogenic secondary aerosol (A/BSOA)) as an ***identical reference point for the onset of atmospheric aging****!*

We thank the reviewer for this comment. We agree that biomass combustion and anthropogenic/biogenic aerosol are not identical reference points for the onset of atmospheric aging. However, these are the pollution events that arrived at the Pico Mountain Observatory and they arrived with very different transport conditions. To provide context regarding our expectations for oxidation, we cited studies that demonstrate both the rapid oxidation of anthropogenic/biogenic aerosol (Jimenez et al. 2009) and the lower average oxidation of biomass combustion aerosol relative to anthropogenic/biogenic aerosol (Bougiatioti et al., 2014) see also lines 30-35, 377-378.

We further strengthened this point to avoid confusion with the following new text (Lines 307-309):
"Although North American outflow of anthropogenic secondary organic aerosol is expected to have

a higher O/C value compared to the wildfire emissions of biomass burning organic aerosol (e.g., Aiken et al., 2008; Jimenez et al., 2009; Bougiatioti et al., 2014) …"

We also added the following sentence to the manuscript (lines 504-505), to clarify the role played by emission sources: "**These observations suggest that the transport pathways, in addition to the emission sources, contribute to the observed differences in the organic aerosol oxidation."**

Regarding the aerosol phase state, we estimated the glass transition temperature (DeRieux et al., 2018) for the identified molecular formulas using the extracted Global Forecast System (GFS) data for the FLEXPART retroplumes. Doing this showed that the majority of species identified in PMO-1 and PMO-3 had T_g values that exceeded the ambient temperature, which suggests solid state during the last 5 days of transport. Considering the length of transport (~7-10 days), these samples demonstrated low O/C and OS_C even compared to biomass burning samples analyzed after less transport (Bougiatioti et al., 2014). As described in several papers (Koop et al., 2011; Shrivastava et al., 2017; Zelenyuk et al., 2017), the solid phase is expected to have decreased susceptibility to oxidation and other chemical processes. For this reason, it was hypothesized that the phase state contributes to ambient observations made in this study.

In contrast to PMO-1 and PMO-3, the estimated T_g values for compounds identified in PMO-2 were often lower than the ambient temperature, indicating a less viscous state and thus an increased susceptibility to oxidation and other chemical processes, relative to PMO-1 and PMO-3. This is consistent with other studies of anthropogenic and biogenic SOA in the planetary boundary layer (Maclean et al., 2017; Ye et al., 2016). Although there are uncertainties in the prediction (DeRieux et al., 2018), PMO-2 organic aerosol species were more likely to be semi-solid/liquid based on the ambient conditions than PMO-1 or PMO-3. Thus, we hypothesized that the higher O/C and oxidation observed in PMO-2 may be due to aqueous phase processing during transport, leading to increased oxidation of atmospheric organic matter (Ervens et al., 2008; Zhao et al., 2014). To support this hypothesis, we examined markers of potential cloud processing. We observed depleted nitrate (Dunlea et al., 2009), elevated sulfate and oxalate (Yu et al. 2005; Sorooshian et al. 2007) in PMO-2 as described in section 3.1.

In the literature it is now well recognized that these two kinds of organic aerosol (BBOA vs SOA from anthropogenic and biogenic VOCs) are already very different on the molecular level at the time when emitted by their sources or formed in the atmosphere: While BBOA is largely composed of lignin- and cellulose-derived condensed aromatic / polyphenolic structures with low O/C ratios (Lin et al., 2016), numerous studies have shown that the auto-oxidation of (mostly biogenic) VOCs results in highly oxygenated molecules within seconds after the initial attack by an oxidant (Crounse et al., 2013; Ehn et al., 2012; Jokinen et al., 2014). Although it is not yet fully understood what happens to these compounds once they condense, the auto-oxidation mechanism still can explain high aerosol O/C from atmospheric oxidation of VOCs.

We agree that the two types of organic aerosol (SOA vs. BBOA) are very different on the molecular level. Auto-oxidation as described by Crounse et al. (2013), Ehn et al. (2012), and Jokinen et al. (2014) does increase the O/C, but it also shows clear carbon number preferences associated with the oxidation of terpene precursors. This trend is consistent with our earlier work on condensed SOA where the concept of "auto-oxidation" was described as "oxygen-increasing-reactions" (Kundu et al., 2012). However, in the case of PMO-2, we did not observe carbon number preferences, which would indicate auto-oxidation. While this does not negate the possible influence of auto-oxidation, it does minimize its relative importance for these long range transported aerosol observations. On the other hand, aqueous phase processing as described by Lim et al. (2010) leads to SOA production with a greater array of carbon

numbers; the greater array of carbon numbers matches more closely with our observations of a continuum of carbon numbers from 2 to 33 in PMO-2.

We also compared the molecular composition of PMO-2 to that of cloud water from the Storm Peak Laboratory (Zhao et al., 2014) and Whiteface Mountain (Cook et al., 2017), and fog water from Fresno, California (Mazzoleni et al. 2010). In these comparisons, the common species observed only in cloud water and PMO-2 had higher O/C and oxidation than the species common to other samples. This likely indicates that at least some degree of aqueous phase processing has occurred. The results comparing our study to the Cook et al. (2017) and Mazzoleni et al. (2010) studies are new and have been added to the Supplement of this paper in Table S6. All three samples contain atmospheric water that was impacted by anthropogenic, biogenic, and biomass burning air plumes at one time or another. These results consistently show that high O/C species in PMO-2 are uniquely common with atmospheric organic matter in fog and cloud, indicating the influence of aqueous phase processing. We note that the comparisons of the molecular compositions from Zhao et al. (2014) and Mazzoleni et al. (2010) were more comprehensive because we had more complete datasets. The species common only to PMO-1 and the Cook et al. (2017) dataset also had high O/C, but the two formulas represent only 2% of the formulas used for comparison. On the other hand, the uniquely common formulas between the Cook et al. (2017) dataset and PMO-2 represent over 20% of the formulas used for comparison. As such it seems reasonable to say the same trend holds.

Table S6. Number of molecular formulas and their average O/C values (unweighted O/C and RA weighted O/C (O/C_w)) uniquely common between this study and ambient aqueous organic matter (Mazzoleni et al., 2010; Zhao et al., 2015; Cook et al., 2017). Uniquely common means that the formula is common between only one of the PMO samples and the aqueous organic matter sample. CW indicates cloud water, the numbers in parentheses are the percentage of total formulas.

Sample	# Common Formula	O/C	O/C_w
PMO and Fog (Mazzoleni et al., 2010)			
PMO-1	202 (6.4%)	0.38	0.39
PMO-2	48 (2.3%)	0.5	0.55
PMO-3	11 (0.60%)	0.29	0.29
PMO and CW (Cook et al., 2017)			
PMO-1	2 (0.063%)	0.82	0.82
PMO-2	23 (1.1%)	0.8	0.81
PMO-3	1 (0.055%)	0.36	0.36
PMO and CW (Zhao et al., 2015)			
PMO-1	197 (6.2%)	0.42	0.42
PMO-2	70 (3.3%)	0.76	0.8
PMO-3	42 (2.3%)	0.38	0.38

In addition to Table S6, the following sentences were added to the manuscript (Lines 483-486):
"Comparisons of the detailed molecular composition of the PMO samples with studies of cloud

(Zhao et al., 2013; Cook et al., 2017) and fog (Mazzoleni et al., 2010) water organic matter indicates that the formulas uniquely common to only PMO-2 and the literature atmospheric water samples have higher O/C consistent with aqueous processing during transport. These results are provided in Fig. S19 and Table S6."

My impression is that the authors do not adequately consider or discuss different reasons for their observations and overemphasize the possible link between atmospheric transport and aging efficiency at different altitudes.

Our previous paper (Dzepina et al., 2015) provided a discussion of a biomass burning plume event intercepted at the PMO. In that paper, we considered several factors, but not phase state. We also did not have any non-biomass burning influenced aerosol samples like PMO-2 for comparison. The new set of samples provides an opportunity for a new perspective. In this work, we examined the meteorological variables from GFS that corresponded to the FLEXPART transport pathways and used the recently developed estimation methods for volatility and phase state to assist in the interpretation of the observations.

Since in Dzepina et al. 2015 we considered photochemical oxidation and fragmentation, it was deemed unnecessary to go over again in detail for this manuscript. For clarity, the following introductory sentences were revised (Lines 100 – 104): **"The low oxidation observed by Dzepina et al. (2015) was attributed to the dominance of persistent aerosol that resisted removal mechanisms, however it is possible that the phase state of the aerosol during transport played a significant role. The increased resistance to photodegradation (Lignell et al., 2014; Hinks et al., 2015) and water diffusivity (Berkemeier et al., 2014) of solid phase organic aerosol provide a basis for this hypothesis."**

To be clear, I am not saying that aerosol phase state does not change aerosol transformation rates, but to extract this effect from ambient observations, one likely needs to consider a larger set of samples (which the authors apparently have).

We would like to have a larger dataset to extract this valuable information. Unfortunately, there were several limiting factors that are not readily apparent:

(1) The Pico Mountain Observatory is a research post that was originally designed to be temporary, located on the caldera top of Pico Mountain in the Azores (see also Image 1 in the Supplement). The mountain-top site is one of the highest points for 1500 km in the North Atlantic. The site is only accessible by foot over rugged terrain (Honrath et al., 2004) and has limited infrastructure for aerosol chemical observations (Dzepina et al., 2015). Thus, we conducted a field study with filter collection and conducted off-line analyses.
(2) The field study and filter collection were limited by the meteorology. Thus, the pollution events were primarily influenced by biomass combustion from North America or dust events from Africa. We also lost samples/observations due to occasional nighttime lenticular cloud formation (Dzepina et al., 2015).
(3) The detailed molecular analyses were done with an ultrahigh resolution FT-ICR MS instrument at the Woods Hole Oceanographic Institution (WHOI). The WHOI instrument is made available with user fees. The costs of the instrument and travel limited our analyses to only those samples with adequate OC loading to ensure reliable measurements.

(2) The authors argue that the aerosol that was captured on the PMO-2 sample travelled at altitudes below 2 km over Eastern U.S. and stayed below 2 km altitude until it reached PMO 2-4 days later (p. 7, l. 251-253). From Figure 1 (e), I cannot see that. For the upwind days 0-5, the mean height of the plume is consistently higher than 2 km. As stated on p.2, l. 65-67, the marine boundary layer (MBL) around PMO ranges between 500 m and 2 km, and thus below the mean height of the plume.

We thank the reviewer for catching our mistake with Fig. 1. We immediately posted the corrected Fig. 1 in Author Comment #1 during the open discussion of this paper. We also added a few more FLEXPART retroplumes for our sampling periods to the Supplement (Figs S1-S3).

*However, the authors argue that **PMO-2 air masses travelled within the MBL layer** to PMO, explaining high relative humidity and a semi-solid phase state during transport. Another argument against the transport within the MBL is given by the authors, mentioning that PMO-2 does not reveal any chemical signature from the MBL (p. 6, l. 232-233). Furthermore, the mean height in PMO-3 appears even lower than PMO-2 for the last five days.*

We thank the reviewer for this comment. We noted that the MBL influence, as inferred from the estimated amount of sea salt sulfate and presence of methane sulfonic acid (MSA), does not seem to be the major influence on that sample. (lines 259-261). The relatively low influence of the MBL does not negate transport within the MBL, especially in this case, because the transport was very fast. Clarification regarding this point was added to lines 263-265. **"The influence of marine sources supports boundary layer transport. However, the results indicate that marine aerosol is not likely a major component of PMO-2, perhaps because the rate of PMO-2 transport was very fast."**

(3) The discussed filters were selected because of their high mass loadings of organic carbon (>1 mg OC / quarter filter). After loading the water-soluble (WS) OC extract onto solid phase extraction (SPE) material for purification, the SPE was then eluted by 2 mL of MeCN/H2O and the extract was used for direct infusion. If we assume that half of the OC is WSOC and assume 100% SPE collection efficiency (neglecting losing the small, polar organic compounds), the concentration of the solution for direct injection ESI would be ~0.25 mg/mL. To me, this appears as a huge concentration in which ion source cluster formation (e.g. x-mers of analytes, clusters with solvents or solvent additives, impurities), can become a serious issue. I understand that SPE was done in order to reduce cluster formation with inorganic ions and that a separation technique was apparently not available. However, the authors could have done straight-forward tests to check the extent of cluster formation in these samples by: (1) sample dilution and checks for non-linear reduction of cluster-signal candidates and (2) MS/MS isolation and recording the fragmentation energy of cluster signal candidates.

Yes, direct infusion of high concentrations can lead to ESI artifacts. We always dilute our samples to the lowest possible level to obtain a stable current during ESI. This has been described in our previous work (Putman et al., 2012). We also note that negative ion ESI is less prone to adduct artifacts. This is mainly because the low molecular weight negative ions are removed by the SPE procedure.

Although, I understand that MS/MS cannot be done on all ion signals, there are some "suspicious" signals standing out in Figure 2 (the signals > 0.3 rel. abundance) that should have been checked using MS/MS when doing direct injection.

Regarding the suspicious signals, we have done a thorough study using ultrahigh resolution FT-ICR MS/MS on PMO-1 similar to LeClair et al. (2012). The results of the MS/MS are the subject of a forthcoming manuscript. To answer the reviewer's concern, we re-examined several of the MS/MS

spectra. Overall, the mass spectra show fragmentation patterns consistent with covalently bonded molecules and not ion clusters. On the following pages, the MS/MS spectra for several of the tallest peaks present in PMO-1 are shown. Note that we cannot isolate 1 and only 1 m/z value. Instead we isolate a range of values (for example 230 ± 3). In this way, the ions of the entire isolated group are simultaneously fragmented.

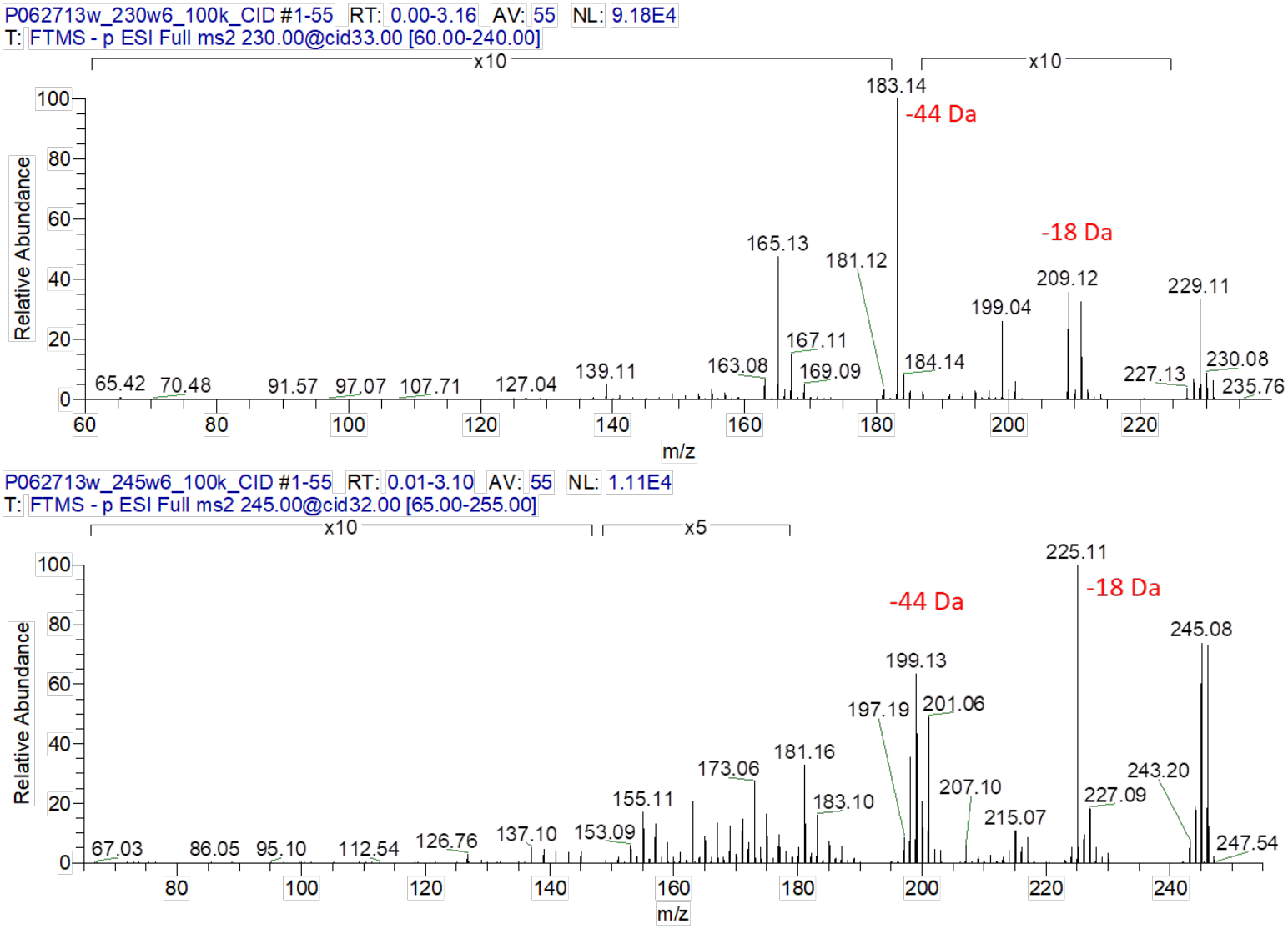
P062713w_230w6_100k_CID #1-55 RT: 0.00-3.16 AV: 55 NL: 9.18E4
T: FTMS - p ESI Full ms2 230.00@cid33.00 [60.00-240.00]
x10
x10
183.14
-44 Da
-18 Da
165.13
181.12
209.12
229.11
199.04
167.11
163.08
169.09
184.14
227.13
230.08
235.76
65.42
70.48
91.57
97.07
107.71
127.04
139.11
Relative Abundance
m/z
P062713w_245w6_100k_CID #1-55 RT: 0.01-3.10 AV: 55 NL: 1.11E4
T: FTMS - p ESI Full ms2 245.00@cid32.00 [65.00-255.00]
x10
x5
225.11
-18 Da
-44 Da
245.08
199.13
197.19
201.06
181.16
173.06
155.11
183.10
207.10
243.20
227.09
215.07
247.54
67.03
86.05
95.10
112.54
126.76
137.10
153.09
Relative Abundance
m/z

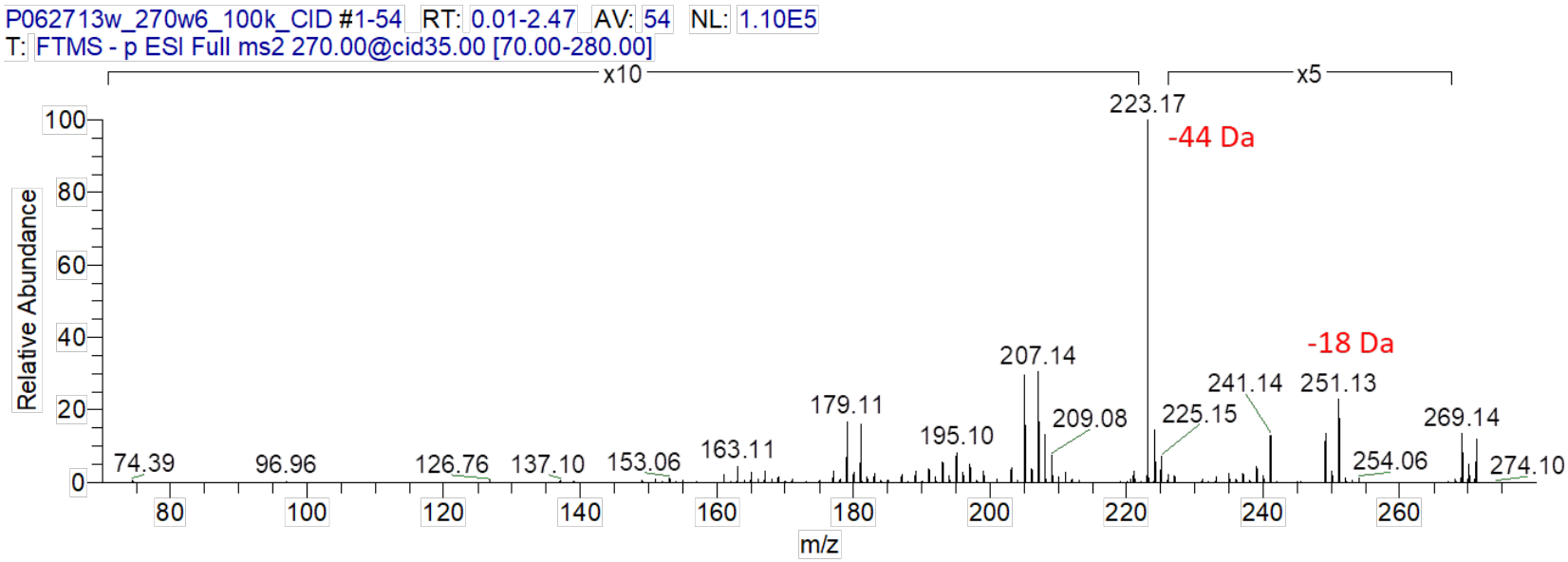
P062713w_270w6_100k_CID #1-54 RT: 0.01-2.47 AV: 54 NL: 1.10E5
T: FTMS - p ESI Full ms2 270.00@cid35.00 [70.00-280.00]
x10
x5
223.17
-44 Da
-18 Da
207.14
241.14
251.13
179.11
209.08
225.15
269.14
195.10
163.11
74.39
96.96
126.76
137.10
153.06
254.06
274.10
Relative Abundance
m/z

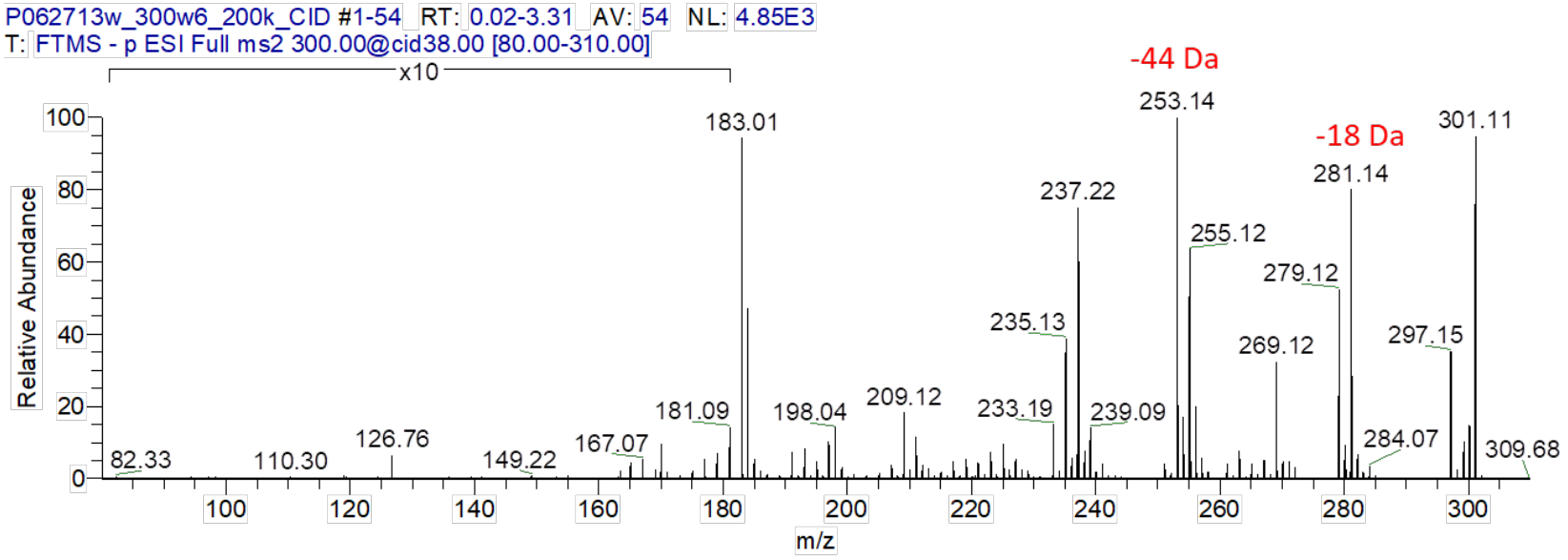
P062713w_300w6_200k_CID #1-54 RT: 0.02-3.31 AV: 54 NL: 4.85E3
T: FTMS - p ESI Full ms2 300.00@cid38.00 [80.00-310.00]
x10
-44 Da
253.14
183.01
301.11
-18 Da
281.14
237.22
255.12
279.12
235.13
269.12
297.15
181.09
198.04
209.12
233.19
239.09
126.76
167.07
284.07
82.33
110.30
149.22
309.68
Relative Abundance
m/z

Ion source cluster formation would introduce a bias on the calculated glass transition temperature (Tg) by artificially increasing the average number of carbon per molecule. Furthermore, the overall Tg is already biased toward higher values since small molecules are very likely lost during the SPE procedure (l. 158-159). The manuscript misses in its current form a critical evaluation of these points and its implications on aerosol phase state and aging.

As shown above, we do not have evidence for ion clustering. However, the lower MW species can be quite important for the average organic aerosol T_g. We chose to address this in two ways, first we report the distribution of T_g values in Figure 7 and second, we estimated the influence of the known low MW compounds. Using the concentrations of organic acids (e.g., Table SM1), we found that the relative abundance weighted T_g for each of the samples changed by $\leq 2.5\%$ when the abundance of the organic acids was considered (Table SM5). This was done by estimating the T_g for each of the following organic acids (formic, acetic, oxalic, malonic, and lactic) using the Boyer-Kauzmann rule ($T_g = g^* T_m$, $g = 0.7$, T_m = melting temperature) (Shiraiwa et al. 2017; DeRieux et al. 2018). Oxalic acid is by far the most abundant of all organic acids in these samples and thus has the largest impact. The percentage of total organic mass that each acid made up was calculated by dividing their concentration by the concentration of organic mass, which was estimated by multiplying the OC value by 2 (El-Zanan et al., 2005). Then the individual low MW compound mass fractions were used to estimate their abundance relative to the sum of the total abundance of species identified by FT-ICR MS using the worst-case scenario assumption that the detected species in the mass spectra represent only 50 % of the total organic mass. These abundance values, along with the estimated T_g values were then used to calculate the abundance weighted average dry T_g for each sample. When compared to the original weighted T_g values, the difference was $\leq 2.5\%$for all samples, indicating that while the organic acids do impact the T_g to some extent, the impact is not so significant as to change any of the conclusions of this study. A series of tables showing the values described here are provided in the Supplement (Tables SM1-SM5).

Table SM1. The concentrations of the ions used for the estimation and the organic mass (OM) concentration. The values are in µg/m^3 air.

Ion	PMO-1	PMO-2	PMO-3
Formate	0.0289 ± 0.0003	0.00438 ± 0.00007	0.0119± 0.0001
Acetate	0.0519 ± 0.0001	0.004587 ± 0.000005	0.0071 ± 0.0002
Oxalate	0.0938 ± 0.00070	0.0897 ± 0.00181	0.0522 ± 0.00002
Malonate	0.00605 ± 0.0003	0.00548 ± 0.0007	0.0045± 0.0003
Lactate	0.0292 ± 0.0004	0.0019 ± 0.0001	0.00467 ± 0.0001
OM	4.14 ± 0.04	0.956 ± 0.052	1.74 ± 0.20

Table SM5. Estimated average T_g values when the ions are considered. The table contains the results for 3 assumptions of the organic mass fraction represented by the FT-ICR MS identified species (100%, 70%, 50%). The numbers in parentheses show the percent change in average T_g from the T_g without ions considered. All T_g values are in K.

Sample	RA Weighted T_g without Ions (100%)	Ions and RA Weighted T_g (100%)	Ions and RA Weighted T_g (70%)	Ions and RA Weighted T_g (50%)
PMO-1	328.75	324.38 (1.33%)	322.67 (1.85%)	320.51 (2.51%)
PMO-2	326.45	324.43 (0.619%)	323.71 (0.839%)	322.85 (1.10%)
PMO-3	326.88	324.41 (0.756%)	323.44 (1.05%)	322.22 (1.43%)

A comment about the estimated impact of small organic acids to the T_g has been added to the manuscript as follows (lines: 164-171): **"The procedural loss of ionic low MW compounds such as oxalate can lead to an underprediction of the organic aerosol O/C and overprediction of the average glass transition temperatures (T_g). To investigate this, we used the concentrations of the prominent organic anions measured with ion chromatography to estimate the abundance of these compound relative to the compounds detected by FT-ICR MS. The low MW corrected average O/C values correlated with the trends of the original O/C values, however the significance of impacts varies with the measured analyte concentrations and the assumptions associated with the uncertain mass fraction of the molecular formula composition (Table SM4). When low MW organic anions were included in the estimated average dry T_g values, they dropped by ≤ 2.5 %, which was deemed relatively insignificant (Table SM5).**

In the supplement, a discussion of the estimation method was added (pg. 5). In addition, the tables shown above were added to the supplement as well.

Finally, it would have been interesting to measure also in the positive ESI mode, in which one can observe levoglucosan or nitrogen-heterocycles that are expected in biomass burning aerosol samples.

We agree with the reviewer, analyses with positive mode ESI would have been interesting. Time constraints limited our ability to do multiple ionization method and we were interested in the oxidation characteristics of long-range transported aerosol. Since oxidation leads to the addition of carboxylic acid groups and in general more polar molecular species, negative mode ESI was the most practical way to analyze the samples.

Moreover, it is not clear how the blank signal of the DI/ESI-UHRMS was determined. I would expect a measurement of a blank filer that undergoes the whole procedure incl. transport from the field site, sample preparation procedure in laboratory (sonication, filtration, SPE, etc). Only a good blank measurement allows determining the significance level at which individual signals are present in the samples and identifying those signals that emerge from sample preparation. Here, it is especially important since the paper discusses the number of identified compounds between the different samples. If a compound was identified as "not present" in one sample, does that mean after blank subtraction? It is not described what were procedures involving a blank filter, nor are mentioned the criteria and the thresholds for this kind of filtering!

Blank subtraction is a non-trivial matter in ultrahigh resolution MS (e.g., Zielinski et al., 2018) due to the difference in ion collection times for a sample compared to a blank, and the possibility of resuspension of

sample residues within the instrument when a blank (i.e., clean solvent) is infused. Ion trap instruments (including hybrid FT-ICR MS and Orbitrap MS instruments) also use an auto-gain control (AGC) to avoid space charge artifacts. In our analysis, the AGC was set at the recommended setting of 1×10^6 ions. Since samples and blanks generate ions at very different rates, the time necessary for the analysis varies and often a maximum injection period is required. Our maximum inject period was 500 ms for samples and 800 ms for blanks. The actual average injections times for samples were in the range of 20-80 ms, however the blanks "timed-out" at 800 ms before the mass analysis was performed. The injection time differences indicated that the blanks were very clean and the potential for resuspension was non-negligible due to increased accumulation time. Therefore, we compared the intensities of the analytes in the samples and blanks and used a ratio of 3 to determine whether or not a peak should be removed.

In this study, we had both technical instrument blanks and field blanks. We applied the ratio of 3 criteria to both types of blanks, where all of the analytes with a ratio < 3 relative to the technical blank were removed and those < 3 relative to the field blanks were flagged. This led to 2 formulas being flagged because they didn't meet the criteria in 1 of the 3 samples. If the 2 analytes were contamination, they should have appeared equally in all 3 samples, but they were not. Further the 2 analytes were part of a homologous series that was not otherwise in common with the field blanks. The two flagged analytes are $C_{17}H_{34}O_4$ and $C_{19}H_{38}O_4$, which showed very low intensity in that sample. We deemed this to be a fair assessment, especially in light of the very different amounts of time required for the ion injection.

The QA that was performed for the samples is consistent with what has been described in other studies from our group (Putman et al., 2012; Mazzoleni et al., 2012; Dzepina et al., 2015). In short, we removed formulas with extremely high or low O/C (>2, <0.1), H/C (>2.2, <0.3), and DBE (>20). We also removed known solvent contaminant peaks and isolated assignments that were not part of a CH_2 homologous series. After this was done, we aligned the two replicate analyses of the samples and kept only the formulas that were present in both replicates. If a formula is described as "not present" it means that formula was not present in the sample being referred to after the QA steps described above were performed. This description of the QA procedure was added to the Supplement of the manuscript. To the main manuscript we added the following (lines: 185-188): **"Specifically, two formulas ($C_{17}H_{34}O_4$ and $C_{19}H_{38}O_4$) observed in PMO-1 could not be classified as pertaining only to the field blank and so they were not removed. Further discussion about the blank subtraction is provided in the Supplement. To produce the final data set for each sample, the replicates were aligned and only the molecular formulas found in both replicates after QA were retained. "**

The description of the blank subtraction procedure given above will be added to the Supplement pg. 4.

Overall, I cannot recommend the article to be published in ACP, since the conclusions reached remain far too speculative and are not convincingly supported by the presented data. I miss a more critical discussion and evaluation of other potentially important processes (both atmospheric and instrumental) throughout the manuscript. The description of the mass spectrometry analysis is not sufficiently complete and leaves the reader with open questions (e.g. What was the workflow of the data analysis? What did they use as blank samples?). Last but not least, the presentation and language is in many cases not precise.

Based on the combination of reviewer and editor impressions, we substantially revised the discussion in section 3.5 regarding the observed organic aerosol and its glass transition temperatures (T_g). This aspect of the paper is one that is especially unique because we pulled out the GFS ambient conditions along the

FLEXPART retroplume to consider the role of the ambient conditions on the observed chemistry. We paired this with a discussion of the markers of aqueous phase chemistry.

To avoid unnecessary length, our original paper referenced several of our previous papers regarding instrumental method details. However, the reviewers have raised a few interesting questions that we answered more directly in the revised manuscript and the corresponding supplement.

A key point that is especially important to keep in mind is that very little research has been done on the chemistry of free tropospheric aerosol as opposed to the more extensive knowledge of aerosol chemistry from within the continental boundary layer. Our detailed analysis contributes much needed insight to the chemistry of free tropospheric aerosol, where the ambient conditions are colder and drier than in the boundary layer.

The manuscript has been edited for grammar corrections and clarity.

Specific comments
p.3, l. 106-109: Please provide a reference stating that long-range transported aerosol is generally acidic in nature. Furthermore, negative ESI is not only sensitive to organic acids, but also to important biomass burning markers (e.g. nitro-phenols (Iinuma et al., 2010)). Have you seen nitro-phenols or similar biomass burning tracers in the biomass burning samples?

Long range transported aerosol generally has an acidic nature as mentioned in a study by Bougiatioti et al. (2016). Additionally, it is known that during oxidation, carboxylic acid groups will be formed in organic aerosol (Iinuma et al., 2004), providing additional evidence that aged aerosol is generally acidic in nature. The following reference has been added to the manuscript for the citation of acidic transported aerosol at line 112: **(Bougiatioti et al., 2016)**

To clarify our use of negative mode ESI and the reasons for it, the following has been added to lines 175-176 of the manuscript: **"Negative polarity is effective for the deprotonation of polar organic molecules (Mazzoleni et al., 2010), which are expected to dominate the organic aerosol mass fraction and were the focus of this study."**

Formulas such as $C_6H_5NO_3$ (nitro-phenol) and $C_6H_{10}O_5$ (levoglucosan) were detected in the samples. Additionally, all but three of the CHNO and CHO negative mode ESI species connected to brown carbon by Lin et al. (2016) were detected in one or more of the aerosol samples in this study. PMO-1 contained all of them, which supports the biomass combustion source for this sample in particular. For a list of matching formulas see Table S4. This table was added to the Supplement.

Table S4. Molecular formulas identified in brown carbon by Iinuma et al. 2010 and Lin et al. 2016.

Formula	Observed	Citation
		Iinuma et al. 2010;
$C_7H_7NO_4$	Yes	Lin et al. 2016
$C_6H_5NO_3$	Yes	Lin et al. 2016
$C_6H_5NO_4$	Yes	Lin et al. 2016
$C_6H_6N_2O_6$	No	Lin et al. 2016
$C_6H_4NO_4$	No	Lin et al. 2016
$C_{10}H_9NO_3$	No	Lin et al. 2016
$C_8H_7NO_4$	Yes	Lin et al. 2016
$C_8H_7NO_3$	Yes	Lin et al. 2016
$C_9H_7NO_4$	Yes	Lin et al. 2016
$C_{10}H_7NO_4$	Yes	Lin et al. 2016
$C_8H_8O_3$	Yes	Lin et al. 2016
$C_9H_6O_3$	Yes	Lin et al. 2016
$C_{10}H_8O_4$	Yes	Lin et al. 2016
$C_{13}H_8O_5$	Yes	Lin et al. 2016
$C_{13}H_8O_6$	Yes	Lin et al. 2016
$C_{15}H_{10}O_6$	Yes	Lin et al. 2016
$C_{16}H_{12}O_6$	Yes	Lin et al. 2016
$C_{16}H_{12}O_7$	Yes	Lin et al. 2016
$C_{17}H_{14}O_8$	Yes	Lin et al. 2016

p. 5, l. 169: The two references describe different criteria for the molecular formula assignments: Dzepina et al.: max. 100 C, 400 H, 100 O, 3 N, and 1 S. Mazzoleni et al.: max. 70 C, 140 H, 25 O, 3 N, and 1 S.

The maximum range for C, H, and O is a function of the molecular weight range. Our highest m/z value is 752.3636, thus assuming 100% C (752.3636/12 = 62.7), 50% O (752.3636/32 = 23.5) and an H/C = 2 (62.7 *2 = 125.4). Thus, it is not necessary to have higher maximum values.

The elemental windows for nitrogen and sulfur seem very strict. The used limits exclude for example the identification of nitrogen-heterocycles with four nitrogen (e.g Kampf et al., 2012). Given the clear isotopic signature of sulfur, why was not more sulfur allowed? Were the isotopic patterns used to confirm the molecular formulas in case multiple elemental compositions appeared within the instrumental accuracy limits?

Based on our observations over several iterations of molecular formula assignment with varied elemental tolerances, the number of unreliable (aka chemically unreasonable) molecular formula assignments increases with an increased number of N and S.

Isotopic patterns were used to provide confidence in the molecular formula assignment. Roughly 90% of all species identified were found to have a corresponding ^{13}C peak and roughly 70% of all sulfur containing formulas were found to have a corresponding ^{34}S peak. The molecular formulas without isotope confirmation had low relative abundances, thus the polyisotopic ions were likely below the noise threshold.

Reduced S and N (including heterocyclic compounds) are unlikely to be detected in negative ion ESI-MS. Furthermore, several studies have shown that the number of elements and especially the number of multivalent elements must be restricted to obtain reliable molecular formula assignment (Koch et al., 2007; Herzsprung et al., 2015). On the other hand, not allowing probable heteroatoms leads to incorrect assignments (Ohno et al., 2013).

p. 5, l. 172: According to Putman et al., allowing nitrogen for compounds larger than 500 amu results in multiple results within 1 ppm. Does that mean that the number of elements allowed was chosen such strict that only one molecular formula per signal was obtained?

In the Putman et al. (2012) paper we discussed the importance of having a *de novo* (aka first in series) cutoff of 500 u when assigning molecular formulas with heteroatoms such as nitrogen. This means that the molecular formula assignments above 500 u are restricted to homologous series of molecular formulas below 500 u. In Composer this relationship is based on Kendrick mass defects to identify homologous series of CH_2. This is necessary because the number of chemically reasonable formulas with N and S heteroatoms is greater than 1.

p. 6, l. 205-222: As mentioned by the editor, this paragraph is not well structured and needs rewriting.

Upon receipt of the editor's comments, we revised the paragraph from a single long paragraph to 3 shorter paragraphs. To further clarify the paragraph, we removed the following sentence (from Section 3.1) as it was slightly off topic: "**Generally, increased cloud processing is expected to lead to increased oxidation of atmospheric organic species (Ervens et al., 2008; Zhao et al., 2013), but has also been hypothesized that cloud scavenging of oxidized components could lead to lower overall oxidation by leaving behind reduced aerosol (Dzepina et al., 2015).**"

p. 8, l. 308: Is the high O/C of the CHNO species potentially driven by organic nitrates?

Yes, we expect the oxygen of nitrate functional groups to contribute to the O/C value. This is why the O/C ratios of CHO and CHNO species were never directly compared and contrasted within a single sample, instead they were only compared across the samples.

p. 8, l. 310-311: Does the common number of identified molecules in a certain group (here CHNO) really tell us something about the similarity of samples? This is mentioned several times in the manuscript, and I don't understand why intensity of compounds is not given more weight in the discussions.

The peak intensity is not the only consideration for these compounds, because intensity is not based entirely on the abundance of the compound in the sample. Ionization efficiency also plays an important role (this is mentioned in lines 324-326). For this reason, we tried to limit our reliance on interpreting the samples solely through abundance. However, because the ions represent a mixture of isomers, the trends associated with the molecular formulas are important. For example, although a majority of the CHO molecular formulas between the three samples were in common, we observed much higher normalized relative abundances of the CHO with higher O/C values in PMO-2. It is the same for CHNO species as well, the species with high O/C are more abundant in PMO-2 than in the other two samples.

To eliminate confusion, we moved the non-intensity weighted values to the supplement.

Why not visualizing the similarity of two different samples by simple scatter plots of the intensity of all ions of sample A vs intensity of all ions of sample B. This would also allow determining the Pearson correlation coefficient.

As requested, we made a scatter plot (see below). The scatter plots are consistent with our observations regarding the similarities between PMO-1 and PMO-3 and the relative difference between these two and PMO-2. The Pearson coefficients are shown in each plot and demonstrate PMO-1 and PMO-3 are more similar to each other than PMO-2.

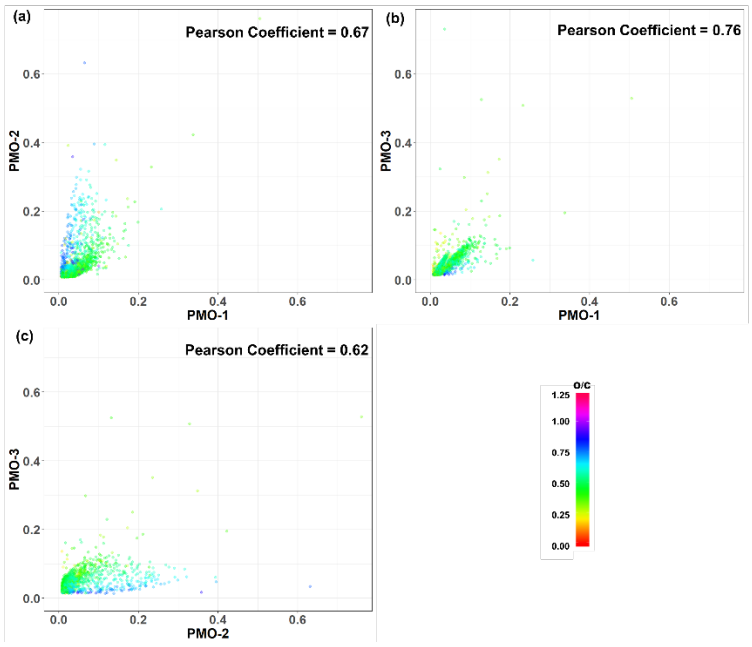

Figure AR1. Scatter plot of the normalized relative abundance of one sample vs. the normalized relative abundance of another. The sample name is on each axis and the numbers denote the normalized relative abundance.

Another way of demonstrating the differences and similarities between these samples while considering their abundance can be done using difference mass spectra. We added 3 difference mass spectra to the Supplement (Fig. S23). In these plots, PMO-2 contains nearly all of the high O/C species, while PMO-1 and/or PMO-3 show the lower O/C species, as described in the manuscript. The plots also show where the species are more abundant. Likewise, similar abundances cancel each other toward zero.

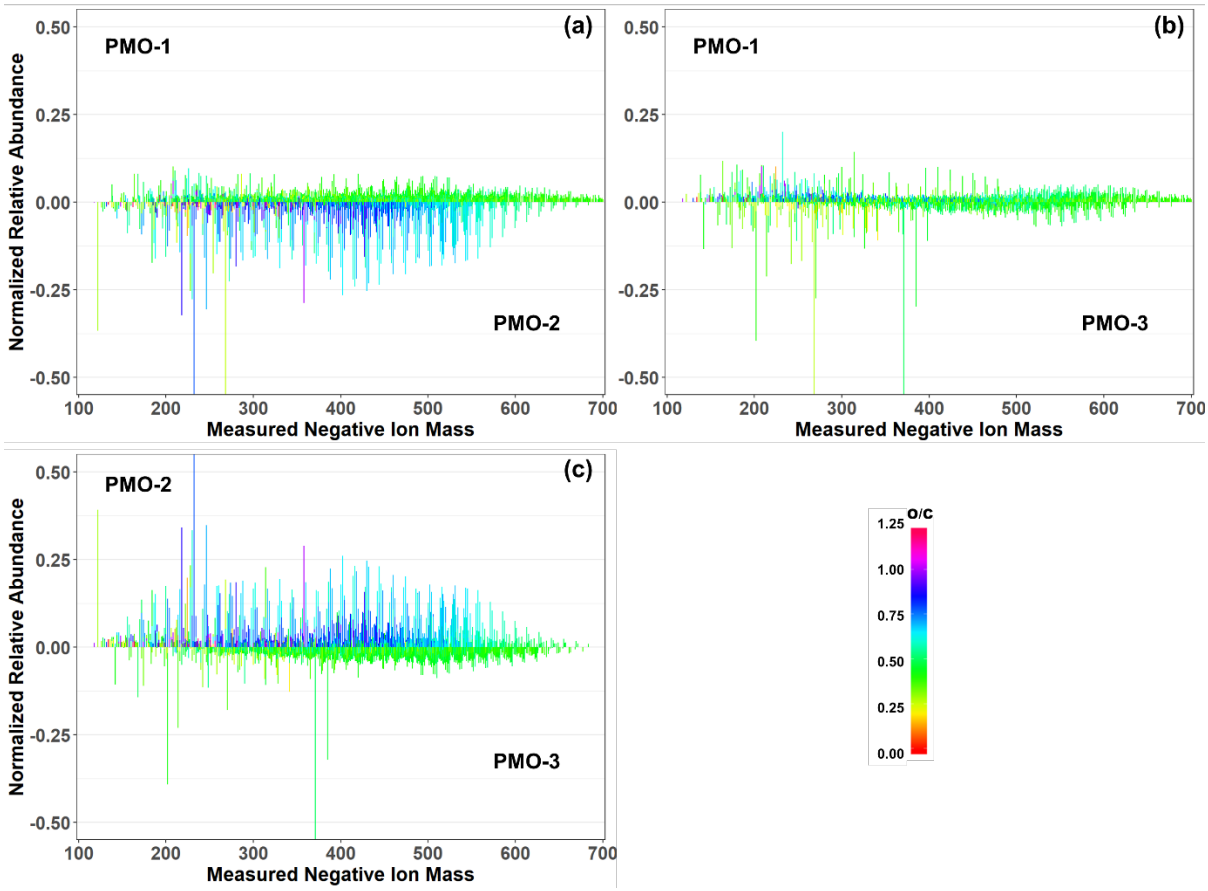

Figure S23. Difference mass spectra comparing the three PMO samples. The species more abundant in one sample or another are elevated in the correspondingly labeled half of the plot. PMO-1 vs. PMO-2 (a), PMO-1 vs. PMO-3 (b), and PMO-2 vs. PMO-3 (c).

p. 8, l. 319: Is the high O/C of the CHOS species potentially driven by organic sulfates? What would be the O/C after accounting for organic sulfates? Is it then still different from the CHO value?

Yes, the O/C of the CHOS species is impacted by the presence of organic sulfates. If 4 oxygen are removed from the molecular formulas and the O/C is recalculated the O/C decreases to a level somewhat below that of the CHO group (O/C = 0.44 for PMO-2 and O/C = 0.27 for PMO-1 when "sulfate" is removed). This is why the O/C values of the CHOS compounds are not directly compared to the other groups.

p. 9, l. 334 ff.: The oxygen that originates from organic nitrates and sulfates artificially increases the oxidation state of carbon.

Yes, this is correct, and in Fig. 4 (manuscript) the OS_C values used were calculated using the assumption that nitrogen and sulfur were both fully oxidized (Kroll et al., 2011). The average values reported in the tables calculated without this assumption were corrected. To clarify this, a sentence was added to lines 370-371: **"Additionally, we assumed all nitrogen and sulfur were present as nitrate and sulfate functional groups and calculated the OS_C with the appropriate corrections (Equation S1)."**

p. 10, l. 394: Was the glass transition temperature determined only for single molecules and not for the intensity weighted population of all ion signals? Obviously the atmospheric particles are mixtures and therefore only the glass transition temperature derived from the whole spectrum is meaningful.

We thank the reviewer for this question. A similar question was raised by Reviewer 2. Prompting much additional consideration of this topic. Please see also the Authors Response to Reviewer 2.

First, we calculated the T_g for all components because it provides the distribution of T_g values. This can be useful because it is unlikely that all particles contain all the species identified (e.g. Riemer and West, 2013), and so some particles may contain species that are more likely to be liquid, while another may be more likely solid. A determination of the chemical mixing at the single particle level would require a different type of analysis (e.g., O'Brien et al., 2015) and is not possible with our samples. The single compound information is lost when all species are treated as if they were uniformly mixed by calculating a single average T_g.

We agree that the overall T_g for a particle is what matters in determining the phase state of said particle, but as we have no way of knowing the exact composition of every aerosol particle we feel that showing the distribution of estimated T_g values is more appropriate. In any case, we did calculate the compositional arithmetic average dry T_g values for all three samples (RA Weighted T_g without Ions (100%)), which is shown in the table below. This table has also been added to the Supplement as Table S5.

Table SM5. Estimated average T_g values when the ions are considered. The table contains the results for 3 assumptions of the organic mass fraction represented by the FT-ICR MS identified species (100%, 70%, 50%). The numbers in parentheses show the percent change in average T_g from the T_g without ions considered. All T_g values are in K.

Sample	RA Weighted T_g without Ions (100%)	Ions and RA Weighted T_g (100%)	Ions and RA Weighted T_g (70%)	Ions and RA Weighted T_g (50%)
PMO-1	328.75	324.38 (1.33%)	322.67 (1.85%)	320.51 (2.51%)
PMO-2	326.45	324.43 (0.619%)	323.71 (0.839%)	322.85 (1.10%)
PMO-3	326.88	324.41 (0.756%)	323.44 (1.05%)	322.22 (1.43%)

Accounting for the fact that small organics are lost during the SPE (which would reduce Tg of the mixture), what would be the effect on Tg of the mixture if one assumes that 10, 20 or 50% of total OC consist of small organics?

It is correct that low MW species are lost during SPE and this can bias the T_g towards higher values. However, the bias is very minor based on estimations made using the ion concentrations and OM concentrations for these samples, as discussed in the response to reviewer comment #3 (Table SM5). The most prevalent organic anion in all three samples, is oxalate, which has a T_g estimated to be 324.21 according to the Boyer-Kauzmann rule ($T_g = g*T_m$, g= 0.7, T_m = melting point) (Koop et al., 2011; Shiraiwa et al., 2017; DeRieux et al., 2018). If the assumption is made that half of the total OM is small organics, oxalate would likely make up the largest percentage of the total and would thus have the

greatest effect on the impact of small organics on the T_g. Just as a theoretical exercise, if we use the assumption that 50% of the OM is oxalate and the method described in detail above, the average dry T_g drops ≤ 2.5 K. It would be lower if we assumed that formate or acetate were the major small organic being lost, but based on our measurements that is not expected.

As explained earlier, our intention was not to definitively calculate the glass transition temperature for the entire mixture in the particle. To clarify this we altered Figure 7 in the manuscript to instead show the distribution of estimated T_g values based on the ambient relative humidity. In this plot, we included the T_g and abundance of the most abundant low MW organic ions removed by SPE. This sheds light on their potential impact toward the overall T_g of the particles. We also plotted the ambient temperature to guide the eye and illustrate where the estimated T_g values exceed the ambient temperature, which implies a greater likelihood for solid state aerosol (Shiraiwa et al., 2017). Furthermore, the text of the manuscript has been revised to reflect these changes from discussing phase state predictions to estimates of T_g and their implications.

Figure 3: The three dots with H/C<0.6 are cyan in PMO-1, which should mean unique in PMO-1. Why are these three signals in PMO-2 and PMO-3 then grey (common signals)?

We thank the reviewer for the comment, the figure caption was inaccurate, and the grey symbols were actually all CHNO formulas detected in the three samples. They were included in each plot to make it clear where the differences are between the three samples. The colored circles are the formulas that are unique to each sample, as stated in the figure caption. We clarified the wording by replacing **"common species"** with **"all identified CHNO species".**

Figure 1: The Figure quality is not appropriate.

Corrected.

Figure 2: X-axis ticks are missing for (a),(b),(d) and (e). It seems as the highest peaks in (b) and (c) are cut at the top, or are they all the same height?

The tick marks on the bottom plot are accurate for all plots. The tallest peaks are cut off at the top in order to better show the lower intensity species. A comment to clarify this has been added to the caption for Figure 2: **"The tallest peaks in the mass spectra exceed the range, this was done to improve the visibility of the lower abundance species (see also Fig. S6)."** In addition, a plot that shows the entire range of abundance values was added to the Supplement (Fig. S6).

Figure 4: X-axis ticks are missing for (a), (b), (d) and (e).

Corrected

Figure 4: The y-label is number of formulas. The caption is not clear on that. What is the "normalized abundance"? On what is it normalized?

Thank you for catching this oversight. Instead of normalized abundance, it should have been number of formulas. However, we decided to use the histogram based on the normalized abundance instead of the one that was there, so the caption is now correct as written, and no additional changes are needed. The abundance is normalized to the total abundance of the assigned species.

Figure 6: X-axis ticks are missing for PMO-1.

Corrected

Literature

Crounse, J. D., Nielsen, L. B., Jorgensen, S., Kjaergaard, H. G., and Wennberg, P. O.: Autoxidation of Organic Compounds in the Atmosphere, Journal of Physical Chemistry Letters, 4, 3513–3520, doi:10.1021/jz4019207, 2013.

Ehn, M., Kleist, E., Junninen, H., Petaja, T., Lonn, G., Schobesberger, S., Dal Maso, M., Trimborn, A., Kulmala, M., Worsnop, D. R., Wahner, A., Wildt, J., and Mentel, T. F.: Gas phase formation of extremely oxidized pinene reaction products in chamber and ambient air, Atmos. Chem. Phys., 12, 5113–5127, doi:10.5194/acp-12-5113-2012, 2012.

Iinuma, Y., Boege, O., Graefe, R., and Herrmann, H.: Methyl-Nitrocatechols: Atmospheric Tracer Compounds for Biomass Burning Secondary Organic Aerosols, Environ. Sci. Technol., 44, 8453–8459, doi:10.1021/es102938a, 2010.

Jokinen, T., Sipila, M., Richters, S., Kerminen, V.-M., Paasonen, P., Stratmann, F., Worsnop, D., Kulmala, M., Ehn, M., Herrmann, H., and Berndt, T.: Rapid Autoxidation Forms Highly Oxidized RO2 Radicals in the Atmosphere, Angewandte Chemie-International Edition, 53, 14596–14600, doi:10.1002/anie.201408566, 2014.

Kampf, C. J., Jakob, R., and Hoffmann, T.: Identification and characterization of aging products in the glyoxal/ammonium sulfate system - implications for light-absorbing material in atmospheric aerosols, Atmos. Chem. Phys., 12, 6323–6333, doi:10.5194/acp-12-6323-2012, 2012.

Lin, P., Aiona, P. K., Li, Y., Shiraiwa, M., Laskin, J., Nizkorodov, S. A., and Laskin, A.: Molecular Characterization of Brown Carbon in Biomass Burning Aerosol Particles, Environ. Sci. Technol., 50, 11815–11824, doi:10.1021/acs.est.6603024, 2016.

Additional References

Aiken, A. C., DeCarlo, P. F., Kroll, J. H., Worsnop, D. R., Huffman, J. A., Docherty, K. S., Ulbrich, I. M., Mohr, C., Kimmel, J. R., Sueper, D., Sun, Y., Zhang, Q., Trimborn, A., Northway, M., Ziemann, P. J., Canagaratna, M. R., Onasch, T. B., Alfarra, M. R., Prevot, A. S. H., Dommen, J., Duplissy, Metzger, A., Baltensperger, U., and Jimenez J. L.: O/C and OM/OC Ratios of Primary, Secondary, and Ambient Organic Aerosols with High-Resolution Time-of-Flight Aerosol Mass Spectrometry, Environ. Sci. Technol., 42(12), 4478–4485, doi:10.1021/es703009q, 2008.

Bougiatioti, A., Stavroulas, I., Kostenidou, E., Zarmpas, P., Theodosi, C., Kouvarakis, G., Canonaco, F., Prevot, A. S. H., Nenes, A., Pandis, S. N. and Mihalopoulos, N.: Processing of biomass-burning aerosol in the eastern Mediterranean during summertime, Atmos. Chem. Phys., 14(9), 4793–4807, doi:10.5194/acp-14-4793-2014, 2014.

Bougiatioti, A., Nikolaou, P., Stavroulas, I., Kouvarakis, G., Weber, R., Nenes, A., Kanakidou, M. and Mihalopoulos, N.: Particle water and pH in the eastern Mediterranean: source variability and implications for nutrient availability, Atmos. Chem. Phys., 16(7), 4579–4591, doi:10.5194/acp-16-4579-2016, 2016.

Cook, R. D., Lin, Y.-H., Peng, Z., Boone, E., Chu, R. K., Dukett, J. E., Gunsch, M. J., Zhang, W., Tolic, N., Laskin, A. and Pratt, K. A.: Biogenic, urban, and wildfire influences on the molecular composition of dissolved organic compounds in cloud water, Atmos. Chem. Phys., 17(24), 15167–15180, doi:10.5194/acp-17-15167-2017, 2017.

DeRieux, W.-S. W., Li, Y., Lin, P., Laskin, J., Laskin, A., Bertram, A. K., Nizkorodov, S. A. and Shiraiwa, M.: Predicting the glass transition temperature and viscosity of secondary organic

material using molecular composition, Atmos. Chem. Phys., 18(9), 6331–6351, doi:10.5194/acp-18-6331-2018, 2018.

Dunlea, E. J., DeCarlo, P. F., Aiken, A. C., Kimmel, J. R., Peltier, R. E., Weber, R. J., Tomlinson, J., Collins, D. R., Shinozuka, Y., McNaughton, C. S., Howell, S. G., Clarke, A. D., Emmons, L. K., Apel, E. C., Pfister, G. G., van Donkelaar, A., Martin, R. V., Millet, D. B., Heald, C. L. and Jimenez, J. L.: Evolution of Asian aerosols during transpacific transport in INTEX-B, Atmos. Chem. Phys., 9(19), 7257–7287, doi:10.5194/acp-9-7257-2009, 2009.

Dzepina, K., Mazzoleni, C., Fialho, P., China, S., Zhang, B., Owen, R. C., Helmig, D., Hueber, J., Kumar, S., Perlinger, J. A., Kramer, L. J., Dziobak, M. P., Ampadu, M. T., Olsen, S., Wuebbles, D. J., and Mazzoleni, L. R.: Molecular characterization of free tropospheric aerosol collected at the Pico Mountain Observatory: a case study with a long-range transported biomass burning plume, Atmos. Chem. Phys., 15(9), 5047–5068, doi:10.5194/acp-15-5047-2015, 2015.

El-Zanan, H. S., Lowenthal, D. H., Zielinska, B., Chow, J. C. and Kumar, N.: Determination of the organic aerosol mass to organic carbon ratio in IMPROVE samples, Chemosphere, 60(4), 485–496, doi:10.1016/j.chemosphere.2005.01.005, 2005.

Ervens, B., Carlton, A. G., Turpin B. J., Altieri, K. E., Kreidenweis, S. M., and Feingold, G.: Secondary organic aerosol yields from cloud- processing of isoprene oxidation products, Geophy. Res. Lett., 35(2), doi:10.1029/2007gl031828, 2008.

Herzsprung, P., Tümpling, W. v, Hertkorn, N., Harir, M., Friese, K. and Schmitt-Kopplin, P.: High-Field FTICR-MS Data Evaluation of Natural Organic Matter: Are CHON5S2Molecular Class Formulas Assigned to13C Isotopicm/zand in Reality CHO Components?, Analytical Chemistry, 87(19), 9563–9566, doi:10.1021/acs.analchem.5b02549, 2015.

Honrath, R., Owen, R., Martín, M., Reid, J., Lapina, K., Fialho, P., Dziobak, M., Kleissl, J. and Westphal, D.: Regional and hemispheric impacts of anthropogenic and biomass burning emissions on summertime CO and O3 in the North Atlantic lower free troposphere, J. of Geophys. Res. Atmos., 109(D24), doi:10.1029/2004jd005147, 2004.

Iinuma, Y., Böge, O., Gnauk, T. and Herrmann, H.: Aerosol-chamber study of the α-pinene/O3 reaction: influence of particle acidity on aerosol yields and products, Atmos. Environ., 38(5), 761–773, doi:10.1016/j.atmosenv.2003.10.015, 2004.

Jimenez, J. L., Canagaratna, M. R., Donahue, N. M., Prevot, A. S. H., Zhang, Q., Kroll, J. H., DeCarlo, P. F., Allan, J. D., Coe, H., Ng, N. L., Aiken, A. C., Docherty, K. S., Ulbrich, I. M., Grieshop, A. P., Robinson, A. L., Duplissy, J., Smith, J. D., Wilson, K. R., Lanz, V. A., Hueglin, C., Sun, Y, L., Tian, J., Laaksonen, A., Raatikainen, T., Rautiainen, J., Vaattovaara, P., Ehn, M., Kulmala, M., Tomlinson, J. M., Collins, D. R., Cubison, M. J., Dunlea, E. J., Huffman, J. A., Onasch, T. B., Alfarra, M. R., Williams, P. I., Bower, K., Kondo, Y., Schneider, J., Drewnick, F., Borrmann, S., Weimer, S., Demerjian, K., Salcedo, D., Cottrell, L., Griffin, R., Takami, A., Miyoshi, T., Hatakeyama, S., Shimono, A., Sun, J. Y., Zhang, Y. M., Dzepina, K., Kimmel, J. R., Sueper, D., Jayne, J. T., Herndon, S. C., Trimborn, A. M., Williams, L. R., Wood, E. C., Middlebrook, A. M., Kolb, C. E., Baltensperger U. and Worsnop D. R.: Evolution of Organic Aerosols in the Atmosphere, Science, 326(5959), 1525–1529, doi:10.1126/science.1180353, 2009.

Koop, T., Bookhold, J., Shiraiwa, M. and Pöschl, U.: Glass transition and phase state of organic compounds: dependency on molecular properties and implications for secondary organic aerosols in the atmosphere, Phys. Chem. Chem. Phys., 13(43), 19238–19255, doi:10.1039/c1cp22617g, 2011.

Kroll, J. H., Donahue, N. M., Jimenez, J. L., Kessler, S. H., Canagaratna, M. R., Wilson, K. R., Altieri, K. E., Mazzoleni, L. R., Wozniak, A. S., Bluhm, H., Mysak, E. R., Smith, J. D., Kolb, C. E. and Worsnop, D. R.: Carbon oxidation state as a metric for describing the chemistry of atmospheric organic aerosol, Nat. Chem., 3(2), nchem.948, doi:10.1038/nchem.948, 2011.

Koch, B. P., Dittmar, T., Witt, M. and Kattner, G.: Fundamentals of Molecular Formula Assignment to Ultrahigh Resolution Mass Data of Natural Organic Matter, Anal Chem, 79(4), 1758–1763, doi:10.1021/ac061949s, 2007.

Kundu, S., Fisseha, R., Putman, A. L., Rahn, T. A. and Mazzoleni, L. R.: High molecular weight SOA formation during limonene ozonolysis: insights from ultrahigh-resolution FT-ICR mass spectrometry characterization, Atmos. Chem. and Phys., 12(12), 5523–5536, doi:10.5194/acp-12-5523-2012, 2012.

LeClair, J. P., Collett, J. L. and Mazzoleni, L. R.: Fragmentation Analysis of Water-Soluble Atmospheric Organic Matter Using Ultrahigh-Resolution FT-ICR Mass Spectrometry, Environ. Sci. Technol., 46(8), 4312–4322, doi:10.1021/es203509b, 2012.

Lim, Y. B., Tan, Y., Perri, M. J., Seitzinger, S. P. and Turpin, B. J.: Aqueous chemistry and its role in secondary organic aerosol (SOA) formation, Atmos. Chem. and Phys., 10(21), 10521–10539, doi:10.5194/acp-10-10521-2010, 2010.

Maclean, A. M., Butenhoff, C. L., Grayson, J. W., Barsanti, K., Jimenez, J. L. and Bertram, A. K.: Mixing times of organic molecules within secondary organic aerosol particles: a global planetary boundary layer perspective, Atmos. Chem. Phys., 17(21), 13037–13048, doi:10.5194/acp-17-13037-2017, 2017.

Mazzoleni, L. R., Ehrmann, B. M., Shen, X., Marshall, A. G. and Collett, J. L.: Water-Soluble Atmospheric Organic Matter in Fog: Exact Masses and Chemical Formula Identification by Ultrahigh-Resolution Fourier Transform Ion Cyclotron Resonance Mass Spectrometry, Environ. Sci. Technol., 44(10), 3690–3697, doi:10.1021/es903409k, 2010.

Mazzoleni, L. R., Saranjampour, P., Dalbec, M. M., Samburova, V., Hallar, A. G., Zielinska, B., Lowenthal, D. H. and Kohl, S.: Identification of water-soluble organic carbon in non-urban aerosols using ultrahigh-resolution FT-ICR mass spectrometry: organic anions, Environ. Chem., 9(3), 285–297, doi:10.1071/en11167, 2012.

O'Brien, R. E., Wang, B., Laskin, A., Riemer, N., West, M., Zhang, Q., Sun, Y., Yu, X., Alpert, P., Knopf, D. A., Gilles, M. K. and Moffet, R. C.: Chemical imaging of ambient aerosol particles: Observational constraints on mixing state parameterization, J. Geophys. Res. Atmos., 120(18), 9591–9605, doi:10.1002/2015jd023480, 2015.

Ohno, T. and Ohno, P. E.: Influence of heteroatom pre-selection on the molecular formula assignment of soil organic matter components determined by ultrahigh resolution mass spectrometry, Anal. Bioanal. Chem., 405(10), 3299–3306, doi:10.1007/s00216-013-6734-3, 2013.

Putman, A. L., Offenberg, J. H., Fisseha, R., Kundu, S., Rahn, T. A. and Mazzoleni, L. R.: Ultrahigh-resolution FT-ICR mass spectrometry characterization of α-pinene ozonolysis SOA, Atmos. Env., 46, 164–172, doi:10.1016/j.atmosenv.2011.10.003, 2012.

Riemer, N. and West, M.: Quantifying aerosol mixing state with entropy and diversity measures, Atmos. Chem. Phys., 13(22), 11423–11439, doi:10.5194/acp-13-11423-2013, 2013.

Shiraiwa, M., Li, Y., Tsimpidi, A., Karydis, V., Berkemeier, T., Pandis, S., Lelieveld, J., Koop, T. and Pöschl, U.: Global distribution of particle phase state in atmospheric secondary organic aerosols, Nat. Commun., 8, ncomms15002, doi:10.1038/ncomms15002, 2017.

Shrivastava, M., Lou, S., Zelenyuk, A., Easter, R., Corley, R., Thrall, B., Rasch, P., Fast, J., Simonich, S., Shen, H. and Tao, S.: Global long-range transport and lung cancer risk from polycyclic aromatic hydrocarbons shielded by coatings of organic aerosol, P. Natl. Acad. Sci., 114(6), 1246–1251, doi:10.1073/pnas.1618475114, 2017.

Sorooshian, A., Lu, M.-L., Brechtel, F., Jonsson, H., Feingold, G., Flagan, R. and Seinfeld, J.: On the Source of Organic Acid Aerosol Layers above Clouds, Environ. Sci. Technol., 41(13), 4647–4654, doi:10.1021/es0630442, 2007.

Ye, Q., Robinson, E. S., Ding, X., Ye, P., Sullivan, R. C. and Donahue, N. M.: Mixing of secondary organic aerosols versus relative humidity, P. Natl. Acad. of Sci., 113(45), 12649–12654, doi:10.1073/pnas.1604536113, 2016.

Yu, J. Z., Huang, X., Xu, J. and Hu, M.: When Aerosol Sulfate Goes Up, So Does Oxalate: Implication for the Formation Mechanisms of Oxalate, Environ. Sci. Technol., 39(1), 128–133, doi:10.1021/es049559f, 2005.

Zelenyuk, A., Imre, D. G., Wilson, J., Bell, D. M., Suski, K. J., Shrivastava, M., Beránek, J., Alexander, M. L., Kramer, A. L. and Massey-Simonich, S. L.: The effect of gas-phase polycyclic aromatic hydrocarbons on the formation and properties of biogenic secondary organic aerosol particles, Faraday Discuss., 200, 143–164, doi:10.1039/c7fd00032d, 2017.

Zhang, B., Owen, R. C., Perlinger, J. A., Helmig, D., Val Martín, M., Kramer, L., Mazzoleni, L. R. and Mazzoleni, C.: Ten-year chemical signatures associated with long-range transport observed in the free troposphere over the central North Atlantic, Elem. Sci. Anth., 5, doi:10.1525/elementa.194, 2017.

Zhao, Y., Hallar, A. G. and Mazzoleni, L. R.: Atmospheric organic matter in clouds: exact masses and molecular formula identification using ultrahigh-resolution FT-ICR mass spectrometry, Atmos. Chem. Phys., 13(24), 12343–12362, doi:10.5194/acp-13-12343-2013, 2013.

Zielinski, A. T., Kourtchev, I., Bortolini, C., Fuller, S. J., Giorio, C., Popoola, O. A. M., Bogialli, S., Tapparo, A., Jones, R. L. and Kalberer, M.: A new processing scheme for ultra-high resolution direct infusion mass spectrometry data, Atmos. Environ., doi:10.1016/j.atmosenv.2018.01.034, 2018.

Author Responses to Reviewer #2

The *Reviewer comments are in black italic font* and the Author responses are in blue font.

Schum et al. present a unique dataset collected on Pico Mountain Observatory to study the physiochemical properties of aerosol in the remote marine free troposphere. They analyzed three aerosol samples that had elevated organic carbon concentration, and attributed the differences in their molecular and physical characteristics to emission sources as well as their transport pathways. They observed a lower O/C ratio in two samples that they believed were likely from biomass burning plumes that were transported mostly in the free troposphere, and the aerosols were in a solid state that resisted oxidation. Before this work is published in ACP, the authors need to provide careful clarification and further discussion of several important aspects in this manuscript. Please find the comments below.

We thank the reviewer for their helpful comments. We made several changes to both the main paper and the supplemental information. In particular, we made major revisions to section 3.5.

Major comments

1. The O/C values for PMO-1 and PMO-3 are surprisingly low for particles that had been transported for 7-10 days. In Section 2.3, the authors pointed out that "losses of highly water soluble, low molecular weight organic compounds are expected". Highly water soluble compounds are presumably quite polar and thus should have higher O/C. Authors need to address how the SPE artifacts affect the overall sample O/C. The same issue applies to the artifacts of water extraction that the water-soluble compounds in the samples were preferably collected for the subsequent analysis. Please provide a discussion of possible bias, what is roughly the fraction that had been extracted versus not-extracted, and how it might affect the results of the analysis.

We thank the reviewer for this comment. The sample preparation step is necessary because electrospray ionization (ESI) is used to study complex organic matter. The soft ionization method is susceptible to salt adducts that can complicate the mass spectra. Furthermore, low molecular weight (MW) compounds can be analyzed using other analytical techniques (e.g., gradient anion chromatography is suitable for several common low MW organic anions).

As suggested by the reviewer, the loss of low MW compounds with high O/C values does likely correspond to a decrease in the total water-soluble organic carbon O/C value. The magnitude of this depends on how the O/C value is determined. An overall larger difference is associated with relative abundance weighted O/C values (RA-weighted or O/C_w). On the other hand, a negligible difference is associated with arithmetic mean values (due to the very high number of identified molecular formulas). For this reason, a majority of the values reported in the discussion paper were arithmetic mean values. For a more complete comparison of arithmetic mean values of O/C from several studies, we refer the reviewer to Table 3 from Dzepina et al. (2015) shown below.

Table 3. Chemical characterization of the molecular assignments detected in selected studies. All values are average (arithmetic mean).

Sample name	Sample type	Measurement site	O / C	H / C	OM / OC	DBE	DBE / C	MW	Reference
Pico 9/24	Aerosol	Free troposphere	0.46	1.17	1.73	10.7	0.47	478	This study
Pico 9/25	Aerosol	Free troposphere	0.42	1.28	1.67	9.4	0.42	462	
Storm Peak Lab S4SXA	Aerosol	Remote	0.53	1.48	1.91	6.2	0.34	414	Mazzoleni et al. (2012)
Millbrook, NY[1]	Aerosol	Rural	0.32	1.46	1.60	6.30	0.33	366	Wozniak et al. (2008)
Harcum, VA[1]	Aerosol	Rural	0.28	1.37	1.54	7.45	0.38	360	
K-Puszta 2004 (KP2004)[2]	Aerosol	Rural	0.48	1.40	1.84	7.36	0.37	408	Schmitt-Kopplin et al. (2010)
K-Puszta 2005 (KP2005)[2]	Aerosol	Rural	0.39	1.22	1.69	10.1	0.46	430	
Pearl River Delta, China	Aerosol	Urban, Suburban, Rural, Regional	0.46	1.34	1.85	5.3	0.45	265	Lin et al. (2012a)
Atlantic Ocean[3]	Aerosol	Marine boundary layer	0.35	1.59	1.67	4.37	0.28	317	Schmitt-Kopplin et al. (2012)
North Atlantic Ocean – All[4]	Aerosol	Marine boundary layer	0.42	1.49	1.74	6.76	0.32	445	Wozniak et al. (2014)
North Atlantic Ocean – Aged Marine[4]	Aerosol	Marine boundary layer	0.36	1.56	1.70	5.88	0.28	423	
Storm Peak Lab CW1	Cloud water	Remote	0.62	1.46	2.08	6.3	0.38	402	Zhao et al. (2013)
Storm Peak Lab CW2	Cloud water	Remote	0.61	1.46	2.06	6.3	0.38	400	
Fresno fog	Fog water	Rural	0.43	1.39	1.77	5.6	0.40	289	Mazzoleni et al. (2010)
Camden and Pinelands, NJ[5]	Rainwater	Urban impacted	1.02	1.49	2.73	3.24	0.44	220	Altieri et al. (2009a, b)

Values were calculated: [1] For each sample presented in Wozniak et al. (2008). [2] For only two samples (KP2004 and KP2005) presented in Schmitt-Kopplin et al. (2010). [3] For only one, marine aerosol, sample presented in Schmitt-Kopplin et al. (2012). [4] For all samples (and only one PCA group) presented in Wozniak et al. (2014). [5] By combining the negative mode FT-ICR MS data available in Altieri et al. (2009a) (CHO, CHOS and CHNOS) and Altieri et al. (2009b) (CHON).

After consideration of all of the comments (including those of Reviewer 1 and the editor), we opted to instead focus on the RA-weighted values consistently throughout the manuscript. These values do help distinguish important trends in the data (e.g., Fig. 2 and 4). However, we note both here, and in the manuscript (lines 327-328), that the RA is not expected to directly correspond to the analyte concentrations because the ionization efficiencies depend on several factors such polarity, surface activity, and pH (Cech and Enke, 2001).

We estimated the impact of the missing low MW species on the overall O/C using the five highest mass concentrations (oxalate, acetate, lactate, formate, and malonate) as measured using ion chromatography. The measured mass concentrations were converted to their percent abundance relative to the total organic mass (estimated using an OM/OC conversion of 2 (El-Zanan et al., 2005)). The total ion abundance identified using ultrahigh resolution FT-ICR MS was assumed to represent as little as 50% of the total WSOC. Then the individual low MW compound mass fractions were used to estimate their abundance relative to the sum of the total abundance of species identified by FT-ICR MS. These abundance values were then used to estimate the weighted average O/C value for each of the samples. The following table was added to the Supplement (Table SM4).

Table SM4. Estimated average O/C values when the ions are considered. The table contains the results for 3 assumptions of the organic mass fraction represented by the FT-ICR MS identified species (100%, 70%, 50%). The numbers in parentheses show the percent change in average O/C from the O/C without ions considered.

Sample	RA Weighted O/C without Ions (100%)	Ions and RA Weighted O/C (100%)	Ions and RA Weighted O/C (70%)	Ions and RA Weighted O/C (50%)
PMO-1	0.48	0.53 (10.42%)	0.55 (14.58%)	0.58 (20.83%)
PMO-2	0.57	0.70 (22.81%)	0.75 (31.58%)	0.81 (42.11%)
PMO-3	0.45	0.52 (15.56%)	0.54 (20.00%)	0.57 (26.67%)

PMO-2 is still by far the most oxidized sample overall. PMO-1 and PMO-3 were still somewhat un-oxidized relative to our pre-conceived expectations based on transport time (Bougiatioti et al., 2014; Aiken et al., 2008). Oxalate is by far the most abundant organic ion and has the highest O/C, thus it yields the largest impact. Note that these O/C values are likely the upper limit of the average high MW O/C for these samples. The ionization preferences associated with negative mode ESI favor more highly oxidized higher molecular weight species, thus high MW molecular species detected by other ionization methods would likely only decrease the O/C.

To clarify the impact of the missing anions on the average O/C, the following has been added (see lines 164-171): **"The procedural loss of ionic low MW compounds such as oxalate can lead to an underprediction of the organic aerosol O/C and overprediction of the average glass transition temperatures (T_g). To investigate this, we used the concentrations of the prominent organic anions measured with ion chromatography to estimate the abundance of these compound relative to the compounds detected by FT-ICR MS. The low MW corrected average O/C values correlated with the trends of the original O/C values, however the significance of impacts varies with the measured analyte concentrations and the assumptions associated with the uncertain mass fraction of the molecular formula composition (Table SM4). When low MW organic anions were included in the estimated average dry T_g values, they dropped by ≤ 2.5 %, which was deemed relatively insignificant (Table SM5)."**

A description of the estimation method and data discussed above were added to the Supplement (Page 5).

2. The authors use the method developed by DeRieux et al. to estimate particle phase state and heavily rely on the result to explain their findings. However, the authors use this method without further comment and discussion, especially regarding its uncertainty. Solid, semisolid and liquid state are qualitative descriptions which do not provide much insight into diffusion time-scale of water or organic molecules into/out of particles. Diffusion is a key process that determines the evolution of particle composition, and the connection of phase state and diffusivity involves multiple-step estimations with large uncertainties, as shown in a couple of studies [1][2]. Is it possible that the uncertainty of the method is large enough that it changes the major conclusions of this paper? The authors need to provide a much more comprehensive discussion of these issues.

We thank the reviewer for this comment.

This work expands the understanding of the long-range transported aerosol collected at the Pico Mountain Observatory (PMO) presented in previous studies (Dzepina et al., 2015, China et al., 2015; China et al. 2017; Zhang et al., 2015; Zhang et al., 2017). As described, the site is located in the North Atlantic free troposphere on the Azores archipelago, and as such, it is quite remote. Additionally, the site is uniquely well-suited for the observation of long range transported aerosol due to the low marine boundary layer which is frequently below the site (See also Image 1 in the Supplement for a photo of the site and the mountain). Specifically, this paper attempts to advance the interpretation of pollution events arriving from North America using the detailed molecular chemistry.

We agree that diffusion is a key process in determining the evolution of particle compositions; however according to the FLEXPART retroplumes, the aerosol have been aloft for several days and the compositions that we measured are mostly low volatility compounds (Fig. 6 of manuscript). Our intent was not to provide exact predictions of diffusion or viscosity for the aerosol collected during the sampling periods (predictions for which our available sample and measurements would not be appropriate), but to provide an estimate of the most probable phase state for the organic aerosol during transport using the GFS meteorological fields (specifically ambient T and RH) associated with the FLEXPART retroplumes for a few upwind days. We then used the ratio of glass transition temperatures (T_g) to the ambient temperature (T_g/T) coupled with chemical markers to assist in the interpretation of our observations of the samples.

At present, we do not have enough information to predict the diffusion of species in the aerosol particles. Insufficient knowledge on the composition of aerosol particles and a lack of available methods to accurately measure viscosity for ambient samples at low concentrations limit the possibility to estimate diffusion, as described in a recent review by Reid et al. (2018). Therefore, we used general literature ideas about phase state and its impact on diffusion and viscosity to support the hypothesis that phase state limits the atmospheric oxidation of organic aerosol, which is consistent with several other studies (Shrivastava et al. 2017, Berkemeier et al., 2014, Lignell et al., 2014, Zelenyuk et al., 2017). Research reported in Ye et al. (2016), has shown that low volatility compounds resist diffusion even at high RH.

To be more accurate and avoid confusion, we removed the classification of molecular species as “solid”, “semi-solid”, and “liquid”, and instead show only the estimated T_g. We also focused our discussion on the uncertainties in the T_g estimates with respect to the DeRieux et al. (2018) defined error and the range of meteorological conditions extracted from FLEXPART. In fact, the range of ambient conditions presents a larger range of estimated T_g values. As such, Figure 7 from the revised manuscript has revised and an additional version of the plot which demonstrates the distribution of T_g values using just the mean RH for the RH dependent T_g was added to the supplement (Fig. S17).

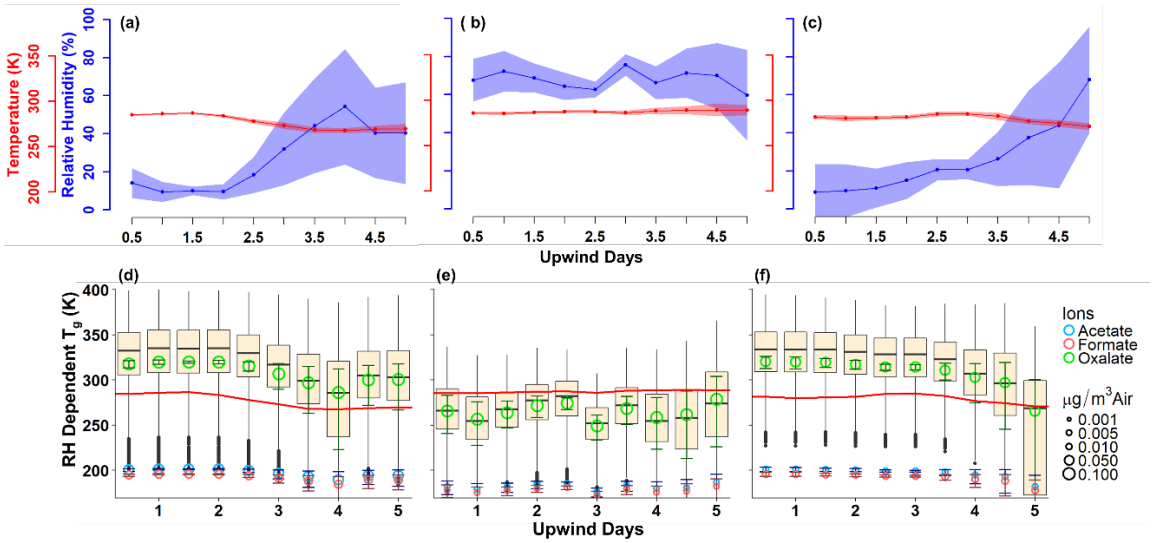

Figure 7. Panels a-c contain the ambient conditions extracted from the GFS analysis along the FLEXPART modeled path weighted by the residence time for PMO-1, PMO-2, and PMO-3, respectively. The line represents the mean value and the shading represents one standard deviation of values. Panels d-f contain the boxplot distributions of the relative humidity dependent T_g values for molecular formulas using the maximum, mean, and minimum RH for PMO-1, PMO-2, and PMO-3, respectively. The T_g values for the full composition of each sample were calculated using the maximum, mean, and minimum RH and then all three sets of data are combined and plotted as a single distribution for each time period. The open circles represent the abundance and Boyer-Kauzmann estimated T_g for the acid forms of the three most abundant low MW organic ions, the bars around the circles represent the range of possible T_g values for those compounds when the range of RH is considered. The red line demonstrates the ambient temperature at each time point, as extracted from GFS. The centerline of the boxplot represents the median, the top and bottom of the "box" represent the third and first quartiles, respectively. The "whiskers" represent Q3 + 1.5* interquartile range (IQR, Q3-Q1) (maximum), and Q1 – 1.5*(IQR) (minimum).

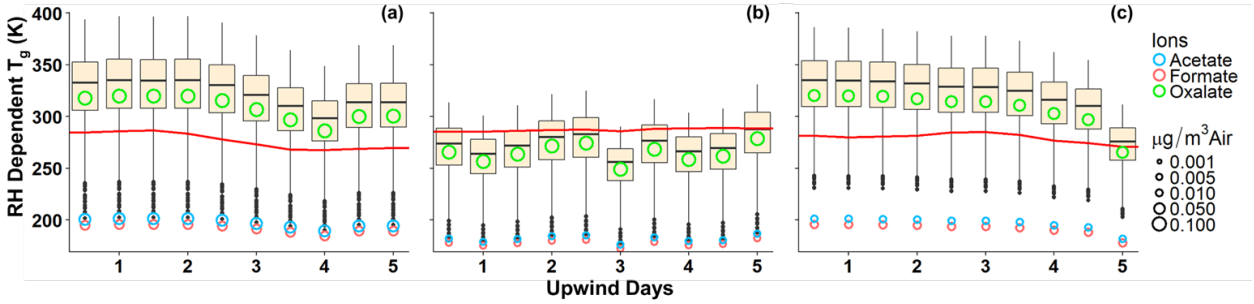

Figure S17. Boxplots showing the distributions of the relative humidity dependent T_g values for each sample over the last five days of transport. The open circles represent the Boyer-Kauzmann estimated T_g values for the acid forms of the three most abundant low MW organic ions not observed in FT-ICR mass spectra. The symbols are scaled by their ambient concentration. The red line represents the mean ambient temperature from the GFS analysis. The samples PMO-1, PMO-2, and PMO-3 are shown in panels (a), (b), and (c), respectively. The centerline of the boxplot represents the median, the top and bottom of the "box" represent the third and first quartiles, respectively. The "whiskers" represent Q3 + 1.5* interquartile range (IQR, Q3-Q1) (maximum) and Q1 – 1.5*(IQR) (minimum).

According to DeRieux et al. 2018, the estimation of T_g has an error of ±21 K when considering only a single compound. They also mention that when considered as a group, the error decreases substantially, owing largely to some species being overestimated and some being underestimated, leading to the final result being reasonably accurate. In order to test the limit of the potential error, we added and subtracted 21 K from all the estimated T_g values and replotted the distributions as presented in the manuscript.

As expected, the range of T_g values increased. However, despite this increase, the majority of the T_g distribution was still below the ambient temperature for PMO-2. Figure S18 (below) illustrates the results of these tests. However, to have the equation under or overestimate the T_g of all formulas by the maximum reported error and the same extent with the same direction is highly unlikely and so it seems likely that our results are robust. Furthermore, an individual molecular formula represents a mixture of isomers with slightly different T_g values, thereby potentially decreasing the error consistent with the description by DeRieux et al. (2018). For example, ultrahigh resolution MS/MS work by LeClair et al. (2012) has shown that most molecular formulas have more functional group losses (neutral losses of hydroxyl, carboxyl, etc.) than could be expected from a single isomer of a molecule. This has also been observed in the MS/MS analysis of PMO-1 which is the subject of a forthcoming paper.

To make the potential error due to the estimation clear the following has been added to the manuscript (Lines 213-217): **"DeRieux et al. (2018) reported an uncertainty of ± 21 K for the prediction of any single compound, but the uncertainty is expected to decrease when a mixture of compounds is considered. Nonetheless, we assumed an uncertainty range of ± 21 K on T_g and found that it did not significantly change the T_g trends presented in Section 3.5. Further discussion the uncertainty on T_g is provided in the Supplement."**

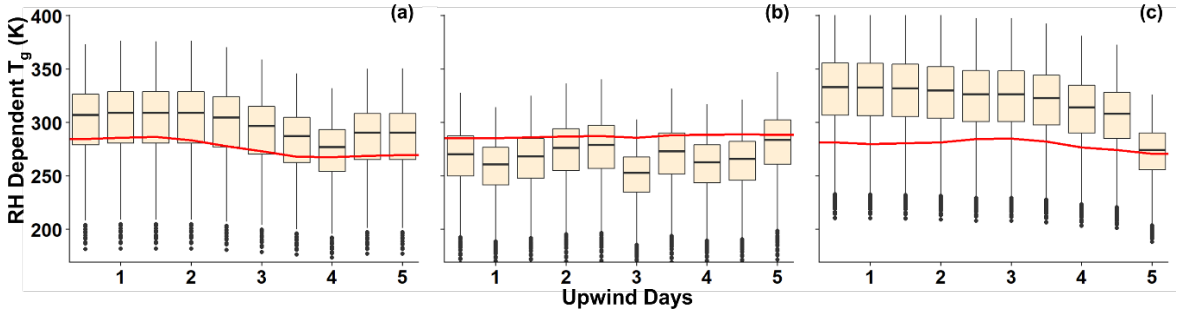

Figure S18. Relative humidity dependent T_g distribution box plots with ± 21 K uncertainty (DeRieux et al., 2018) applied. Panels (a), (b), and (c) show the distributions for PMO-1, PMO-2, and PMO-3, respectively. Three distributions were calculated for each sample, one with 21 K added to the dry T_g, one with 21 K subtracted from the dry T_g, and one with the original T_g values. The three data sets were combined here. The inclusion of the ± 21 K uncertainty does not significantly impact the range of observations. The centerline of the boxplot represents the median, the top and bottom of the "box" represent the third and first quartile respectively. The "whiskers" represent Q3 + 1.5* interquartile range (IQR, Q3-Q1) (maximum) and Q1 – 1.5*(IQR) (minimum).

Minor comments

1. In line 20, "This suggests that biomass burning emissions injected into the free troposphere are longer-lived than emissions in the boundary layer." The term "longer lived" is vaguely used here, as well as in a couple places in the main text. Do the authors mean the particles from biomass burning have lower oxidation state, or the authors are referring to the chemical life time of the compounds from biomass burning that were transported in the free troposphere?

The intent was to indicate that aerosol in the free troposphere appear to be more resistant to removal, due in part to the ambient conditions. In this case, we specifically contrast this finding to previously reported lifetimes of biomass burning brown carbon species, which were predicted to have a lifetime of ~1 day within the boundary layer (Forrister et al., 2016; Laing et al., 2016). To clarify, we changed "long lived" to "persistent", everywhere as appropriate in the manuscript.

2. In Section 3.1, chloride is presented in Table 1 but not discussed in the main text. Some studies show that biomass burning can produce chlorine-containing particles [3][4].

We thank the reviewer for this interesting observation. To reflect this, we added the following to Section 3.1 (lines 250-251) of the paper: **"Chloride was also present in PMO-1 and PMO-3, which has been shown in some studies to be a minor product of biomass burning, depending on the fuel burned (Levin et al., 2010; Liu et al., 2017)."**

3. In Figure 1 (c), the air mass spent a couple of days over Europe, and based on (f), the height of the air mass was quite low during those days. Could there be any influence from emissions from Europe on the sample?

We thank the reviewer for this comment. First, the altitude profile plots were inadvertently misplaced, so the altitude of the airmass over Europe was not as low as shown there. We corrected this as soon as we realized the mistake during the discussion. We also corrected the plot in the final manuscript and added additional retroplumes with 12 hour time differences. Looking at the correct plots, the altitude was still somewhat low and the RH increased indicating potential influence from Europe. However, the molecular species identified in PMO-3 were much more similar to the more strongly influenced biomass burning sample (PMO-1) than they were to the anthropogenic, albeit North American, influenced sample (PMO-2). There is the possibility of European influence roughly 5 days before reaching the PMO, shown by the spike in altitude and RH during that time period, but it does not seem to be a major component based on the chemical comparisons of the three samples. Additionally, the source apportionment modeling did not predict European influence for that sample.

4. In Section 3.2, regarding the CO source apportionment in Figure S1, what is the uncertainty associated with the CO modeling?

We add a few sentences in Section 2.4 (highlighted in bold below) to discuss the uncertainty and features associated with the FLEXPART CO simulations. We would like to point out that the FLEXPART CO tracer does not reproduce the actual CO concentration at the site because FLEXPART only simulates the transport of emissions but not the chemistry or deposition. FLEXPART CO was set to have a cutoff lifetime of 20 days in the model, but in reality, the CO lifetime varies from weeks to months depending on the location and atmospheric conditions. In this work, FLEXPART CO simulations were used as an indicator to show the relative contributions from anthropogenic and biomass burning emissions rather than an estimate of CO concentrations at Pico.

Manuscript excerpt (Lines 191-207):

"FLEXPART ~~**modeling**~~ was used to determine the sources, ages, and transport pathways of the aerosol samples collected at PMO. FLEXPART backward simulations (also called retroplumes) were driven by meteorology fields from the Global Forecast System (GFS) and its Final Analysis (FNL) with 3-hour

temporal resolution, 1° horizontal resolution, and 26 vertical levels. The output was saved in a grid with a horizontal resolution of 1° latitude by 1° longitude, and eleven vertical levels from the surface to 15,000 m a.s.l. **For each simulation, 80 thousand air parcels were released from the receptor and transported backwards for 20 days to calculate a source-receptor relationship (in units of s kg^{-1}, Seibert and Frank, 2004)**. FLEXPART retroplumes **~~(upwind distributions of residence time)~~** are **then** multiplied with CO emission inventories **(kg s^{-1})** from the Emissions Database for Global Atmospheric Research (EDGAR version 3.2 (Olivier and Berdowski, 2001)) and the Global Fire Assimilation System (Kaiser et al., 2012) to estimate the influence from anthropogenic and wildfire sources, respectively. **The FLEXPART CO tracer calculated with this approach indicates the relative contributions from anthropogenic and biomass burning emissions. Since CO chemistry and dry deposition are not considered in the FLEXPART setup, the absolute FLEXPART CO value does not reproduce the actual CO concentrations at Pico. FLEXPART does not consider the background CO accumulated in the atmosphere. The difference between FLEXPART CO and the actual CO largely depends on these factors. In previous applications of this approach, FLEXPART CO was able to estimate the episodes of CO enhancement due to transport of emissions (e.g., Brown et al., 2009; Stohl et al., 2007; Warneke et al., 2009).** This **~~modeling~~** approach has been used in several PMO studies **and successfully captured elevated CO periods** (e.g., Dzepina et al., 2015; Zhang et al., 2014, 2017) **and it is used here to assist in** the interpretation of the chemical composition in this work"

5. In Section 3.3, line 285-287, 78% of the formulas in PMO-2 are found to be common with sample from the boundary layer aerosol, and PMO-3 has similarity of 76%. Are 78% and 76% significantly different? This piece of information might not be a strong evidence to support the conclusion that PMO-2 was largely influenced by North America outflow transported within the boundary layer while PMO-3 was not.

As mentioned in the manuscript, there are many species (especially CHO molecular formulas) that are present in all samples. In addition, PMO-3 does not have a large number of unique species relative to PMO-1 or PMO-2. This is largely due to the sampled air as shown in the retroplume being somewhat more diffuse with a less certain path of transport and also origin, than either PMO-1 or PMO-2. Despite the large percentage of common species between PMO-3 and the boundary layer sample from Storm Peak Laboratory (SPL), PMO-3 had much more in common with a previous free troposphere wildfire sample (91%) (September 24, 2012, Dzepina et al., 2015). This suggests PMO-3 is more similar to PMO-1 than PMO-2, but there is the potential for a non-negligible influence from the European boundary layer. The point of the percentages, was to show that PMO-1 and PMO-3 have more in common with free tropospheric wildfire aerosol, than they do with the continental boundary layer aerosol of somewhat mixed sources (SPL aerosol).

To clarify, we revised the text (lines 313 – 318): **"In fact, when we compared the molecular formula composition of the free tropospheric aerosol sample "9/24" from the study by Dzepina et al. (2015) to the free tropospheric samples in this study (PMO-1 and PMO-3), we observed that 86% and 91% of the formulas are common. FLEXPART simulations from both studies suggested these samples were all affected by wildfire emissions, contributing to their similarity. In contrast, only 75% of the formulas found in the boundary layer sample (PMO-2) were common with those in Dzepina et al. (2015). These comparisons are provided in Table S2."**

6. In Figure 2, an obvious difference of the three spectra is the much higher fraction of high molecular weight materials in PMO-2. Little is discussed about the sources of the high molecular weight compounds in the text. Are they from oligomerization? In contrast, Lee et al. [5] observed abundant high molecular weight compounds from biomass burning in Canada using an aerosol mass spectrometer.

Considering the percentage of species with a mass greater than 350, PMO-2 actually has the smallest percentage of its total formulas in that range both by number of formulas and percentage of total abundance. PMO-1 has 70% of its formulas above 350 and PMO-3 has 71% of it formulas in that range, and PMO-2 has 64% of the formulas in this range. In terms of percentage of total abundance, they make up 63% of PMO-1, 59% of PMO-2, and 65% of PMO-3. These numbers are admittedly similar, but PMO-1 and PMO-3 are more similar and are both somewhat higher than PMO-2. These results may support the observations made in Lee et al. (2016) regarding high molecular weight compounds from biomass burning in Canada.

The main reason why those species (m/z > 350) stand out so much is due to their normalized relative abundance, where each measured intensity was normalized by the total ion intensity of the assigned molecular formulas in each sample. The implications of this increased O/C and subsequently, oxidation is the major focus of this paper and is discussed several times. The tall peaks that really stand out (norm. RA > 0.1) only make up 136 of 1349 masses above m/z 350 in PMO-2. Additionally, while analyzing the samples, we investigated the potential of SOA type oligomerization, and were unable to find any clear evidence, and thus did not include it in this manuscript. Also, interestingly, the fire studied by Lee et al. (2016) is likely the same fire that impacted the air mass that intercepted PMO on June 27-28, 2013 (PMO-1), so the relative increase in higher molecular mass compounds is consistent between the two studies.

7. In section 3.5, line 387, "Volatility can also play a role in the phase state". This expression is vague. Do the authors mean phase state depends on volatility? Or they both relate to structures of molecules in particles? Please make clarification.

The sentence was replaced with the following (Lines 424-426): **"In general, lower volatility typically inversely correlates with T_g (Shiraiwa et al., 2017) and viscosity. As such it was important to estimate the volatility of the PMO aerosol."**

8. In section 3.5, line 392, "This highlights the correlation between O/C and volatility, where volatility is expected to decrease as O/C increases." What about fragmentation?

Fragmentation can definitely contribute to both a decrease in O/C and an increase in volatility which requires other chemical changes in the compounds, namely a decrease in mass. The general mass ranges for all three samples is consistent and so fragmentation is unlikely to be the source of lower O/C in PMO-1 or PMO-3. Fragmentation may have occurred in PMO-2, helping to contribute to the increased O/C value observed, but it does not change the observation that the predicted volatility for the high abundance species in PMO-2 was lower than for the high abundance species in PMO-1 or PMO-3, or that the high abundance species in PMO-2 were also those with elevated O/C. Furthermore, the estimation of volatility includes a term regarding the carbon and oxygen interactions (Donahue et al., 2011; Li et al., 2016) indicating a relationship between O/C and volatility. Also, studies have shown a relationship between O/C and volatility before (Ng et al., 2011).

To address this, the following has been added (Lines 429-432):
"This highlights the relationship between O/C and volatility, where volatility is expected to decrease as O/C increases when the mass range is constant (Ng et al., 2011); the relationship between oxygen and carbon and its effect on volatility is used by both Donahue et al. (2011) and (Li et al., 2016) to estimate volatility. Similarly, lower volatility is expected to lead to lower diffusivity in aerosol even at elevated RH as demonstrated by Ye et al. (2016)."

9. Lastly, how generalizable are these findings in the paper in terms of predicting the oxidation state of aerosols having different transport pathways?

We thank the reviewer for this interesting question. The idea of phase state having an impact is likely fairly generalizable because it has been shown in several studies to have an impact on the rate of chemical reaction in aerosol samples (Koop et al., 2011; Berkemeier et al., 2014; Lignell et al., 2014; Shrivastava et al., 2017; Zelenyuk et al., 2017). Thus, it is fair to say that aerosol traveling high in the atmosphere, effectively since emission, can be anticipated to have a relatively low oxidation state. However, more samples are needed to be studied using multiple ionization modes to get a more complete analysis of what is present in these samples.

Regarding this question we added the following to the manuscript (lines 512-514):

"More work is needed to better constrain the molecular composition of long range transported aerosol and the processes that affect it during transport. The presented results have broader implications for the aging of long range transported biomass burning organic aerosol rapidly convected to the free troposphere."

References

[1] Frances H Marshall, Rachael EH Miles, Young-Chul Song, Peter B Ohm, Rory M Power, Jonathan P Reid, and Cari S Dutcher. Diffusion and reactivity in ultraviscous aerosol and the correlation with particle viscosity. Chemical Science, 7(2):1298–1308, 2016.
[2] Lindsay Renbaum-Wolff, James W Grayson, Adam P Bateman, Mikinori Kuwata, Mathieu Sellier, Benjamin J Murray, John E Shilling, Scot T Martin, and Allan K Bertram. Viscosity of alpha-pinene secondary organic material and implications for particle growth and reactivity. Proc Natl Acad Sci U S A, 110(20):8014–9, May 2013.
[3] EJT Levin, GR McMeeking, CM Carrico, LE Mack, SM Kreidenweis, CE Wold, H Moosmuller, WP Arnott, WM Hao, JL Collett, et al. Biomass burning smoke aerosol properties measured during fire laboratory at missoula experiments (FLAME). Journal of Geophysical Research: Atmospheres, 115(D18), 2010.
[4] Xiaoxi Liu, L Gregory Huey, Robert J Yokelson, Vanessa Selimovic, Isobel J Simpson, Markus Muller, Jose L Jimenez, Pedro Campuzano-Jost, Andreas J Beyersdorf, Donald R Blake, et al. Airborne measurements of western US wildfire emissions: Comparison with prescribed burning and air quality implications. Journal of Geophysical Research: Atmospheres, 122(11):6108–6129, 2017.
[5] Alex KY Lee, Megan D Willis, Robert M Healy, Jon M Wang, Cheol-Heon Jeong, John C Wenger, Greg J Evans, and Jonathan PD Abbatt. Single-particle characterization of biomass burning organic aerosol (BBOA): evidence for non-uniform mixing of high molecular weight organics and potassium. Atmospheric Chemistry and Physics, 16(9):5561–5572, 2016.

Additional References

Aiken, A. C., DeCarlo, P. F., Kroll, J. H., Worsnop, D. R., Huffman, J. A., Docherty, K. S., Ulbrich, I. M., Mohr, C., Kimmel, J. R., Sueper, D., Sun, Y., Zhang, Q., Trimborn, A., Northway, M., Ziemann, P. J., Canagaratna, M. R., Onasch, T. B., Alfarra, M. R., Prevot, A. S. H., Dommen, J., Duplissy, Metzger, A., Baltensperger, U., and Jimenez J. L.: O/C and OM/OC Ratios of Primary, Secondary, and Ambient Organic Aerosols with High-Resolution Time-of-Flight Aerosol Mass Spectrometry, Environ. Sci. Technol., 42(12), 4478–4485, doi:10.1021/es703009q, 2008.

Berkemeier, T., Shiraiwa, M., Pöschl, U. and Koop, T.: Competition between water uptake and ice nucleation by glassy organic aerosol particles, Atmos. Chem. Phys., 14(22), 12513–12531, doi:10.5194/acp-14-12513-2014, 2014.

Bougiatioti, A., Stavroulas, I., Kostenidou, E., Zarmpas, P., Theodosi, C., Kouvarakis, G., Canonaco, F., Prevot, A. S. H., Nenes, A., Pandis, S. N. and Mihalopoulos, N.: Processing of biomass-burning aerosol in the eastern Mediterranean during summertime, Atmos. Chem. Phys., 14(9), 4793–4807, doi:10.5194/acp-14-4793-2014, 2014.

Cech, N. B. and Enke, C. G.: Practical implications of some recent studies in electrospray ionization fundamentals, Mass Spec. Rev., 20(6), 362–387, doi:10.1002/mas.10008, 2001.

China, S., Scarnato, B., Owen, R. C., Zhang, B., Ampadu, M. T., Kumar, S., Dzepina, K., Dziobak, M. P., Fialho, P., Perlinger, J. A., Hueber, J., Helmig, D., Mazzoleni, L.R. and Mazzoleni, C.: Morphology and mixing state of aged soot particles at a remote marine free troposphere site: Implications for optical properties, Geophys. Res. Lett., 42(4), 1243–1250, doi:10.1002/2014gl062404, 2015.

China, S., Alpert, P. A., Zhang, B., Schum, S., Dzepina, K., Wright, K., Owen, R. C., Fialho, P. Mazzoleni, L.R., Mazzoleni, C., and Knopf, D. A.: Ice cloud formation potential by free tropospheric particles from long- range transport over the Northern Atlantic Ocean, J. Geophys. Res-Atmos., 122(5), 3065–3079, doi:10.1002/2016jd025817, 2017.

DeRieux, W.-S. W., Li, Y., Lin, P., Laskin, J., Laskin, A., Bertram, A. K., Nizkorodov, S. A. and Shiraiwa, M.: Predicting the glass transition temperature and viscosity of secondary organic material using molecular composition, Atmos. Chem. Phys., 18(9), 6331–6351, doi:10.5194/acp-18-6331-2018, 2018.

Donahue, N., Epstein, S., Pandis, S. and Robinson, A.: A two-dimensional volatility basis set: 1. organic-aerosol mixing thermodynamics, Atmos. Chem. Phys., 11(7), 3303–3318, doi:10.5194/acp-11-3303-2011, 2011.

Dzepina, K., Mazzoleni, C., Fialho, P., China, S., Zhang, B., Owen, R. C., Helmig, D., Hueber, J., Kumar, S., Perlinger, J. A., Kramer, L. J., Dziobak, M. P., Ampadu, M. T., Olsen, S., Wuebbles, D. J., and Mazzoleni, L. R.: Molecular characterization of free tropospheric aerosol collected at the Pico Mountain Observatory: a case study with a long-range transported biomass burning plume, Atmos. Chem. Phys., 15(9), 5047–5068, doi:10.5194/acp-15-5047-2015, 2015.

El-Zanan, H. S., Lowenthal, D. H., Zielinska, B., Chow, J. C. and Kumar, N.: Determination of the organic aerosol mass to organic carbon ratio in IMPROVE samples, Chemosphere, 60(4), 485–496, doi:10.1016/j.chemosphere.2005.01.005, 2005.

Forrister, H., Liu, J., Scheuer, E., Dibb, J., Ziemba, L., Thornhill, K. L., Anderson, B., Diskin, G., Perring, A. E., Schwarz, J. P., Campuzano- Jost, P., Day, D. A., Palm, B. B., Jimenez, J. L., Nenes, A. and Weber, R. J.: Evolution of brown carbon in wildfire plumes, Geophys. Res. Lett., 42(11), 4623–4630, doi:10.1002/2015gl063897, 2015.

Kaiser, J. W., Heil, A., Andreae, M. O., Benedetti, A., Chubarova, N., Jones, L., Morcrette, J.-J., Razinger, M., Schultz, M. G., Suttie M., and van der Werf, G. R.: Biomass burning emissions estimated with a global fire assimilation system based on observed fire radiative power, Biogeosciences, 9(1), 527–554, doi:10.5194/bg-9-527-2012, 2012.

Koop, T., Bookhold, J., Shiraiwa, M. and Pöschl, U.: Glass transition and phase state of organic compounds: dependency on molecular properties and implications for secondary organic aerosols in the atmosphere, Phys. Chem. Chem. Phys., 13(43), 19238–19255, doi:10.1039/c1cp22617g, 2011.

Laing, J. R., Jaffe, D. A., and Hee, J. R.: Physical and optical properties of aged biomass burning aerosol from wildfires in Siberia and the Western USA at the Mt. Bachelor Observatory, Atmos. Chem. Phys., 16(23), 15185–15197, doi:10.5194/acp-16-15185-2016, 2016.

LeClair, J. P., Collett, J. L. and Mazzoleni, L. R.: Fragmentation Analysis of Water-Soluble Atmospheric Organic Matter Using Ultrahigh-Resolution FT-ICR Mass Spectrometry, Environ. Sci. Technol., 46(8), 4312–4322, doi:10.1021/es203509b, 2012.

Li, Y., Pöschl, U. and Shiraiwa, M.: Molecular corridors and parameterizations of volatility in the chemical evolution of organic aerosols, Atmos. Chem. Phys., 16(5), 3327–3344, doi:10.5194/acp-16-3327-2016, 2016.

Lignell, H., Hinks, M. and Nizkorodov, S.: Exploring matrix effects on photochemistry of organic aerosols, P. Natl. Acad. Sci., 111(38), 13780–13785, doi:10.1073/pnas.1322106111, 2014.

Ng, N. L., Canagaratna, M. R., Jimenez, J. L., Chhabra, P. S., Seinfeld, J. H. and Worsnop, D. R.: Changes in organic aerosol composition with aging inferred from aerosol mass spectra, Atmos. Chem. Phys., 11(13), 6465–6474, doi:10.5194/acp-11-6465-2011, 2011.

Olivier, J.G.J. and Berdowski, J.J.M.: Global emissions sources and sinks, in: The Climate System, Berdowski, J., Guicherit, R. and Heij, B.J., A.A. Balkema Publishers/Swets & Zeitlinger Publishers, Lisse, The Netherlands. 33-78, 2001.

Reid, J. P., Bertram, A. K., Topping, D. O., Laskin, A., Martin, S. T., Petters, M. D., Pope, F. D. and Rovelli, G.: The viscosity of atmospherically relevant organic particles, Nat. Commun., 9(1), 956, doi:10.1038/s41467-018-03027-z, 2018.

Seibert, P. and Frank, A.: Source-receptor matrix calculation with a Lagrangian particle dispersion model in backward mode, Atmos. Chem. Phys., 4, 51-63, https://doi.org/10.5194/acp-4-51-2004, 2004.

Shiraiwa, M., Li, Y., Tsimpidi, A., Karydis, V., Berkemeier, T., Pandis, S., Lelieveld, J., Koop, T. and Pöschl, U.: Global distribution of particle phase state in atmospheric secondary organic aerosols, Nat. Commun., 8, ncomms15002, doi:10.1038/ncomms15002, 2017.

Shrivastava, M., Lou, S., Zelenyuk, A., Easter, R., Corley, R., Thrall, B., Rasch, P., Fast, J., Simonich, S., Shen, H. and Tao, S.: Global long-range transport and lung cancer risk from polycyclic aromatic hydrocarbons shielded by coatings of organic aerosol, P. Natl. Acad. Sci., 114(6), 1246–1251, doi:10.1073/pnas.1618475114, 2017.

Stohl, A., Forster, C., Frank, A., Seibert, P. and Wotawa, G.: Technical note: The Lagrangian particle dispersion model FLEXPART version 6.2, Atmos. Chem. Phys., 5(9), 2461–2474, doi:10.5194/acp-5-2461-2005, 2005.

Ye, Q., Robinson, E. S., Ding, X., Ye, P., Sullivan, R. C. and Donahue, N. M.: Mixing of secondary organic aerosols versus relative humidity, P. Natl. Acad. Sci., 113(45), 12649–12654, doi:10.1073/pnas.1604536113, 2016.

Zelenyuk, A., Imre, D. G., Wilson, J., Bell, D. M., Suski, K. J., Shrivastava, M., Beránek, J., Alexander, M. L., Kramer, A. L. and Massey-Simonich, S. L.: The effect of gas-phase polycyclic aromatic hydrocarbons on the formation and properties of biogenic secondary organic aerosol particles, Faraday Discuss., 200, 143–164, doi:10.1039/c7fd00032d, 2017.

Zhang, B., Owen, R., Perlinger, J., Kumar, A., Wu, S., Martin, M., Kramer, L., Helmig, D. and Honrath, R.: A semi-Lagrangian view of ozone production tendency in North American outflow in the summers of 2009 and 2010, Atmos. Chem. Phys., 14(5), 2267–2287, doi:10.5194/acp-14-2267-2014, 2014.

Zhang, B., Owen, R. C., Perlinger, J. A., Helmig, D., Val Martín, M., Kramer, L., Mazzoleni, L. R. and Mazzoleni, C.: Ten-year chemical signatures associated with long-range transport observed in the free troposphere over the central North Atlantic, Elem. Sci. Anth., 5, doi:10.1525/elementa.194, 2017.

Molecular and physical characteristics of aerosol at a remote marine free troposphere site: Implications for atmospheric aging

Simeon K. Schum[1], Bo Zhang[2,a], Katja Dzepina[1,b], Paulo Fialho[3], Claudio Mazzoleni[2,4] and Lynn R. Mazzoleni[1,2]

[1]Department of Chemistry, Michigan Technological University, Houghton, MI, USA
[2]Atmospheric Sciences Program, Michigan Technological University, Houghton, MI, USA
[3]Institute for Volcanology and Risk Assessment – IVAR, University of the Azores, Angra do Heroísmo, Portugal
[4]Department of Physics, Michigan Technological University, Houghton, MI, USA
[a]now at the National Institute of Aerospace, Hampton, VA, USA
[b]now at the Department of Biotechnology, University of Rijeka, Croatia

Correspondence to: Lynn R. Mazzoleni (lrmazzol@mtu.edu)

Abstract. Aerosol properties are transformed by atmospheric processes during long-range transport and play a key role in the Earth's radiative balance. To understand the molecular and physical characteristics of free tropospheric aerosol, we studied samples collected at the Pico Mountain Observatory in the North Atlantic. The observatory is located in the marine free troposphere at 2225 m above sea level, on Pico Island in the Azores archipelago. The site is ideal for the study of long-range transported free tropospheric aerosol with minimal local influence. Three aerosol samples with elevated organic carbon concentrations were selected for detailed analysis. FLEXPART retroplumes indicated that two of the samples were influenced by North American wildfire emissions transported in the free troposphere and one by North American outflow mainly transported within the marine boundary layer. To determine the detailed molecular composition of the samples, we used ultrahigh resolution Fourier transform ion cyclotron resonance mass spectrometry. Thousands of molecular formulas were assigned to each of the individual samples. On average ~60 % of the molecular formulas contained only carbon, hydrogen, and oxygen atoms (CHO), ~30 % contained nitrogen (CHNO), and ~10 % contained sulfur (CHOS). The molecular formula compositions of the two wildfire influenced aerosol samples transported mainly in the free troposphere had relatively low average O/C ratios (0.48 ± 0.13 and 0.45 ± 0.11) despite the 7 - 10 days of transport time according to FLEXPART. In contrast, the molecular composition of North American outflow transported mainly in the boundary layer had a higher average O/C ratio (0.57 ± 0.17) with 3 days of transport time. Thus, aerosol oxidation appears to be related to environmental factors during transport and not simply aging time. We used meteorological conditions extracted from the Global Forecast System analysis for model grids along the FLEXPART simulated transport pathways and the observed molecular chemistry to predict the relative humidity dependent glass transition temperatures (T_g) of the aerosol components. Comparisons of the T_g to the ambient temperature, indicated that a majority of the organic aerosol components transported in the free troposphere were more viscous and therefore less oxidized than the organic aerosol components transported in the boundary layer. This suggests that biomass burning organic aerosol injected into the free troposphere are more persistent than those in the boundary layer having broader implications for aerosol aging.

1 Introduction

Atmospheric organic aerosol composition and mass concentrations are transformed by atmospheric processes including oxidization (Dunlea et al., 2009; Jimenez et al., 2009; Kroll et al., 2011), cloud processing (Ervens et al., 2007, 2011; Zhao et al., 2013), and wet or dry deposition (Pöschl, 2005). Oxidation of organic aerosol impacts its lifetime, cloud droplet and ice nucleation (Massoli et al., 2010; Lambe et al., 2011; China et al., 2017), aerosol morphology, and optical properties (Pöschl,

Formatted: Level 1
Deleted: Science
Formatted: Level 1
Formatted: Level 1
Deleted: composition
Deleted: 46
Deleted: 12
Deleted: 47
Deleted: 15
Deleted: However
Deleted: the
Deleted: 55
Deleted: 19
Deleted: Meteorological
Deleted: GFS
Deleted: were used
Deleted: phase state
Deleted: samples, indicating
Deleted: was
Deleted: likely to be solid
Deleted: emissions
Deleted: longer-lived
Deleted: emissions
Deleted: aerosol
Deleted: and aerosol-cloud interactions, including

2005; China et al., 2015; Laskin et al., 2015 and references therein). As such, the chemistry of atmospheric aerosol oxidation has received much attention (George and Abbatt, 2010; Lee et al., 2011; Kroll et al., 2011). Jimenez et al. (2009) studied the oxidation of anthropogenic organic aerosol emitted from Mexico City as it was transported downwind. They used an aerosol mass spectrometer (AMS) instrument on board an aircraft to measure the magnitude of the *m/z* 44 fragment as a proxy for the oxidation of organic aerosol. After 6 hours and 63 km of transport, a noticeable increase in the overall chemical oxidation was observed. Rapid oxidation was also observed using an AMS in studies of biomass burning organic aerosol in Africa (Capes et al., 2008; Vakkari et al., 2014) and over the Mediterranean Sea (Bougiatioti et al., 2014). These analyses found that most of the marker species for biomass burning were oxidized within 24 hours (Vakkari et al., 2014) suggesting that after 24 hours, organic aerosol is nearly indistinguishable regardless of source. Except for the study by Capes et al. (2008) the aerosol in these studies was generally collected relatively close (up to 30 hours, but mostly < 10 hours downwind) to the emission sources. These studies all show the importance of oxidation to the aging of organic aerosol and provide motivation for studies of long-range transported organic aerosol.

A study of predominately Asian anthropogenic aerosol transported in the free troposphere over the Pacific Ocean found that the oxidation, inferred by the average oxygen to carbon ratio (O/C), continued to increase over the course of roughly a week (Dunlea et al., 2009). In a study of biomass burning aerosol transported in the free troposphere across the North Atlantic Ocean, Dzepina et al. (2015) observed a relatively low O/C ratio (0.46 ± 0.13), considering the aerosol transport time of more than 10 days (Aiken et al., 2008). Dzepina et al. (2015) hypothesized that cloud processing and other oxidative processes led to the formation and subsequent removal of oxidized species, leaving behind the more persistent aerosol species. Other recent studies of long-range transported brown carbon (BrC) from biomass burning in the boundary layer found that the aging of aerosol led to a near complete depletion of BrC within 24 hours (Forrister et al., 2015; Laing et al., 2016). The remaining BrC was found to lead to a 6 % increase of BrC over background levels and may represent the ubiquitous BrC present in the atmosphere far from the source (Forrister et al., 2015). This leftover BrC aerosol could impact large areas globally because much of it is located within the free troposphere and above clouds, due to the typically elevated injection heights of aerosol over wildfires (Val Martin et al., 2008a). These studies indicate that free tropospheric aerosol chemistry is particularly important because this aerosol can have a longer atmospheric lifetime than boundary layer aerosol (Laing et al., 2016) allowing it to be transported over greater distances.

Studies of transported biomass burning aerosol are typically performed using instrumentation either onboard aircrafts (Capes et al., 2008) or located at low altitude (Bougiatioti et al., 2014; Vakkari et al., 2014) and continental mountain (Laing et al., 2016) sites. Aircraft measurements have the advantage of sampling aerosol over wide spatial and altitudinal ranges, but they are limited to short time periods, typically of a few days to a week (Capes et al., 2008; Dunlea et al., 2009). Ground sites are less constricted by time, but because of the high injection heights of wildfires, biomass burning aerosol are often above the boundary layer (Val Martin et al., 2008a). Thus, low altitude sites are less often affected by pyro-convective wildfire plumes. Continental mountain sites typically have seasonally limited access to the free troposphere, because high summer temperatures can lead to planetary boundary layer influence through convection (Collaud Coen et al., 2011). Thus, many of the continental mountain sites have long-term access to the free troposphere in the winter, but not in the summer when most wildfire activity occurs. The Pico Mountain Observatory (PMO, see the Supplement for additional information), is located 2225 m above sea level (a.s.l) on the caldera summit of Pico Mountain, on Pico Island in the Azores archipelago in the North Atlantic. The marine boundary layer in the region has been measured and estimated to range from 500 to 2000 m a.s.l in the summer months (Kleissl et al., 2007; Remillard et al., 2012; Zhang et al., 2017), well below the observatory. This permits access to free tropospheric

Moved (insertion) [1]
Deleted: Changes in
Moved up [1]: Jimenez et al.
Deleted: was studied by
Deleted: (2009).
Deleted: in an AMS
Deleted: had been
Deleted:),
Deleted: (<
Deleted: downwind,
Deleted: the oxidation of
Deleted: The authors
Deleted: long-lived
Deleted: Recent
Deleted: Most studies
Deleted:),
Deleted: sites
Deleted:), or at
Deleted: sites
Deleted:).
Deleted: these
Deleted: within
Deleted:
Deleted: PMO
Deleted: allows

long-range transported aerosol during the wildfire season. This, in conjunction with negligible local emission sources, makes PMO an ideal site for the study of long-range transported free tropospheric aerosol.

As described by Zhang et al. (2017), the Azores-Bermuda anticyclone causes persistent downward mixing from the upper free troposphere and lower stratosphere, and is the dominant meteorological pattern in this region, and strengthens in the summer. The FLEXible PARTicle dispersion model (FLEXPART) retroplumes discussed in Zhang et al. (2017) show that this site is most commonly impacted by North American outflow (30-40%). In the summer months (June – August), 15% of the intercepted air masses have North American anthropogenic influence, and 7.3% have wildfire influence (Zhang et al., 2017). These factors make PMO an excellent site for the study of North American outflow (Val Martin et al., 2008a). In many of the previous studies at PMO, investigators focused on the North American outflows of NO_x, NO_y, CH_4, non-methane hydrocarbons, and O_3 gases (Val Martin et al., 2006; Pfister et al., 2006; Val Martin et al., 2008a; Val Martin et al., 2008b; Helmig et al., 2015) and the physical characteristics of black carbon and mineral dust aerosol and their ice nucleation activity (Fialho et al., 2005; China et al., 2015; China et al., 2017). So far, only Dzepina et al. (2015) has previously looked at the aerosol chemical and molecular characteristics of the organic aerosol collected at the site.

Recent environmental and laboratory studies have shown that under low temperature and low relative humidity (conditions common in the free troposphere), aerosol can be in a solid glassy phase (Zobrist et al., 2008; Virtanen et al., 2010). This observation has been hypothesized to lead to longer atmospheric lifetimes for organic species that are otherwise susceptible to degradation through oxidative processes. As an example, polycyclic aromatic hydrocarbons (PAH) such as benzo[a]pyrene were observed to have a much higher ambient concentration than what could be explained by model simulations without considering the aerosol phase state (Shrivastava et al., 2017). Recently, PAH have been shown to enhance the formation of a viscous phase state in laboratory generated secondary organic aerosol (SOA) (Zelenyuk et al., 2017). Since PAH are common products of biomass burning and anthropogenic emissions, the viscosity could be enhanced in ambient samples as well, leading to a greater likelihood of the occurrence of solid phase aerosol. The solid phase can increase the resistance of aerosol to photodegradation (Lignell et al., 2014; Hinks et al., 2015) and water diffusivity (Berkemeier et al., 2014), which may lead to lower rates of oxidation. Shiraiwa and colleagues developed a set of equations to predict the dry glass transition temperature based on the mass and O/C ratio of organic aerosol components (Shiraiwa et al., 2017; DeRieux et al., 2018). Thus, the phase state of molecular species with respect to ambient conditions can be predicted using the Gordon-Taylor equation (Shiraiwa et al., 2017; DeRieux et al., 2018). Additionally, estimation methods to determine the volatility of organic aerosol were reported by Donahue et al. (2011) and Li et al. (2016). Both the phase state and volatility are potentially important in understanding the processes that affect aerosol during transport and aging. The low oxidation observed by Dzepina et al. (2015) was attributed to the dominance of persistent aerosol that resisted removal mechanisms, however it is possible that the phase state of the aerosol during transport played a significant role. The increased resistance to photodegradation (Lignell et al., 2014; Hinks et al., 2015) and water diffusivity (Berkemeier et al., 2014) of solid phase organic aerosol provide a basis for this hypothesis.

Ultrahigh resolution mass spectrometry (MS) is a necessary tool for determining the molecular characteristics of complex mixtures such as organic aerosol. It has been used to analyze dissolved organic matter (Kido-Soule et al., 2010; Herzsprung et al., 2014), cloud water (Zhao et al., 2013), fog water (Mazzoleni et al., 2010), sea spray (Schmitt-Kopplin et al., 2012), and organic aerosol (Walser et al., 2007; Mazzoleni et al., 2012; O'Brien et al., 2013; Wozniak et al., 2014; Dzepina et al., 2015). Ultrahigh resolution MS techniques are typically paired with electrospray ionization (ESI) because it is a soft ionization technique with little to no fragmentation of the molecular species being analyzed. Negative mode ESI is sensitive to molecules with acidic functional groups, which is ideal for the analysis of long-range transported organic aerosol due to its generally

Deleted: In
Deleted: this
Deleted: The
Deleted: , causing
Deleted: (Zhang et al., 2017).
Deleted: the
Deleted: bulk
Deleted: characterization
Deleted: this enhancement of
Deleted: present
Deleted: .
Deleted: 2017
Deleted: 2017
Deleted: to understand
Deleted: long-lived
Deleted: the
Deleted: such as carboxylic acids in organic species

acidic nature (Bougiatioti et al., 2016). The ultrahigh mass resolution available from Fourier transform ion cyclotron resonance mass spectrometry (FT-ICR MS) and the high field Orbitrap Elite MS instruments (R = 240,000) separates sulfur containing species from carbon, hydrogen, and oxygen containing species (Schmitt-Kopplin et al., 2010), which is important because sulfur containing species are common in atmospheric aerosol (Schmitt-Kopplin et al., 2010; Mazzoleni et al., 2012; Dzepina et al., 2015).

The observations of Dzepina et al. (2015) raised interesting questions regarding the nature of long-range transported free tropospheric aerosol. To further elucidate the detailed molecular characteristics of free tropospheric aerosol, we analyzed three pollution events using ultrahigh resolution FT-ICR MS. We observed key molecular differences in the oxidation related to the transport pathways and their apparent emission sources. In this paper, we present the detailed molecular characteristics of organic aerosol collected at PMO and use the aerosol chemical composition, FLEXPART model simulations, and physical property estimates to interpret those characteristics and infer implications for long-range transported organic aerosol.

2 Methods

2.1 Sample collection

$PM_{2.5}$ samples were collected at PMO on 8.5 x 10 in. quartz fiber filter using high volume air samplers (EcoTech HiVol 3000, Warren, RI, USA) operated at an average volumetric flow rate of 84 $m^3 hr^{-1}$ for 24 h. Prior to sampling, the filters were wrapped in clean, heavy-duty aluminum foil and baked at 500 ^{0}C for ~ 8 hours to remove organic artifacts associated with the filters. Afterward, they were placed in antistatic sealable bags until deployment. We deployed four air samplers at the site, each was set up with a filter simultaneously and programmed to start one day after another, allowing for continuous sample collection for up to four consecutive days. This procedure was used to maximize the number of filters collected. Daily visits and maintenance were prohibited by the time consuming and strenuous hike necessary to reach the site. The sampled filters were removed and returned to the same aluminum wrapper and bag. The samples were then brought down the mountain and stored in a freezer until cold transport back to Michigan Tech where they were stored in a freezer until analysis. Three samples, collected in consecutive years at PMO, on 27-28 June 2013, 5-6 July 2014, and 20-21 June 2015 were analyzed in this study. The sampling time for all samples was 24 hours; on 27-28 June the sampling began at 19:00, on 5-6 July and on 20-21 June the sampling began at 15:00, all local times.

2.2 Chemical analyses

Organic carbon and elemental carbon (OC/EC) measurements were performed using an OC/EC analyzer (Model 4, Sunset Laboratory Inc. Tigard, OR, USA) following the NIOSH protocol. Major anions and cations were analyzed using ion chromatography. Anion analysis was performed using a Dionex ICS-2100 instrument (Thermo Scientific) with an AS-17-C analytical and guard column set (Thermo Scientific) using a KOH generator for gradient elution. Cation analysis was performed using a Dionex ICS-1100 instrument with CS-12A analytical and guard column set (Thermo Scientific) and an isocratic 20 mM methanesulfonic acid eluent. The instruments were operated in parallel using split flow from the autosampler. Additional details can be found in the Supplement.

2.3 Ultrahigh resolution FT-ICR mass spectrometry analysis

The samples for FT-ICR-MS analysis were selected based on the organic carbon concentration. Selected samples typically had more than 1000 µg of organic carbon per quartz filter. Sample preparation was described in detail in previous studies from our group (Mazzoleni et al., 2010, 2012; Zhao et al., 2013; Dzepina et al., 2015). Briefly, one quarter of the quartz filter was cut into strips, placed in a pre-washed and baked 40 mL glass vial, and then extracted using ultrasonic agitation in Optima LC/MS

Deleted: .
Deleted: is used to separate
Deleted: from comparisons of the detailed molecular composition of the pollution events
Deleted: modeling
Formatted: Level 1
Deleted: then
Deleted:
Deleted: , for
Deleted: for
Deleted: ,
Deleted: for
Deleted: local
Formatted: Level 1
Deleted: about the analytical and instrumental methods
Formatted: Level 1
Deleted: quarter of the
Deleted: fiber
Deleted: this

grade deionized water (Fisher Scientific, Waltham, MA, USA) for 30 minutes. The extract was then filtered using a pre-baked quartz filter syringe to remove undissolved material and quartz filter fragments. The sample filter was then sonicated again in 10 mL of Optima LC/MS grade deionized water for 30 minutes, filtered, and then added to the original 30 mL of filtrate, yielding a total of 40 mL. Ice packs were used during the sonication to ensure the water temperature stayed below 25 °C. The water-soluble organic carbon (WSOC) compounds were then isolated using Strata-X (Phenomenex, Torrance, CA, USA) reversed phase solid phase extraction (SPE) cartridges to remove inorganic salts that can adduct with organic compounds during electrospray ionization. During the reversed phase SPE, losses of highly water soluble, low molecular weight (MW) and hydrophobic, high MW organic compounds are expected. Thus, the resulting WSOC is the SPE-recovered fraction. The cartridges were pre-conditioned with acetonitrile and LC/MS grade water before the 40 mL filtrate was applied to the cartridges at a rate of ~ 1 mL/min. The cartridges were eluted with 2 mL of an aqueous acetonitrile solution (90/10 acetonitrile/water by volume) and stored in the freezer until analysis. The procedural loss of ionic low MW compounds such as oxalate can lead to an underprediction of the organic aerosol O/C and overprediction of the average glass transition temperatures (T_g). To investigate this, we used the concentrations of the prominent organic anions measured with ion chromatography to estimate the abundance of these compound relative to the compounds detected by FT-ICR MS. The low MW corrected average O/C values correlated with the trends of the original O/C values, however the significance of impacts varies with the measured analyte concentrations and the assumptions associated with the uncertain mass fraction of the molecular formula composition (Table SM4). When low MW organic anions were included in the estimated average dry T_g values, they dropped by ≤ 2.5 %, which was deemed relatively insignificant (Table SM5).

Ultrahigh resolution mass spectrometric analysis was done using FT-ICR MS with ESI at the Woods Hole Oceanographic Institution (Thermo Scientific LTQ Ultra). The samples were analyzed using direct infusion ESI in the negative ion mode. Negative polarity is effective for the deprotonation of polar organic molecules (Mazzoleni et al., 2010), which are expected to dominate the organic aerosol mass fraction and were the focus of this study. The spray voltage ranged from 3.15 to 3.40 kV depending on the ionization stability with a sample flow rate of 4 to 5 µL/min. We used a scan range of *m/z* 100 – 1000 with a mass resolving power of 400,000 (defined at *m/z* 400) for all samples. The samples were run in duplicate and 200 transient scans were collected. The transients were co-added for each replicate run using the Midas Co-Add tool and molecular formula assignments were made using Composer software (Sierra Analytics), as described in previous studies (Mazzoleni et al., 2012; Dzepina et al., 2015). The resulting molecular formula assignments underwent additional quality assurance (QA) data filtering to remove chemically unreasonable formulas with respect to O/C, hydrogen to carbon ratio (H/C), double bond equivalent (DBE), and absolute PPM error as described in the Supplemental Information of Putman et al. (2012). Molecular formulas in common with the instrument blanks with signal intensity ratios < 3 were removed; meanwhile analytes in common with the field blanks with signal intensity ratios < 3 were flagged. Specifically, two formulas ($C_{17}H_{34}O_4$ and $C_{19}H_{38}O_4$) observed in PMO-1 could not be classified as pertaining only to the field blank and so they were not removed. Further discussion about the blank subtraction is provided in the Supplement. To produce the final data set for each sample, the replicates were aligned and only the molecular formulas found in both replicates after QA were retained.

2.4 FLEXPART numerical simulations

FLEXPART was used to determine the sources, ages, and transport pathways of the aerosol samples collected at PMO. FLEXPART backward simulations (also called retroplumes) were driven by meteorology fields from the Global Forecast System (GFS) and its Final Analysis with 3-hour temporal resolution, 1° horizontal resolution, and 26 vertical levels. The output was saved in a grid with a horizontal resolution of 1° latitude by 1° longitude, and eleven vertical levels from the surface to 15,000 m a.s.l. For each simulation, 80 thousand air parcels were released from the receptor and transported backwards for

Deleted: re-

Deleted: , for

Deleted:

Deleted: all

Deleted: of

Deleted: were put through

Deleted: roughly

Deleted: compounds retained by the cartridge

Deleted: off

Deleted: done

Deleted: make sure the formula assignments were

Deleted: reasonable

Formatted: Level 1

Deleted: FLEXPART modeling was used to determine the sources, ages, and transport pathways of the aerosol samples collected at PMO. FLEXPART backward simulation (also called retroplumes) was driven by meteorology fields from the Global Forecast System (GFS) and its Final Analysis (FNL) with 3-hour temporal resolution, 1° horizontal resolution, and 26 vertical levels. The output was saved in a grid with a horizontal resolution of 1° latitude by 1° longitude, and eleven vertical levels from the surface to 15,000 m a.s.l. FLEXPART retroplumes (upwind distributions of residence time) are multiplied with CO emission inventories from the Emissions Database for Global Atmospheric Research (EDGAR version 3.2 (Olivier and Berdowski, 2001)) and the Global Fire Assimilation System (Kaiser et al., 2012) to estimate the influence from anthropogenic and wildfire sources, respectively. This modeling approach has been used in several PMO studies (e.g., Dzepina et al., 2015; Zhang et al., 2014, 2017). It is an overall powerful tool for the interpretation of the chemical composition in this work. ¶
¶
It

20 days to calculate a source-receptor relationship (in units of s kg^{-1}, Seibert and Frank, 2004). FLEXPART retroplumes were then multiplied with CO emission inventories (kg s^{-1}) from the Emissions Database for Global Atmospheric Research (EDGAR version 3.2 (Olivier and Berdowski, 2001)) and the Global Fire Assimilation System (Kaiser et al., 2012) to estimate the influence from anthropogenic and wildfire sources, respectively. The FLEXPART CO tracer calculated with this approach indicates the relative contributions from anthropogenic and biomass burning emissions. Since CO chemistry and dry deposition are not considered in the FLEXPART setup, the absolute FLEXPART CO value does not reproduce the actual CO concentrations at Pico. FLEXPART does not consider the background CO accumulated in the atmosphere. The difference between FLEXPART CO and the actual CO largely depends on these factors. In previous applications of this approach, FLEXPART CO was able to estimate the episodes of CO enhancement due to transport of emissions (e.g., Brown et al., 2009; Stohl et al., 2007; Warneke et al., 2009). This approach has been used in several PMO studies and successfully captured elevated CO periods (e.g., Dzepina et al., 2015; Zhang et al., 2014; 2017) and it is used here to assist in the interpretation of the chemical composition in this work.

In addition to the typical FLEXPART simulations done for the site (e.g., retroplume, CO source apportionment), we extracted the ambient temperature and relative humidity (RH) from the GFS analysis data for model grids along the FLEXPART simulated transport pathways. These parameters were then used to estimate the glass transition temperatures (T_g) of the organic aerosol components during transport, based on its molecular composition from ultrahigh resolution MS, using estimation methods recently developed by Shiraiwa et al. (2017) and extended to higher masses by DeRieux et al. (2018). DeRieux et al. (2018) reported an uncertainty of ± 21 K for the prediction of any single compound, but the uncertainty is expected to decrease when a mixture of compounds is considered. Nonetheless, we assumed an uncertainty range of ± 21 K on T_g and found that it did not significantly change the T_g trends presented in Section 3.5. Further discussion the uncertainty on T_g is provided in the Supplement. The distributions of the estimated organic aerosol component T_g values provides new insight for the interpretation of long-range transported aerosol.

3 Results and discussion

3.1 Overview of the aerosol chemistry: OC/EC and IC

In this study, we present the detailed composition of three individual samples collected for 24 hours on 27-28 June 2013, 5-6 July 2014, and 20-21 June 2015 at the PMO. These samples, referred to as PMO-1, PMO-2 and PMO-3 hereafter, were selected after analysis of organic and elemental carbon (OC/EC) were performed for all 127 aerosol samples collected in this study. The three selected samples all had elevated organic carbon (OC) concentrations (Table 1) representing the capture of a pollution plume. After blank subtraction, the median OC of the samples collected over the summers of 2013-2015 was 0.16 ± 0.018 µg/m^3. The minimum OC level measured was below the average blank concentration and the maximum was 2.07 ± 0.017 µg/m^3 (PMO-1). The most abundant anions and cations in these samples are also shown in Table 1. The presence of these ions is consistent with the results of other studies (Yu et al., 2005; Aggarwal and Kawamura, 2009). Further discussion of the bulk chemical trends will be presented in a future manuscript.

The concentrations of common anions and cations can offer important insight regarding cloud processing and emission sources (Table 1). Specifically, the elevated level of sulfate observed in the PMO-2 sample can be an indicator of anthropogenic influence, cloud processing, or marine influence (Yu et al., 2005). We also observed elevated oxalate concentrations in PMO-1 and PMO-2. Oxalate is known to co-vary with sulfate concentrations in the atmosphere when they are formed by aerosol-cloud processing (Yu et al., 2005; Sorooshian et al., 2007). Thus, the oxalate to sulfate ratio can be an indication of cloud processing (Sorooshian et al., 2007); in general, a higher ratio is the result of increased cloud processing. As described in

Deleted: modeling
Deleted: Global Forecast System (
Deleted:)
Deleted: predict
Deleted: phase state
Deleted: and
Deleted: .,
Deleted: 2017).
Deleted: phase state determination method
Deleted: information
Deleted: the results that we discuss in Sect. 3.5
Formatted: Level 1
Deleted:
Deleted:
Deleted: composition and
Deleted: for all the study samples
Deleted: of the collected aerosol samples
Deleted:
Deleted:
Deleted:
Deleted:) and

Sorooshian et al. (2007), the oxalate concentrations increase with cloud processing because there is more time for it to be produced, leading to an increased ratio. PMO-1 had the highest oxalate to sulfate ratio (0.278), followed by PMO-3 (0.124), and PMO-2 (0.084). The observed oxalate to sulfate ratios for these samples are all much higher than what was reported in Sorooshian et al. (2007) suggesting other factors may have impacted the ion concentrations. Specifically, an enrichment of oxalate from biomass combustion plumes (Cao et al., 2017) likely contributed to the observed concentrations of these ions in PMO-1 and PMO-3. The bulk concentration of oxalate in PMO-2 is similar to PMO-1, but the sulfate in PMO-2 is much higher, leading to a low oxalate to sulfate ratio. Based on FLEXPART simulations it is likely that PMO-2 underwent aqueous phase processing (see Sect. 3.5), but the high concentration of sulfate from possible anthropogenic and marine sources appears to have obscured the oxalate-sulfate relationship (Yu et al., 2005; Sorooshian et al., 2007).

Despite inconsistencies in the replicate potassium measurements for PMO-1, elevated potassium levels were observed, indicating contributions from biomass combustion (Duan et al., 2004). PMO-3 had slightly elevated potassium relative to PMO-2, but not as high as PMO-1. Chloride was also present in PMO-1 and PMO-3, which has been shown in some studies to be a minor product of biomass burning, depending on the fuel burned (Levin et al., 2010; Liu et al., 2017).

The nitrate levels in PMO-2 were significantly lower than what was observed in PMO-1 and PMO-3, which is consistent with the observation that the marine boundary layer promotes the rapid removal of HNO_3 (Val Martin et al., 2008b). This is also consistent with removal due to cloud scavenging (Dunlea et al., 2009). The elevated nitrate in PMO-1 and PMO-3 is consistent with the observation of elevated NO_y and NO_x in the plumes of wildfire emissions made in previous studies at PMO (Val Martin et al., 2008a) and a lack of recent cloud scavenging (Dunlea et al., 2009).

Despite the low altitude transport, the major ion concentrations in PMO-2 do not strongly support a major influence from marine sources (Quinn et al., 2015; Kirpes et al., 2017). However, the increased concentration of methane sulfonic acid (MSA) in PMO-2 relative to PMO-1 and PMO-3 suggests some degree of marine influence. To estimate this, we used the non-background subtracted sodium concentration as an upper limit to estimate sea salt sulfate according the method described in Chow et al. (2015), this led to a maximum sea salt sulfate contribution of 25 %. The influence of marine sources supports boundary layer transport. However, the results indicate that marine aerosol is not likely a major component of PMO-2, perhaps because the rate of PMO-2 transport was very fast.

3.2 FLEXPART retroplume simulation results

Representative FLEXPART retroplumes for the three samples are shown in Fig. 1, additional time periods are in the Supplement (Figs. S1-S3). PMO-1 was largely influenced by North American outflow transported relatively high in the free troposphere. Based on the FLEXPART carbon monoxide (CO) modeling (Fig. S4), PMO-1 was impacted by wildfire emissions from Canada. The transport time for PMO-1 air masses from North America to PMO was about 7 days. The free tropospheric transport is likely due to the high injection heights (Val Martin et al., 2008a; 2010) of organic aerosol from wildfire events in northwestern Quebec (See Fig. S4, S5). Similar events at PMO have been identified previously by (Val Martin et al., 2006; 2008a). The air masses intercepted during PMO-3 were North American outflows that traveled in the lower free troposphere across the Northern Atlantic Ocean to Western Europe before circling back to PMO. The transport time for the PMO-3 air masses from North America to PMO was roughly 10 days. After a northward transport to Western Europe in the jet stream during the first 4-5 days, the simulated plume turned to the south and west, arriving at PMO from Europe in about 2-4 days. This air mass was most likely influenced by wildfire emissions in western and central Canada (U.S. Air Quality, Smog Blog. alg.umbc.edu). Similar to PMO-1, FLEXPART CO source apportionment (Fig. S4) suggests this sample was influenced by

Deleted: increased

Deleted: impact

Deleted: concentration of these ions

Deleted: Generally, increased cloud processing is expected to lead to increased oxidation of atmospheric organic species (

Moved down [2]: Ervens et al.,

Deleted: 2008; Zhao et al., 2013), but has also been hypothesized that cloud scavenging of oxidized components could lead to lower overall oxidation by leaving behind reduced aerosol (Dzepina et al., 2015).

Deleted: baseline levels

Deleted: appear

Deleted: in PMO-1.

Deleted: .

Deleted: .

Deleted:)

Deleted: of 25 % of the total sulfate classified as

Deleted: .

Formatted: Level 1

Deleted: The

Deleted: 1.

Deleted: Carbon Monoxide

Deleted: S1

Deleted: likely

Deleted: mass

Deleted: S1, S2

Deleted: S2

Deleted: most

fire, although considering the OC concentration and transport time, it was much more diluted than what was observed in PMO-1. In contrast, the PMO-2 air masses traveled relatively low (≤ 2 km) over the "Rust Belt" (Illinois, Indiana, Michigan, Ohio, Pennsylvania, and New York) of the United States and stayed at approximately the same altitude until it reached the observatory 2-4 days later. This transport pattern suggests that the aerosol was predominantly transported in the boundary layer on its way to the PMO and was primarily influenced by a mixture of continental U.S. anthropogenic and biogenic emissions. This was supported by the FLEXPART CO simulations as well (Fig. S4). The height of the boundary layer over the continent generally ranges from 500-2500 m and is strongly affected by diurnal cycles, seasonal effects, and topography (Liu and Liang, 2010); overall, the continental boundary layer height generally increasing during the day and during the summer months. This suggests that PMO-2 was within the boundary layer over the United States.

3.3 Molecular formula oxidation metrics: O/C and OS_C

In this section, we describe the detailed molecular formula composition of the three individual samples PMO-1, PMO-2, and PMO-3. Overall, nearly 80% of the observed mass spectral peaks in the ultrahigh resolution mass spectra were assigned molecular formulas, which is comparable to previous studies (Zhao et al., 2013; Dzepina et al., 2015). After removing the duplicate molecular formulas containing ^{13}C or ^{34}S, a total of 3168 (PMO-1), 2121 (PMO-2), and 1820 (PMO-3) monoisotopic molecular formulas remained. Groups of molecular formulas were assigned based on their elemental composition $C_cH_hN_nO_oS_s$, including: carbon, hydrogen, and oxygen (CHO); carbon, hydrogen, nitrogen, and oxygen (CHNO); and carbon, hydrogen, oxygen, and sulfur (CHOS). The most frequently observed compositions were CHO and CHNO. The reconstructed negative ion mass spectra of the monoisotopic molecular formulas for each of the samples are provided in Fig. 2. Visual comparisons of the mass spectra indicate that PMO-2, which was likely transported through the North American continental and North Atlantic marine boundary layer, has a prevalence of higher O/C ratio formulas compared to the two samples transported through the free troposphere. Considering the ion distribution and normalized relative abundances, PMO-1 and PMO-3 mass spectra look quite similar with a high frequency of individual O/C values < 0.5. This may suggest similar emission sources or aerosol processing. In contrast, PMO-2 has a stronger relative influence of molecular compositions with higher O/C ratios. The O/C histogram plots in Fig. 2 provide additional evidence for the O/C differences between the two types of samples (free troposphere and boundary layer) due to the difference in the O/C distribution.

Although North American outflow of anthropogenic secondary organic aerosol is expected to have a higher O/C value compared to the wildfire emissions of biomass burning organic aerosol (e.g., Aiken et al., 2008; Jimenez et al., 2009; Bougiatioti et al., 2014), we expected that the samples with longer transport times (PMO-1 and PMO-3) would be more oxidized than PMO-2 which had a shorter transport time. However, this expectation was based on results from aging studies of secondary organic aerosol (Volkamer et al., 2006; Jimenez et al., 2009) and continental boundary layer anthropogenic aerosol (Mazzoleni et al., 2012; Huang et al., 2014). The lower oxidation observed in the samples transported for 7+ days is consistent with our previous study at this site by Dzepina et al. (2015). In fact, when we compared the molecular formula composition of the free tropospheric aerosol sample "9/24" from the study by Dzepina et al. (2015) to the free tropospheric samples in this study (PMO-1 and PMO-3), we observed that 86% and 91% of the formulas are common. FLEXPART simulations from both studies suggested these samples were all affected by wildfire emissions, contributing to their similarity. In contrast, only 75% of the formulas found in the boundary layer sample (PMO-2) were common with those in Dzepina et al. (2015). These comparisons are provided in Table S2.

As observed in the mass spectra and histograms presented in Fig. 2, the samples have noticeable differences in the distribution of O/C values. This is also reflected in the abundance weighted mean O/C values for the samples: 0.48 ± 0.13 (PMO-1), 0.57

Deleted: is likely

Deleted: PMO

Deleted: through

Deleted: predicted emission source is

Deleted: modeling

Deleted: S2

Deleted:), which

Deleted: as well

Formatted: Level 1

Deleted: characterization

Deleted:

Deleted: Visual comparison of the mass spectra indicates that PMO-2, which was transported through the

Deleted: continental and North Atlantic marine boundary layer, has

Deleted: prevalence of

Deleted: ratio formulas

Deleted: two samples transported through the free troposphere. It is

Deleted: a sample with

Deleted: (PMO-2).

Deleted: is

Deleted: a longer time

Deleted: the

Deleted: .,

Deleted: -

Deleted: works suggest

Deleted: A comparison with continental boundary layer aerosol (Mazzoleni et al., 2012) finds the opposite trend, with 78% of the formulas in PMO-2 found to be common with the Mazzoleni et al. (2012) study, compared to 62% of PMO-1 formulas and 76% of PMO-3 formulas. These comparisons can be seen

Deleted: 47

Deleted: 15

Deleted: 55

± 0.17 (PMO-2), and 0.45 ± 0.11 (PMO-3). Note that these O/C values are averages of thousands of individual measurements, as such the standard deviation represents the range of values and not uncertainties (see Figs. S7-S8 for violin plots of the distributions). We note that the relative abundance of compounds in ESI mass spectra is not directly proportional to their solution concentration, other factors including surface activity and polarity impact the ionization efficiency (Cech & Enke, 2001). Nonetheless, the abundance does differentiate trends between the samples and the assigned molecular formulas represent a collection of multifunctional isomers (e.g., LeClair et al., 2012). For completeness, both the abundance weighted average values for various metrics of aerosol oxidation and saturation (Table 2) and the unweighted average values (Table S3) are reported. Additional O/C distribution insight was derived from separating the species into CHO, CHNO, CHOS elemental groups. For example, the comparison of the species with CHO formulas in each sample indicates a smaller relative difference between PMO-2 aerosol compared to PMO-1 and PMO-3, with the PMO-2 aerosol having a higher average O/C value (0.55 ± 0.17 (PMO-2) compared to 0.47 ± 0.14 (PMO-1) and 0.44 ± 0.14 (PMO-3)). Meanwhile 85 - 98% of the CHO species in each sample are present in at least one other sample, with 848 (42 - 78%) of the formulas being found in all three samples, as shown in Fig. S9. This suggests that the CHO composition may be fairly uniform throughout the atmosphere, without a significant abundance of clear marker species after long-range transport, regardless of the source region and transport time. This observation is consistent with other studies which have observed the decay of marker species after ~ 24 hours (Bougiatioti et al., 2014; Forrister et al., 2015).

In contrast, the CHNO molecular formulas demonstrate stronger differences that correlate with the overall O/C ratio. The average O/C value for the CHNO formulas in PMO-2 was 0.59 ± 0.14 compared to 0.49 ± 0.15 in PMO-1 and 0.49 ± 0.14 PMO-3 (Table 2). Differences in the elemental ratios are often visualized using the van Krevelen plot, which shows the correlation of H/C *vs.* O/C. The van Krevelen plots for the three samples with the unique CHNO formulas present in each sample are shown in Fig. 3. Most of the unique CHNO species in PMO-2 (68%) fall in the more oxidized region of the plot (Tu et al., 2016) with high overall O/C values. This differs from the PMO-1 unique species that are predominantly on the less oxidized, low O/C side of the plot, or the oxidized aromatic region. Another observation from the CHNO species is more identified species in both PMO-1 (1120) and PMO-3 (608) than in PMO-2 (561), despite the higher total number of molecular species in PMO-2 compared to PMO-3. This is potentially due to the enrichment of NO_x and NO_y species as previously observed in wildfire pollution events (Val Martin et al., 2008a), which may in turn lead to an increased nitrogen content in the organic aerosol species. The nitrogen containing species show a distinct difference in terms of the total oxidation between the two sets of samples, more so than the CHO compounds. This implies that much of the distinction between different aerosol sources may come from heteroatom containing species.

The difference in O/C is even more evident in the sulfur containing formulas (CHOS). The PMO-2 CHOS species have a much higher average O/C ratio (0.74 ± 0.34) than what is observed in PMO-1 (0.48 ± 0.14). Consistent with the CHNO formulas, the PMO-2 unique CHOS formulas (55% of unique formulas) are present in the oxidized region of the plot, whereas those in PMO-1 are nearly completely in the less oxidized region of the van Krevelen plot (Fig. S10). The Kendrick plot (Fig. S10c) also demonstrates a clear difference between the two samples. Most of the unique CHOS compounds in PMO-2 are located on the lower mass, higher defect side of the plot, while the PMO-1 formulas are on the higher mass, lower defect side. This difference is due to the larger amount of oxygen present in the PMO-2 formulas, which would lead to a greater mass defect than the more reduced CHOS formulas present in PMO-1. Higher oxygen content of PMO-2 aerosol is supported by its higher O/C ratio when compared to PMO-1 as shown in box plots (Fig. S10d). Very few CHOS molecular formulas (N = 29) were identified in PMO-3 and most of them (N = 26 of 29 total) were also present in PMO-1. Due to the small number of identified CHOS formulas in this sample, we did not consider it in the comparison between CHOS formulas in the samples. The overall

Deleted: 19
Deleted: 46
Deleted: 12
Deleted: Table S3 and Figs. S3-4 for standard errors and violin plots of the distributions). Additional
Deleted: slightly
Deleted: 51
Deleted: 18
Deleted: 46
Deleted: 16
Deleted: 45
Deleted: 13
Deleted: The smaller difference in O/C is likely reflective of the observation that
Deleted: S5
Deleted: formulas
Deleted: an
Deleted: may also support those made in
Deleted: report
Deleted: about
Deleted:), because the CHO formulas are often the most abundant group of species and easiest to detect.
Deleted: clear
Deleted: 58
Deleted: 15
Deleted: 48
Deleted: 12
Deleted: plot
Deleted: is
Deleted: , and at
Deleted:
Deleted: oxidation
Deleted: 67
Deleted: 26
Deleted: 50
Deleted: are strongly present
Deleted: is
Deleted: S6
Deleted: S6c
Deleted: S6d) This is supported by the box plots showing the O/C values for each sample, where PMO-2 has a higher O/C than PMO-1.
Deleted: do

differences that are observed in the O/C ratios between the boundary layer transported aerosol (PMO-2) compared to the free troposphere transported aerosol (PMO-1 and PMO-3) highlight the differences in the aging and lifetime of aerosol relative to its transport pathway.

Another commonly used metric of aerosol oxidation is the average oxidation state of carbon (OS_C) described by Kroll et al. (2011). The average OS_C includes both hydrogen and oxygen for the average oxidation of carbon in each molecular formula Additionally, we assumed all nitrogen and sulfur were present as nitrate and sulfate functional groups and calculated the OS_C with the appropriate corrections (Equation S1). The average OS_C values (Table 2) for the three samples show again that PMO-2 is more oxidized than the other two samples. The average OS_C values for the CHO formulas in PMO-1 and PMO-2 are very similar (Table 2), but as shown in the histograms in Fig. 4, their relative abundance distributions are quite different. The OS_C *vs.* carbon number plots in Fig. 4 show slight differences between PMO-1 and PMO-2, mostly in the distribution of the sulfur containing formulas. However, the similarity of the PMO-1 and PMO-3 samples and their difference from the PMO-2 sample is quite clear in the visual comparisons of the histograms of the OS_C values with their normalized relative abundances. The observation of an overall lower oxidation in PMO-1 and PMO-3 may support the findings of Aiken et al. (2008) and Bougiatioti et al. (2014) who reported that biomass burning aerosol are less oxidized than other types of aerosol, even after some aging. Conversely, the overall higher oxidation of PMO-2 implies that the sampled aerosol was likely more hygroscopic, included better cloud condensation nuclei (Massoli et al., 2010), and had less volatile components (Ng et al., 2011) than PMO-1 and PMO-3.

3.4 Molecular formula aromaticity and brown carbon

The aromaticity of the samples is also different between the two groups of aerosol. Based on the aromaticity index (AI, Eq. S2; AI_{mod}, Eq. S3; Koch and Dittmar, 2006; 2016), the free tropospheric aerosol samples (PMO-1 and PMO-3) are more aromatic than the convected boundary layer aerosol (PMO-2, Fig. 5). The presence of more aromatic species in the long-range transported wildfire-influenced aerosol may lead to increased light absorption (Bao et al., 2017) or resistance to oxidation (Perraudin et al., 2006). Aromatic species can also be associated with the presence of brown carbon (BrC; Desyaterik et al., 2013). Aromaticity is heavily dependent on the H/C ratio and the DBE (Eq. S4), where low H/C and high DBE indicate aromatic structure. Histograms depicting the distribution of H/C and DBE values for the three samples are shown in Fig. S11. As observed previously, PMO-1 and PMO-3 are more similar to each other than compared to PMO-2. Likewise, PMO-1 and PMO-3 exhibit an increase in the number frequency of higher DBE species, which is not observed in PMO-2, supporting the observation of an increased overall aromaticity for these free tropospheric aerosol. Many aromatic compounds, such as PAH are known to be carcinogens, and are a product of incomplete combustion biomass burning and anthropogenic emissions (Perraudin et al., 2006; Bignal et al., 2008).

Generally, BrC is considered to be aromatic or olefinic in nature (Bao et al., 2017). In our observations, the two samples influenced by wildfire show the greatest amount of olefinic and aromatic species, which is likely associated with the presence of BrC compounds. Additional evidence for the presence of BrC in PMO-1 comes from aethalometer measurements using the 7 wavelength aethalometer (Magee Scientific Company, Berkeley, California, USA) located at the site, which detected a wavelength-dependent peak with an Ångström coefficient of 1.3 during the sampling period. Ångström coefficients above 1 suggest the presence of BrC or iron oxides. Based on the retroplume analysis and comparison to similar samples (Dzepina et al., 2015), the detected peak is most likely the result of BrC. Figure S12 contains the aethalometer observations for this event. Difficulties with the instrument prevented similar data from being collected for PMO-3, although based on the retroplumes, ambient conditions, and molecular characteristics similar results seem likely. In addition to the aethalometer response, PMO-

Deleted: OS_C

Deleted: OS_C considers the impact of

Deleted: (see

Deleted: in the Supplement).

Deleted: OS_C

Deleted: OS_C

Deleted: OS_C

Deleted: some

Deleted: ¶
¶
Many of the molecular formulas that show high oxidation ($OS_C > 0$) are present in more than one sample, but the relative abundance of these formulas is lower in the free tropospheric aerosol samples (PMO-1 and PMO-3) compared to the boundary layer (PMO-2) sample. As observed in the mass spectra in Fig. 2, the oxidized species had a higher abundance in PMO-2 than in the other two samples. To support this observation, Table S4 contains the average values of O/C, OS_C, and other characteristics weighted by the relative abundances for each sample. The O/C_w and

Moved down [3]: OS_{Cw}

Formatted: Font: 9 pt, Bold, Font color: Black

Deleted: values are increased relative to the unweighted averages in the aerosol transported in the boundary layer (PMO-2), while the aerosol transported in the free troposphere (PMO-1 and PMO-3) does not show much difference between weighted and unweighted averages. This suggests that the oxidized species may be more abundant and important to the overall chemical and physical characteristics of PMO-2 in the atmosphere and may imply higher ... [1]

Deleted: wildfire

Deleted: is

Deleted: aged

Formatted: Level 1

Deleted: ;

Deleted: ;

Deleted:) (

Deleted: wildfire

Deleted:) (

Deleted: demonstrative of

Deleted: large

Deleted: an

Deleted: S7

Deleted: for oxidation

Deleted: they are

Deleted: could potentially be

Deleted: very

Deleted: (*pers. comm.*, Paulo Fialho, 2017).

Deleted: S8

Deleted: though

Deleted: (*pers. comm.*, Paulo Fialho, 2017).

1 contained species that were related to BrC in studies by Iinuma et al. (2010) and Lin et al. (2016) (Table S4). This observation provides evidence for the persistence of BrC species, which is contrary to the observations by Forrister et al. (2015) who concluded that BrC is mostly removed within 24 hours. Additionally, the high concentration of OC for this sample makes it seem unlikely that we observed just a minor residual fraction. Perhaps, the lifetime of BrC is dependent on additional ambient conditions that influence aerosol oxidation and phase state.

3.5 Phase state, volatility, and cloud processing: Implications for the observed aerosol oxidation

Atmospheric aging processes are influenced by ambient conditions, such as temperature and water vapor, and the concentrations of reactive species. Recently, Shrivastava et al. (2017) reported observations of long-range transported PAH from Asia to North America and suggested an enhanced lifetime due to a probable glassy aerosol phase state during transport. Additionally, model simulations reported by Shiraiwa et al. (2017) indicated that model SOA is predicted to be semi-solid or glassy at altitudes above 2000 m in the northern hemisphere. Since the PMO aerosol was sampled at 2225 m above sea level, we examined the estimated glass transition temperature (T_g) of the studied WSOC species in addition to the markers of aqueous phase processing for the three PMO samples. Increased aerosol viscosity has been shown to decrease the rate of photodegradation (Lignell et al., 2014; Hinks et al., 2015) and water diffusivity (Berkemeier et al., 2014). Both photodegradation and water diffusion are expected to strongly affect the oxidation and aging of aerosol species during transport.

In general, lower volatility typically inversely correlates with T_g (Shiraiwa et al., 2017) and viscosity. As such it was important to estimate the volatility of the PMO aerosol. Using the parameters reported by Donahue et al. (2011) and Li et al. (2016), we estimated the volatility of the FT-ICR MS identified organic aerosol molecular compositions (Figs. S13 and S14, respectively). As expected based on the length of transport for the samples, the majority of formulas show extremely low volatility. Interestingly, PMO-2 has a larger number of higher abundance molecular formulas with extremely low volatility and elevated oxidation relative to PMO-1 and PMO-3 (Fig. 6). This highlights the relationship between O/C and volatility, where volatility is expected to decrease as O/C increases when the mass range is constant (Ng et al., 2011); the relationship between oxygen and carbon and its effect on volatility is used by both Donahue et al. (2011) and Li et al. (2016) to estimate volatility. Similarly, lower volatility is expected to lead to lower diffusivity in aerosol even at elevated RH as demonstrated by Ye et al. (2016).

As predicted in earlier studies (Shrivastava et al., 2017 and Shiraiwa et al., 2017), particles transported in the free troposphere are likely semi-solid to solid, where the actual particle viscosity depends on the ambient conditions and the composition of the particles. Thus, to better understand the potential phase state associated with the PMO organic aerosol, we first estimated the dry T_g for the identified CHO molecular formulas in each of the PMO aerosol using the estimation method by DeRieux et al. (2018; Eq. S5). We then converted the dry T_g to the RH dependent T_g (below). Currently T_g can only be estimated for CHO species, however the CHO species were the most frequently observed and constituted a major fraction of the total relative abundance in the PMO negative ion mass spectra. Assuming the identified CHO compositions are fairly representative of the total organic aerosol composition, a comparison of the T_g values to the ambient temperature (T_{amb}) provides an indication of the likely phase state of the organic aerosol particles. Generally, if T_g exceeds T_{amb}, a glassy solid state is predicted, likewise, if T_g is less than T_{amb} then either a semi-solid or liquid state is predicted depending on the ratio magnitude (Shiraiwa et al., 2017; DeRieux et al., 2018). Although the exact composition of the total organic aerosol is yet unknown, the identified water-soluble organic compounds provide a reasonable upper limit for the estimated T_g values. Under this assumption, the CHO molecular formulas in PMO-1 and PMO-3 had higher average dry T_g values than PMO-2 (Table S5, Fig. S16), which implies that they would be more viscous than PMO-2, given similar atmospheric conditions.

Deleted: may be
Deleted: long lived
Deleted: suggestion
Deleted: other factors related to
Deleted: , which we will discuss next
Formatted: Level 1
Deleted: Volatility, phase
Deleted: implications
Deleted: In a recent study
Deleted: for PAHs
Deleted: the
Deleted: The
Deleted: solid phase state
Deleted: Additionally, modeling results of
Deleted: . (
Deleted: showed that model SOA is predicted to be solid at altitudes above 2000 m in the northern hemisphere. Volatility can also play a role in
Deleted: phase state (Shiraiwa et al., 2017). Therefore, we used
Deleted:) to estimate
Deleted: sampled in our study
Deleted: S9
Deleted: S10
Deleted: when relative abundance was used to color a plot of OS_C *vs.* volatility calculated using the Li et al. (2016) method (Fig. 6), PMO-2 was observed to have more high abundance formulas of extremely low volatility and elevated oxidation relative to PMO-1 and PMO-3. This highlights the correlation between O/C and volatility, where volatility is expected to decrease as O/C increases. We estimated the phase state using the estimation method by DeRieux et al. (2017) for the PMO aerosol and considered it as a possible explanation for the lower than expected oxidation in PMO-1 and PMO-3. The organic aerosol phase state estimation method is based on the glass transition temperature determined from the molecular mass and the elemental O/C ratio along with the ambient temperature and relative humidity. Using the DeRieux et al. (2017) equation (Eq. S5), we found that the CHO molecular formulas in PMO-1 and PMO-3 typically had higher glass transition temperatures than PMO-2, which implies that they would be more solid than PMO-2, given similar atmospheric conditions. We note that although currently the glass transition temperatures can only be estimated for CHO species, the CHO species were the most frequently observed species and constituted the major fraction of the total relative abundance in the PMO samples. Thus, the results are likely to be reasonably representative of the overall aerosol mass and provide an otherwise unattainable estimate of aerosol phase state during transport.
Deleted: The aerosol phase state during transport was estimated using the Gordon-Taylor equation (Eqs. S6 - S7) with the calculated glass transition temperatures of the identified CHO molecular species and extracted ambient temperature and relative humidity from GFS analysis along the transport pathways using FLEXPART backward simulations. The number fraction of CHO molecular ... [2]

Water is known to be a strong plasticizer relative to typical aerosol species (Koop et al., 2011; Shiraiwa et al., 2017; Reid et al., 2018), thus it can decrease T_g and the overall aerosol viscosity. Therefore, it's important to consider the ambient relative humidity when estimating the T_g. Using the extracted ambient temperature and RH from the GFS along the FLEXPART retroplumes and the Gordon-Taylor equation (Eqs. S6 - S7), the calculated dry T_g were modified to RH-dependent T_g for the CHO molecular species. The distributions of the T_g values for the three PMO samples based on one standard deviation of the ambient conditions are shown as boxplots in Fig. 7. The range of ambient temperature and RH extracted from the GFS along the FLEXPART simulated path yields a wide range of T_g values (Figs. 7, S17). The estimates were taken back only 5 days due to the increasing range of possible meteorological conditions associated with the spread in the air masses as shown in Figs. 1 and S1-S3. Overall, the distributions of T_g values in PMO-1 and PMO-3 generally exceed the ambient temperature (Fig. 7), implying that particles containing a majority of these compounds would likely be solid. To account for the low molecular weight organic anions not observed in the FT-ICR mass spectra, their mass concentrations and T_g values (estimated using the Boyer-Kauzmann rule (Koop et al., 2011; Shiraiwa et al., 2017; DeRieux et al., 2018)) are also shown in Fig. 7. The three most prevalent low molecular weight organic acids indicate the potential impact of those compounds on the overall T_g value of a particle that contains them. Oxalic acid was estimated to have a similar T_g value to a majority of the higher MW species identified in PMO-2, but it is slightly lower than the majority of species in PMO-1 and PMO-3. However, the mass fraction of oxalate is 3 times lower in PMO-1 and PMO-3 (2.3 and 3.0 %) compared to PMO-2 (9.4 %).

The results suggest that aerosol in PMO-1 and PMO-3 was overall less susceptible to atmospheric oxidation due to the aerosol phase state during free tropospheric long-range transport than it may have been in the boundary layer with higher ambient RH and temperature. A more viscous state during transport may also explain the presence of persistent BrC species in PMO-1, where the BrC species are protected from oxidation similarly to the long-lived PAHs observed by Shrivastava et al. (2017). In contrast to the observations from PMO-1 and PMO-3, much of the PMO-2 T_g distribution falls below the ambient temperature indicating a semi-solid or liquid state during the final 5 days of transport. This indicates an increased susceptibility to oxidation processes in the atmosphere (Shiraiwa et al., 2011), such as aqueous phase processing. The possibility of aqueous phase processing is also supported by the extracted GFS RH in Fig. 7, which is above 50% for the last 5 days of PMO-2 transport. The potential for liquid/semi-solid aerosol in the boundary layer is consistent with other studies (Shiraiwa et al., 2017; Maclean et al., 2017) and is expected based on the increased RH in the boundary layer and the plasticizing effect of water. Although, we note the PMO-2 average dry T_g values were lower than those of PMO-1 and PMO-3. The estimates of dry T_g and RH-dependent T_g provide an otherwise unattainable upper limit estimate of the aerosol phase state of the sampled free tropospheric aerosol.

Cloud processing has been shown to increase the oxidation of atmospheric organic matter (e.g., Ervens et al., 2008; Zhao et al., 2013; Cook et al., 2017). Therefore, aqueous phase oxidation may have contributed to the higher oxidation observed in PMO-2 despite its more rapid transport from North America to the PMO. In fact, most of the unique species observed in PMO-2 are in the highly oxidized region of the van Krevelen plot (Fig. 8). Comparisons of the detailed molecular composition of the PMO samples with studies of cloud (Zhao et al., 2013; Cook et al., 2017) and fog (Mazzoleni et al., 2010) water organic matter indicates that the formulas uniquely common to only PMO-2 and the literature atmospheric water samples have higher O/C consistent with aqueous processing during transport. These results are provided in Fig. S19 and Table S6. Additionally, PMO-2 had a strongly elevated non-sea salt sulfate concentration relative to PMO-1 and PMO-3, which supports cloud processing. Oxalate, a marker of cloud processing (Yu et al., 2005; Sorooshian et al., 2007), was also elevated in PMO-2; the mass fraction of oxalate was 9.4 % in PMO-2 compared to 2.3 % and 3.0 % in PMO-1 and PMO-3. Furthermore, nitrate is

Deleted: retroplumes. Another representation of the phase state

Deleted: for the CHO molecular species is shown

Deleted: Fig. S12. In both figures,

Deleted: contain

Deleted: molecular formulas that are predicted to be solid during

Deleted: transport conditions

Deleted: GFS analysis. This suggests that a major reason for the low

Deleted: observed in PMO-1 and PMO-3 is related

Deleted: . Solid phase states during

Deleted: long-lived

Deleted:

Deleted: shows

Deleted: majority of the molecular species to be either

Deleted: modeled relative humidity

Deleted: in PMO-2

Deleted: possibly implying the presence

Deleted: liquid

Deleted: , which would likely contribute to aqueous phase processing

Formatted: Strikethrough

Deleted: was

Moved (insertion) [2]

Deleted: in

Deleted: . (

Deleted:) and so

Deleted: provide an explanation for

Deleted:

Deleted: Comparing

Deleted: cloud water

Deleted: reported in

Deleted: . (2013) to the

Deleted: observed species in each of the PMO samples in ... [3]

Deleted: cloud

Deleted: were highly oxidized (

Deleted: S13). Since, these highly oxidized species were not ... [4]

Deleted: also

Deleted: may indicate

Deleted: or perhaps marine aerosol contributions. In ... [5]

Deleted: strongly

Deleted: oxalate concentration was observed, especially ... [6]

Deleted: to the overall organic mass. The organic mass ... [7]

Deleted: estimated to be 2 times the OC concentration. In

Deleted: , 9.4 % of the organic mass was due to oxalate

Deleted: respectively. Oxalate is also a potential marker of ... [8]

known to be scavenged during cloud processing (Dunlea et al., 2009), leading to its decrease in recently cloud processed aerosol. The nitrate concentration in PMO-2 was very low compared to PMO-1 or PMO-3 (Table 1), supporting the idea of cloud scavenging in PMO-2. Overall, the molecular characteristics and major ion concentrations (Fig. S20) indicate that PMO-2 was likely affected by aqueous phase oxidation during transport.

4 Conclusions

Aerosol samples collected on 27-28 June 2013 (PMO-1), 5-6 July 2014 (PMO-2), and 20-21 June 2015 (PMO-3) at the Pico Mountain Observatory were analyzed using ultrahigh resolution FT-ICR mass spectrometry for molecular formula composition determination. FLEXPART retroplumes for the sampled air masses indicate that: (a) PMO-1 and PMO-3 aerosol were transported predominantly through the free troposphere and were influenced by wildfire emissions; and (b) PMO-2 aerosol were transported primarily through the boundary layer over the Northeast continental U.S. and the North Atlantic Ocean before being intercepted at the observatory. Although elevated levels of OC, sulfate, and oxalate were found in all three samples, PMO-2 had the overall highest mass fractions of oxalate and sulfate. The molecular formula assignments indicated differences in the aerosol oxidation between the free troposphere transported aerosol (PMO-1 and PMO-3) and the boundary layer transported aerosol (PMO-2). These observations suggest that the transport pathways, in addition to the emission sources, contribute to the observed differences in the organic aerosol oxidation. The ambient temperature and RH at upwind times were extracted from the GFS analysis in FLEXPART and were used to estimate the glass transition temperatures of the aerosol species during transport. The results suggest that the organic aerosol components extracted from PMO-1 and PMO-3 were considerably more viscous than those from PMO-2 and less susceptible to aqueous phase oxidation. The concept of increased viscosity leading to less oxidation of aerosol in the free troposphere is supported in the literature (e.g., Koop et al., 2011; Berkemeier et al., 2014; Lignell et al., 2014; Shiraiwa et al., 2017). This suggests that biomass burning emissions and BrC injected into the free troposphere are more resistant to removal than aerosol transported in the boundary layer, due largely to the ambient conditions in the free troposphere. More work is needed to better constrain the molecular composition of long-range transported aerosol and the processes that affect it during transport. The presented results have broader implications for the aging of long-range transported biomass burning organic aerosol rapidly convected to the free troposphere.

Data availability

The molecular formula composition for each sample in this study is available via Digital Commons at the following link: http://digitalcommons.mtu.edu/chemistry-fp/88/.

Acknowledgements

This project was supported with funding from NSF (AGS-1110059) and DOE (DE-SC0006941). Logistical support for the operation of the Pico Mountain Observatory was provided by the Regional Secretariat of the Environment and the Sea of the Portuguese Regional Government of the Azores. Major equipment cost share and graduate student support associated with this project was provided by the Earth, Planetary, and Space Science Institute at Michigan Technological University. We thank Mike Dziobak, Kendra Wright, Sumit Kumar, Andrea Baccarini, Stefano Viviani, Jacques Huber, and Detlev Helmig for assistance in the field. We thank Manabu Shiraiwa, Sarah Petters, and Marcus Petters for helpful discussion regarding aerosol phase state. Finally, we thank Melissa Soule and Elizabeth Kujawinski of the Woods Hole Oceanographic Institution (WHOI) Mass Spectrometry Facility for FT-ICR MS instrument time and assistance with data acquisition (NSF OCE-0619608 and Gordon and Betty Moore Foundation).

References

Deleted: in
Deleted: levels
Deleted: are
Deleted: S14
Formatted: Level 1
Deleted: ,
Deleted: ,
Deleted: was
Deleted: intercepting PMO
Deleted: PMO-1 and PMO-3 had elevated nitrate and PMO-1 had elevated potassium.
Deleted: marine
Formatted: Font: 12 pt, Bold
Deleted: indicate
Deleted: of aerosol
Deleted: relative humidity and
Deleted: data using
Deleted: phase state
Deleted: These
Deleted: suggested
Deleted: aerosols in
Deleted: mainly in the solid phase during transport. This would increase their resistance to oxidation and lead to a lower
Deleted: expected
Deleted: . This also
Deleted: longer-lived
Deleted: emissions
Deleted: . PMO-2 was estimated to be mainly semi-solid or liquid, suggesting an increased susceptibility to aqueous phase oxidation relative to PMO-1 and PMO-3, and offering an explanation
Deleted: observed increase in oxidation.
Formatted: Level 1
Formatted: Level 1
Formatted: Level 1

Aggarwal, S. G. and Kawamura, K.: Carbonaceous and inorganic composition in long-range transported aerosols over northern Japan: Implication for aging of water-soluble organic fraction, Atmos. Env., 43(16), 2532–2540, doi:10.1016/j.atmosenv.2009.02.032, 2009.

Aiken, A. C., DeCarlo, P. F., Kroll, J. H., Worsnop, D. R., Huffman, J. A., Docherty, K. S., Ulbrich, I. M., Mohr, C., Kimmel, J. R., Sueper, D., Sun, Y., Zhang, Q., Trimborn, A., Northway, M., Ziemann, P. J., Canagaratna, M. R., Onasch, T. B., Alfarra, M. R., Prevot, A. S. H., Dommen, J., Duplissy, Metzger, A., Baltensperger, U., and Jimenez J. L.: O/C and OM/OC Ratios of Primary, Secondary, and Ambient Organic Aerosols with High-Resolution Time-of-Flight Aerosol Mass Spectrometry, Environ. Sci. Technol., 42(12), 4478–4485, doi:10.1021/es703009q, 2008.

Bao, H., Niggemann, J., Luo, L., Dittmar, T. and Kao, S.: Aerosols as a source of dissolved black carbon to the ocean, Nat. Commun., 8(1), 510, doi:10.1038/s41467-017-00437-3, 2017.

Berkemeier, T., Shiraiwa, M., Pöschl, U. and Koop, T.: Competition between water uptake and ice nucleation by glassy organic aerosol particles, Atmos. Chem. Phys., 14(22), 12513–12531, doi:10.5194/acp-14-12513-2014, 2014.

Berkemeier, T., Steimer, S., Krieger, U., Peter, T., Pöschl, U., Ammann, M. and Shiraiwa, M.: Ozone uptake on glassy, semi-solid and liquid organic matter and the role of reactive oxygen intermediates in atmospheric aerosol chemistry, Phys. Chem. Chem. Phys., 18(18), 12662–12674, doi:10.1039/c6cp00634e, 2016.

Bignal, K. L., Langridge, S. and Zhou, J. L.: Release of polycyclic aromatic hydrocarbons, carbon monoxide and particulate matter from biomass combustion in a wood-fired boiler under varying boiler conditions, Atmos. Env., 42(39), 8863–8871, doi:10.1016/j.atmosenv.2008.09.013, 2008.

Bougiatioti, A., Stavroulas, I., Kostenidou, E., Zarmpas, P., Theodosi, C., Kouvarakis, G., Canonaco, F., Prevot, A. S. H., Nenes, A., Pandis, S. N. and Mihalopoulos, N.: Processing of biomass-burning aerosol in the eastern Mediterranean during summertime, Atmos. Chem. Phys., 14(9), 4793–4807, doi:10.5194/acp-14-4793-2014, 2014.

Bougiatioti, A., Nikolaou, P., Stavroulas, I., Kouvarakis, G., Weber, R., Nenes, A., Kanakidou, M. and Mihalopoulos, N.: Particle water and pH in the eastern Mediterranean: source variability and implications for nutrient availability, Atmos. Chem. Phys., 16(7), 4579–4591, doi:10.5194/acp-16-4579-2016, 2016.

Brown, S. S., deGouw, J. A., Warneke, C., Ryerson, T. B., Dubé, W. P., Atlas, E., Weber, R. J., Peltier, R. E., Neuman, J. A., Roberts, J. M., Swanson, A., Flocke, F., McKeen, S. A., Brioude, J., Sommariva, R., Trainer, M., Fehsenfeld, F. C. and Ravishankara, A. R.: Nocturnal isoprene oxidation over the Northeast United States in summer and its impact on reactive nitrogen partitioning and secondary organic aerosol, Atmos. Chem. Phys., 9(9), 3027–3042, doi:10.5194/acp-9-3027-2009, 2009.

Cao, F., Zhang, S., Kawamura, K., Liu, X., Yang, C., Xu, Z., Fan, M., Zhang, W., Bao, M., Chang, Y., Song, W., Liu, S., Lee, X., Li, J., Zhang, G., and Zhang, Y.: Chemical characteristics of dicarboxylic acids and related organic compounds in PM2.5 during biomass-burning and non-biomass-burning seasons at a rural site of Northeast China, Environ. Pollut., 231(Pt 1), 654–662, doi:10.1016/j.envpol.2017.08.045, 2017.

Capes, G., Johnson, B., McFiggans, G., Williams, P. I., Haywood, J. and Coe, H.: Aging of biomass burning aerosols over West Africa: Aircraft measurements of chemical composition, microphysical properties, and emission ratios, J. Geophys. Res-Atmos., 113(D23), doi:10.1029/2008jd009845, 2008.

Cech, N. B. and Enke, C. G.: Practical implications of some recent studies in electrospray ionization fundamentals, Mass Spec. Rev., 20(6), 362–387, doi:10.1002/mas.10008, 2001.

China, S., Scarnato, B., Owen, R. C., Zhang, B., Ampadu, M. T., Kumar, S., Dzepina, K., Dziobak, M. P., Fialho, P., Perlinger, J. A., Hueber, J., Helmig, D., Mazzoleni, L.R. and Mazzoleni, C.: Morphology and mixing state of aged soot particles at a remote marine free troposphere site: Implications for optical properties, Geophys. Res. Lett., 42(4), 1243–1250, doi:10.1002/2014gl062404, 2015.

China, S., Alpert, P. A., Zhang, B., Schum, S., Dzepina, K., Wright, K., Owen, R. C., Fialho, P. Mazzoleni, L.R., Mazzoleni, C., and Knopf, D. A.: Ice cloud formation potential by free tropospheric particles from long- range transport over the Northern Atlantic Ocean, J. Geophys. Res-Atmos., 122(5), 3065–3079, doi:10.1002/2016jd025817, 2017.

Chow, J. C., Lowenthal, D. H., Chen, L.W.A., Wang, X., and Watson, J. G.: Mass reconstruction methods for PM2.5: a review, Air Qual. Atmos. Hlth., 8(3), 243–263, doi:10.1007/s11869-015-0338-3, 2015.

Collaud Coen, M., Weingartner, E., Furger, M., Nyeki, S., Prevot, A. S. H., Steinbacher, M. and Baltensperger, U.: Aerosol climatology and planetary boundary influence at the Jungfraujoch analyzed by synoptic weather types, Atmos. Chem. Phys., 11(12), 5931–5944, doi:10.5194/acp-11-5931-2011, 2011.

Cook, R. D., Lin, Y.-H., Peng, Z., Boone, E., Chu, R. K., Dukett, J. E., Gunsch, M. J., Zhang, W., Tolic, N., Laskin, A. and Pratt, K. A.: Biogenic, urban, and wildfire influences on the molecular composition of dissolved organic compounds in cloud water, Atmos. Chem. Phys., 17(24), 15167–15180, doi:10.5194/acp-17-15167-2017, 2017.

Deleted:

Formatted: Font: Times New Roman

DeRieux, W.-S. W., Li, Y., Lin, P., Laskin, J., Laskin, A., Bertram, A. K., Nizkorodov, S. A. and Shiraiwa, M.: Predicting the glass transition temperature and viscosity of secondary organic material using molecular composition, Atmos. Chem. Phys., 18(9), 6331–6351, doi:10.5194/acp-18-6331-2018, 2018.

Desyaterik, Y., Sun, Y., Shen, X., Lee, T., Wang, X., Wang, T. and Collett, J. L.: Speciation of "brown" carbon in cloud water impacted by agricultural biomass burning in eastern China, J. Geophys. Res-Atmos., 118(13), 7389–7399, doi:10.1002/jgrd.50561, 2013.

Donahue, N., Epstein, S., Pandis, S. and Robinson, A.: A two-dimensional volatility basis set: 1. organic-aerosol mixing thermodynamics, Atmos. Chem. Phys., 11(7), 3303–3318, doi:10.5194/acp-11-3303-2011, 2011.

Duan, F., Liu, X., Yu, T. and Cachier, H.: Identification and estimate of biomass burning contribution to the urban aerosol organic carbon concentrations in Beijing, Atmos. Env., 38(9), 1275–1282, doi:10.1016/j.atmosenv.2003.11.037, 2004.

Dunlea, E. J., DeCarlo, P. F., Aiken, A. C., Kimmel, J. R., Peltier, R. E., Weber, R. J., Tomlinson, J., Collins, D. R., Shinozuka, Y., McNaughton, C. S., Howell, S. G., Clarke, A. D., Emmons, L. K., Apel, E. C., Pfister, G. G., van Donkelaar, A., Martin, R. V., Millet, D. B., Heald, C. L. and Jimenez, J. L.: Evolution of Asian aerosols during transpacific transport in INTEX-B, Atmos. Chem. Phys., 9(19), 7257–7287, doi:10.5194/acp-9-7257-2009, 2009.

Dzepina, K., Mazzoleni, C., Fialho, P., China, S., Zhang, B., Owen, R. C., Helmig, D., Hueber, J., Kumar, S., Perlinger, J. A., Kramer, L. J., Dziobak, M. P., Ampadu, M. T., Olsen, S., Wuebbles, D. J., and Mazzoleni, L. R.: Molecular characterization of free tropospheric aerosol collected at the Pico Mountain Observatory: a case study with a long-range transported biomass burning plume, Atmos. Chem. Phys., 15(9), 5047–5068, doi:10.5194/acp-15-5047-2015, 2015.

Ervens, B., Cubison, M., Andrews, E., Feingold, G., Ogren, J. A., Jimenez, J. L., DeCarlo, P. and Nenes, A.: Prediction of cloud condensation nucleus number concentration using measurements of aerosol size distributions and composition and light scattering enhancement due to humidity, J. Geophys. Res-Atmos., 112(D10), doi:10.1029/2006jd007426, 2007.

Ervens, B., Carlton, A. G., Turpin B. J., Altieri, K. E., Kreidenweis, S. M., and Feingold, G.: Secondary organic aerosol yields from cloud- processing of isoprene oxidation products, Geophys. Res. Lett., 35(2), doi:10.1029/2007gl031828, 2008.

Ervens, B., Turpin, B. J. and Weber, R. J.: Secondary organic aerosol formation in cloud droplets and aqueous particles (aqSOA): a review of laboratory, field and model studies, Atmos. Chem. Phys., 11(21), 11069–11102, doi:10.5194/acp-11-11069-2011, 2011.

Fialho, P., Hansen, A. D. A. and Honrath, R. E.: Absorption coefficients by aerosols in remote areas: a new approach to decouple dust and black carbon absorption coefficients using seven-wavelength Aethalometer data, J. Aerosol Sci., 36(2), 267–282, doi:10.1016/j.jaerosci.2004.09.004, 2005.

Forrister, H., Liu, J., Scheuer, E., Dibb, J., Ziemba, L., Thornhill, K. L., Anderson, B., Diskin, G., Perring, A. E., Schwarz, J. P., Campuzano- Jost, P., Day, D. A., Palm, B. B., Jimenez, J. L., Nenes, A. and Weber, R. J.: Evolution of brown carbon in wildfire plumes, Geophys. Res. Lett., 42(11), 4623–4630, doi:10.1002/2015gl063897, 2015.

George, I. J. and Abbatt, J. P. D.: Heterogeneous oxidation of atmospheric aerosol particles by gas-phase radicals, Nat. Chem., 2(9), nchem.806, doi:10.1038/nchem.806, 2010.

Helmig, D., Muoz, M., Hueber, J., Mazzoleni, C., Mazzoleni, L., Owen, R. C., Val-Martin, M., Fialho, P., Plass-Duelmer, C., Palmer, P. I., Lewis, A. C. and Pfister G.: Climatology and atmospheric chemistry of the non-methane hydrocarbons ethane and propane over the North Atlantic, Elem. Sci. Anth., 3, 000054, doi:10.12952/journal.elementa.000054, 2015.

Herzsprung, P., Hertkorn, N., Tümpling, W., Harir, M., Friese, K. and Schmitt-Kopplin, P.: Understanding molecular formula assignment of Fourier transform ion cyclotron resonance mass spectrometry data of natural organic matter from a chemical point of view, Anal. Bioanal. Chem., 406(30), 7977–7987, doi:10.1007/s00216-014-8249-y, 2014.

Hinks, M., Brady, M., Lignell, H., Song, M., Grayson, J., Bertram, A., Lin, P., Laskin, A., Laskin, J. and Nizkorodov, S.: Effect of viscosity on photodegradation rates in complex secondary organic aerosol materials, Phys. Chem. Chem. Phys., 18(13), 8785–8793, doi:10.1039/c5cp05226b, 2015.

Huang, R., Zhang, Y., Bozzetti, C., Ho, K., Cao, J., Han, Y., Daellenbach, K. R., Slowik, J. G., Platt, S. M., Canonaco, F., Zotter, P., Wolf, R., Pieber, S. M., Bruns, E. A., Crippa, M., Ciarelli, G., Piazzalunga, A., Schwikowski, M., Abbaszade, G., Schnelle-Kreis, J., Zimmermann, R., An, Z., Szidat, S., Baltensperger, U., El Haddad, I. and Prevot, A. S. H.: High secondary aerosol contribution to particulate pollution during haze events in China, Nature, 514(7521), nature13774, doi:10.1038/nature13774, 2014.

Iinuma, Y., Boege, O., Graefe, R., and Herrmann, H.: Methyl-Nitrocatechols: Atmospheric Tracer Compounds for Biomass Burning Secondary Organic Aerosols, Environ. Sci. Technol., 44, 8453–8459, doi:10.1021/es102938a, 2010.

Deleted: . Disc., 1–41

Deleted: 2017-1066, 2017

Deleted: Geophy

Deleted:

Deleted:

Deleted:

Jimenez, J. L., Canagaratna, M. R., Donahue, N. M., Prevot, A. S. H., Zhang, Q., Kroll, J. H., DeCarlo, P. F., Allan, J. D., Coe, H., Ng, N. L., Aiken, A. C., Docherty, K. S., Ulbrich, I. M., Grieshop, A. P., Robinson, A. L., Duplissy, J., Smith, J. D., Wilson, K. R., Lanz, V. A., Hueglin, C., Sun, Y, L., Tian, J., Laaksonen, A., Raatikainen, T., Rautiainen, J., Vaattovaara, P., Ehn, M., Kulmala, M., Tomlinson, J. M., Collins, D. R., Cubison, M. J., Dunlea, E. J., Huffman, J. A., Onasch, T. B., Alfarra, M. R., Williams, P. I., Bower, K., Kondo, Y., Schneider, J., Drewnick, F., Borrmann, S., Weimer, S., Demerjian, K., Salcedo, D., Cottrell, L., Griffin, R., Takami, A., Miyoshi, T., Hatakeyama, S., Shimono, A., Sun, J. Y., Zhang, Y. M., Dzepina, K., Kimmel, J. R., Sueper, D., Jayne, J. T., Herndon, S. C., Trimborn, A. M., Williams, L. R., Wood, E. C., Middlebrook, A. M., Kolb, C. E., Baltensperger U. and Worsnop D. R.: Evolution of Organic Aerosols in the Atmosphere, Science, 326(5959), 1525–1529, doi:10.1126/science.1180353, 2009

Kaiser, J. W., Heil, A., Andreae, M. O., Benedetti, A., Chubarova, N., Jones, L., Morcrette, J.-J., Razinger, M., Schultz, M. G., Suttie M., and van der Werf, G. R.: Biomass burning emissions estimated with a global fire assimilation system based on observed fire radiative power, Biogeosciences, 9(1), 527–554, doi:10.5194/bg-9-527-2012, 2012.

Kido-Soule, M., Longnecker, K., Giovannoni, S. and Kujawinski, E.: Impact of instrument and experiment parameters on reproducibility of ultrahigh resolution ESI FT-ICR mass spectra of natural organic matter, Org. Geochem., 41(8), 725–733, doi:10.1016/j.orggeochem.2010.05.017, 2010.

Kirpes, R. M., Bondy, A. L., Bonanno D., Moffet, R. C., Wang, B., Laskin, A., Ault, A. P., and Pratt, K. A.: Secondary Sulfate is Internally Mixed with Sea Spray Aerosol and Organic Aerosol in the Winter-Spring Arctic, Atmos. Chem. Phys. Disc., 1–29, doi:10.5194/acp-2017-998, 2017.

Kleissl, J., Honrath, R. E., Dziobak, M. P., Tanner, D., Val Martín, M., Owen, R. C. and Helmig, D.: Occurrence of upslope flows at the Pico mountaintop observatory: A case study of orographic flows on a small, volcanic island, J. Geophys. Res-Atmos., 112(D10), doi:10.1029/2006jd007565, 2007.

Koch, B. P. and Dittmar, T.: From mass to structure: an aromaticity index for high- resolution mass data of natural organic matter, Rapid Commun. Mass Sp., 20(5), 926–932, doi:10.1002/rcm.2386, 2006

Koch, B. P. and Dittmar, T.: From mass to structure: an aromaticity index for high- resolution mass data of natural organic matter, Rapid Commun. Mass Sp., 30(1), 250, doi: 10.1002/rcm.7433, 2016.

Koop, T., Bookhold, J., Shiraiwa, M. and Pöschl, U.: Glass transition and phase state of organic compounds: dependency on molecular properties and implications for secondary organic aerosols in the atmosphere, Phys. Chem. Chem. Phys., 13(43), 19238–19255, doi:10.1039/c1cp22617g, 2011.

Kroll, J. H., Donahue, N. M., Jimenez, J. L., Kessler, S. H., Canagaratna, M. R., Wilson, K. R., Altieri, K. E., Mazzoleni, L. R., Wozniak, A. S., Bluhm, H., Mysak, E. R., Smith, J. D., Kolb, C. E. and Worsnop, D. R.: Carbon oxidation state as a metric for describing the chemistry of atmospheric organic aerosol, Nat. Chem., 3(2), nchem.948, doi:10.1038/nchem.948, 2011.

Laing, J. R., Jaffe, D. A., and Hee, J. R.: Physical and optical properties of aged biomass burning aerosol from wildfires in Siberia and the Western USA at the Mt. Bachelor Observatory, Atmos. Chem. Phys., 16(23), 15185–15197, doi:10.5194/acp-16-15185-2016, 2016.

Lambe, A. T., Onasch, T. B., Massoli, P., Croasdale, D. R., Wright, J. P., Ahern, A. T., Williams, L. R., Worsnop, D. R., Brune, W. H., and Davidovits, P.: Laboratory studies of the chemical composition and cloud condensation nuclei (CCN) activity of secondary organic aerosol (SOA) and oxidized primary organic aerosol (OPOA), Atmos. Chem. Phys., 11(17), 8913–8928, doi:10.5194/acp-11-8913-2011, 2011

Laskin, A., Laskin, J. and Nizkorodov, S.: Chemistry of Atmospheric Brown Carbon, Chemical Reviews, 115(10), 4335–4382, doi:10.1021/cr5006167, 2015

Lee, A. K. Y., Herckes, P., Leaitch, W. R., Macdonald, A. M. and Abbatt, J. P. D.: Aqueous OH oxidation of ambient organic aerosol and cloud water organics: Formation of highly oxidized products, Geophys. Res. Lett., 38(11), n/a-n/a, doi:10.1029/2011gl047439, 2011.

Levin, E., McMeeking, G. R., Carrico, C. M., Mack, L. E., Kreidenweis, S. M., Wold, C. E., Moosmüller, H., Arnott, W. P., Hao, W. M., Collett, J. L. and Malm, W. C.: Biomass burning smoke aerosol properties measured during Fire Laboratory at Missoula Experiments (FLAME), J. Geophys. Res-Atmos, 115(D18), doi:10.1029/2009jd013601, 2010.

Li, Y., Pöschl, U. and Shiraiwa, M.: Molecular corridors and parameterizations of volatility in the chemical evolution of organic aerosols, Atmos. Chem. Phys., 16(5), 3327–3344, doi:10.5194/acp-16-3327-2016, 2016.

Lignell, H., Hinks, M. and Nizkorodov, S.: Exploring matrix effects on photochemistry of organic aerosols, P. Natl. Acad. Sci., 111(38), 13780–13785, doi:10.1073/pnas.1322106111, 2014.

Lin, P., Aiona, P. K., Li, Y., Shiraiwa, M., Laskin, J., Nizkorodov, S. A., and Laskin, A.: Molecular Characterization of Brown Carbon in Biomass Burning Aerosol Particles, Environ. Sci. Technol., 50, 11815–11824, doi:10.1021/acs.est.6603024, 2016.

Deleted:

Deleted:

Deleted:

Liu, S. and Liang, X.: Observed Diurnal Cycle Climatology of Planetary Boundary Layer Height, J. Climate, 23(21), 5790–5809, doi:10.1175/2010jcli3552.1, 2010.

Liu, X., Huey, L. G., Yokelson, R. J., Selimovic, V., Simpson, I. J., Müller, M., Jimenez, J. L., Campuzano- Jost, P., Beyersdorf, A. J., Blake, D. R., Butterfield, Z., Choi, Y., Crounse, J. D., Day, D. A., Diskin, G. S., Dubey, M. K., Fortner, E., Hanisco, T. F., Hu, W., King, L. E., Kleinman, L., Meinardi, S., Mikoviny, T., Onasch, T. B., Palm, B. B., Peischl, J., Pollack, I. B., Ryerson, T. B., Sachse, G. W., Sedlacek, A. J., Shilling, J. E., Springston, S., Clair, J., Tanner, D. J., Teng, A. P., Wennberg, P. O., Wisthaler, A. and Wolfe, G. M.: Airborne measurements of western U.S. wildfire emissions: Comparison with prescribed burning and air quality implications, J. Geophys. Res-Atmos, 122(11), 6108–6129, doi:10.1002/2016jd026315, 2017.

Massoli, P., Lambe, A. T., Ahern, A. T., Williams, L. R., Ehn, M., Mikkilä, J., Canagaratna, M. R., Brune, W. H., Onasch, T. B., Jayne, J. T., Petäjä, T., Kulmala, M., Laaksonen, A., Kolb, C. E., Davidovits, P. and Worsnop, D. R.: Relationship between aerosol oxidation level and hygroscopic properties of laboratory generated secondary organic aerosol (SOA) particles, Geophys. Res. Lett., 37(24), n/a-n/a, doi:10.1029/2010gl045258, 2010.

Mazzoleni, L. R., Ehrmann, B. M., Shen, X., Marshall, A. G. and Collett, J. L.: Water-Soluble Atmospheric Organic Matter in Fog: Exact Masses and Chemical Formula Identification by Ultrahigh-Resolution Fourier Transform Ion Cyclotron Resonance Mass Spectrometry, Environ. Sci. Technol., 44(10), 3690–3697, doi:10.1021/es903409k, 2010.

Mazzoleni, L. R., Saranjampour, P., Dalbec, M. M., Samburova, V., Hallar, A. G., Zielinska, B., Lowenthal, D. H. and Kohl, S.: Identification of water-soluble organic carbon in non-urban aerosols using ultrahigh-resolution FT-ICR mass spectrometry: organic anions, Environ. Chem., 9(3), 285–297, doi:10.1071/en11167, 2012.

Ng, N. L., Canagaratna, M. R., Jimenez, J. L., Chhabra, P. S., Seinfeld, J. H. and Worsnop, D. R.: Changes in organic aerosol composition with aging inferred from aerosol mass spectra, Atmos. Chem. Phys., 11(13), 6465–6474, doi:10.5194/acp-11-6465-2011, 2011.

O'Brien, R. E., Laskin, A., Laskin, J., Liu, S., Weber, R., Russell, L. M. and Goldstein, A. H.: Molecular characterization of organic aerosol using nanospray desorption/electrospray ionization mass spectrometry: CalNex 2010 field study, Atmospheric Environment, 68, 265–272, doi:10.1016/j.atmosenv.2012.11.056, 2013.

Olivier, J.G.J. and Berdowski, J.J.M.: Global emissions sources and sinks, in: The Climate System, Berdowski, J., Guicherit, R. and Heij, B.J., A.A. Balkema Publishers/Swets & Zeitlinger Publishers, Lisse, The Netherlands. 33-78, 2001.

Perraudin, E., Budzinski, H. and Villenave, E.: Kinetic Study of the Reactions of Ozone with Polycyclic Aromatic Hydrocarbons Adsorbed on Atmospheric Model Particles, J. Atmos. Chem., 56(1), 57–82, doi:10.1007/s10874-006-9042-x, 2006.

Pfister, G. G., Emmons, L. K., Hess, P. G., Honrath, R. E., Lamarque, J. F., Val Martin, M., Owen, R. C., Avery, M. A., Browell, E. V., Holloway, J. S., Nedelec, P., Purvis, R., Ryerson, T. B., Sachse, G. W. and Schlager, H.: Ozone production from the 2004 North American boreal fires, J. Geophys. Res-Atmos., 111(D24), doi:10.1029/2006jd007695, 2006.

Pöschl, U.: Atmospheric Aerosols: Composition, Transformation, Climate and Health Effects, Angew. Chem. Int. Edit., 44(46), 7520–7540, doi:10.1002/anie.200501122, 2005.

Putman, A. L., Offenberg, J. H., Fisseha, R., Kundu, S., Rahn, T. A. and Mazzoleni, L. R.: Ultrahigh-resolution FT-ICR mass spectrometry characterization of α-pinene ozonolysis SOA, Atmos. Env., 46, 164–172, doi:10.1016/j.atmosenv.2011.10.003, 2012.

Quinn, P. K., Collins, D. B., Grassian, V. H., Prather, K. A., and Bates, T. S.: Chemistry and Related Properties of Freshly Emitted Sea Spray Aerosol, Chem. Rev., 115(10), 4383–4399, doi:10.1021/cr500713g, 2015.

Rémillard, J., Kollias, P., Luke, E. and Wood, R.: Marine Boundary Layer Cloud Observations in the Azores, J. Climate, 25(21), 7381–7398, doi:10.1175/jcli-d-11-00610.1, 2012.

Schmitt-Kopplin, P., Gelencsér, A., Dabek-Zlotorzynska, E., Kiss, G., Hertkorn, N., Harir, M., Hong, Y. and Gebefügi, I.: Analysis of the Unresolved Organic Fraction in Atmospheric Aerosols with Ultrahigh-Resolution Mass Spectrometry and Nuclear Magnetic Resonance Spectroscopy: Organosulfates As Photochemical Smog Constituents, Anal. Chem., 82(19), 8017–8026, doi:10.1021/ac101444r, 2010.

Schmitt-Kopplin, P., Liger-Belair, G., Koch, B., Flerus, R., Kattner, G., Harir, M., Kanawati, B., Lucio, M., Tziotis, D., Hertkorn, N. and Gebefügi, I.: Dissolved organic matter in sea spray: a transfer study from marine surface water to aerosols, Biogeosciences, 9(4), 1571–1582, doi:10.5194/bg-9-1571-2012, 2012.

Seibert, P. and Frank, A.: Source-receptor matrix calculation with a Lagrangian particle dispersion model in backward mode, Atmos. Chem. Phys., 4, 51-63, https://doi.org/10.5194/acp-4-51-2004, 2004.

Shiraiwa, M., Ammann, M., Koop, T. and Pöschl, U.: Gas uptake and chemical aging of semisolid organic aerosol particles, P. Natl. Acad. Sci., 108(27), 11003–11008, doi:10.1073/pnas.1103045108, 2011.

Formatted: csl-entry, Font: Helvetica

Deleted:

Deleted:

Formatted: Font: Times New Roman

Shiraiwa, M., Li, Y., Tsimpidi, A., Karydis, V., Berkemeier, T., Pandis, S., Lelieveld, J., Koop, T. and Pöschl, U.: Global distribution of particle phase state in atmospheric secondary organic aerosols, Nat. Commun., 8, ncomms15002, doi:10.1038/ncomms15002, 2017.

Shrivastava, M., Lou, S., Zelenyuk, A., Easter, R., Corley, R., Thrall, B., Rasch, P., Fast, J., Simonich, S., Shen, H. and Tao, S.: Global long-range transport and lung cancer risk from polycyclic aromatic hydrocarbons shielded by coatings of organic aerosol, P. Natl. Acad. Sci., 114(6), 1246–1251, doi:10.1073/pnas.1618475114, 2017.

Sorooshian, A., Lu, M.-L., Brechtel, F., Jonsson, H., Feingold, G., Flagan, R. and Seinfeld, J.: On the Source of Organic Acid Aerosol Layers above Clouds, Environ. Sci. Technol., 41(13), 4647–4654, doi:10.1021/es0630442, 2007.

Stohl, A., Forster, C., Frank, A., Seibert, P. and Wotawa, G.: Technical note: The Lagrangian particle dispersion model FLEXPART version 6.2, Atmospheric Chemistry and Physics, 5(9), 2461–2474, doi:10.5194/acp-5-2461-2005, 2005.

Tu, P., Hall, W. and Johnston, M.: Characterization of Highly Oxidized Molecules in Fresh and Aged Biogenic Secondary Organic Aerosol, Anal. Chem., 88(8), 4495–4501, doi:10.1021/acs.analchem.6b00378, 2016.

U.S. Air Quality, Smog Blog. alg.umbc.edu, last access: 9 January 2018.

Vakkari, V., Kerminen, V., Beukes, J., Tiitta, P., Zyl, P., Josipovic, M., Venter, A., Jaars, K., Worsnop, D., Kulmala, M. and Laakso, L.: Rapid changes in biomass burning aerosols by atmospheric oxidation, Geophys. Res. Lett., 41(7), 2644–2651, doi:10.1002/2014gl059396, 2014.

Val Martin, M., Honrath, R., Owen, R., Pfister, G., Fialho, P. and Barata, F.: Significant enhancements of nitrogen oxides, black carbon, and ozone in the North Atlantic lower free troposphere resulting from North American boreal wildfires, J. Geophys. Res-Atmos., 111(D23), n/a-n/a, doi:10.1029/2006jd007530, 2006.

Val Martin, M., Honrath, R., Owen, R. and Lapina, K.: Large- scale impacts of anthropogenic pollution and boreal wildfires on the nitrogen oxides over the central North Atlantic region, J. Geophys. Res-Atmos., 113(D17), doi:10.1029/2007jd009689, 2008a.

Val Martin, M., Honrath, R., Owen, R. and Li, Q.: Seasonal variation of nitrogen oxides in the central North Atlantic lower free troposphere, J. Geophys. Res-Atmos., 113(D17), doi:10.1029/2007jd009688, 2008b.

Val Martin, M., Logan, J. A., Kahn, R. A., Leung, F.-Y., Nelson, D. L. and Diner, D. J.: Smoke injection heights from fires in North America: analysis of 5 years of satellite observations, Atmos. Chem. Phys., 10(4), 1491–1510, doi:10.5194/acp-10-1491-2010, 2010.

Virtanen, A., Joutsensaari, J., Koop, T., Kannosto, J., Yli-Pirilä, P., Leskinen, J., Mäkelä, J., Holopainen, J., Pöschl, U., Kulmala, M., Worsnop, D. and Laaksonen, A.: An amorphous solid state of biogenic secondary organic aerosol particles, Nature, 467(7317), nature09455, doi:10.1038/nature09455, 2010.

Volkamer, R., Jimenez, J. L., San Martini, F., Dzepina, K., Zhang, Q., Salcedo, D., Molina, L. T., Worsnop, D. R. and Molina, M. J.: Secondary organic aerosol formation from anthropogenic air pollution: Rapid and higher than expected, Geophys. Res. Lett., 33(17), doi:10.1029/2006gl026899, 2006.

Walser, M. L., Desyaterik, Y., Laskin, J., Laskin, A. and Nizkorodov, S.: High-resolution mass spectrometric analysis of secondary organic aerosol produced by ozonation of limonene, Phys. Chem. Chem. Phys., 10(7), 1009–1022, doi:10.1039/b712620d, 2007.

Warneke, C., Bahreini, R., Brioude, J., Brock, C. A., Gouw, J., Fahey, D. W., Froyd, K. D., Holloway, J. S., Middlebrook, A., Miller, L., Montzka, S., Murphy, D. M., Peischl, J., Ryerson, T. B., Schwarz, J. P., Spackman, J. R. and Veres, P.: Biomass burning in Siberia and Kazakhstan as an important source for haze over the Alaskan Arctic in April 2008, Geophys. Res. Lett., 36(2), n/a-n/a, doi:10.1029/2008gl036194, 2009.

Wozniak, A. S., Willoughby, A. S., Gurganus, S. C. and Hatcher, P. G.: Distinguishing molecular characteristics of aerosol water soluble organic matter from the 2011 trans-North Atlantic US GEOTRACES cruise, Atmos. Chem. Phys., 14(16), 8419–8434, doi:10.5194/acp-14-8419-2014, 2014.

Ye, Q., Robinson, E. S., Ding, X., Ye, P., Sullivan, R. C. and Donahue, N. M.: Mixing of secondary organic aerosols versus relative humidity, Proc. Natl. Acad. Sci., 113(45), 12649–12654, doi:10.1073/pnas.1604536113, 2016.

Yu, J. Z., Huang, X., Xu, J. and Hu, M.: When Aerosol Sulfate Goes Up, So Does Oxalate: Implication for the Formation Mechanisms of Oxalate, Environ. Sci. Technol., 39(1), 128–133, doi:10.1021/es049559f, 2005.

Zelenyuk, A., Imre, D. G., Wilson, J., Bell, D. M., Suski, K. J., Shrivastava, M., Beránek, J., Alexander, M. L., Kramer, A. L. and Massey-Simonich, S. L.: The effect of gas-phase polycyclic aromatic hydrocarbons on the formation and properties of biogenic secondary organic aerosol particles, Faraday Discuss., 200, 143–164, doi:10.1039/c7fd00032d, 2017.

Zhang, B., Owen, R. C., Perlinger, J. A., Kumar, S., Wu, S., Val Martin, M., Kramer, L. Helmig, D. and Honrath, R. E.: A semi-Lagrangian view of ozone production tendency in North American outflow in the summers of 2009 and 2010, Atmos. Chem. Phys., 14(5), 2267–2287, doi:10.5194/acp-14-2267-2014, 2014.

Zhang, B., Owen, R. C., Perlinger, J. A., Helmig, D., Val Martín, M., Kramer, L., Mazzoleni, L. R. and Mazzoleni, C.: Ten-year chemical signatures associated with long-range transport observed in the free troposphere over the central North Atlantic, Elem. Sci. Anth., 5, doi:10.1525/elementa.194, 2017.

Zhao, Y., Hallar, A. G. and Mazzoleni, L. R.: Atmospheric organic matter in clouds: exact masses and molecular formula identification using ultrahigh-resolution FT-ICR mass spectrometry, Atmos. Chem. Phys., 13(24), 12343–12362, doi:10.5194/acp-13-12343-2013, 2013.

Zobrist, B., Marcolli, C., Pedernera, D. and Koop, T.: Do atmospheric aerosols form glasses?, Atmos. Chem. Phys., 8(17), 5221–5244, doi:10.5194/acp-8-5221-2008, 2008.

Tables

Table 1. Average concentrations (μg/m^3) of major ions and organic carbon.

Component	PMO-1	PMO-2	PMO-3
Acetate	0.0519 ± 0.0001	0.004587 ± 0.000005	0.0071 ± 0.0002
Formate	0.0289 ± 0.0003	0.00438 ± 0.00007	0.0119 ± 0.0001
MSA	0	0.00439 ± 0.00006	0.00232 ± 0.00002
Chloride	0.0104 ± 0.0003	0	0.0310 ± 0.0001
Nitrate	0.189 ± 0.002	0.0173 ± 0.0004	0.3010 ± 0.00028
Sulfate	0.338 ± 0.004	1.07 ± 0.01	0.421 ± 0.003
Oxalate	0.0938 ± 0.00070	0.0897 ± 0.00181	0.05222 ± 0.00002
Sodium	0.2101±0.0004*	0.2560±0.0001*	0.548±0.005*
Ammonium	0.1364 ± 0.0004	0.2394 ± 0.00001	0.1193 ± 0.00062
Potassium	0.0791 ± 0.0020**	0.0126 ± 0.0002	0.0197 ± 0.0003
OC	2.07 ± 0.02	0.478 ± 0.026	0.87 ± 0.10

*Sodium concentrations were not background subtracted due to inconsistent and high blank levels, they are included to provide an upper limit on the approximate sodium concentrations.

**Replicate measurements of potassium were inconsistent. The sample could not be re-analyzed because there was no remaining sample. Standard deviation was determined by looking at the average standard deviation of 36 potassium measurements in other samples. This sample should only be considered as elevated potassium and only minimal importance placed on the actual measured value.

Table 2. Molecular formula composition with abundance weighted average values and the numbers of formulas for each elemental group.

Sample	Group	O/C_w	H/C_w	DBE_w	OS_{Cw}	Number
PMO-1	All	0.48 ± 0.13	1.30 ± 0.28	7.74 ± 3.38	-0.42 ± 0.43	3168
PMO-2	All	0.57 ± 0.17	1.36 ± 0.22	6.42 ± 2.54	-0.30 ± 0.46	2121
PMO-3	All	0.45 ± 0.11	1.34 ± 0.41	7.45 ± 3.15	-0.50 ± 0.41	1820
PMO-1	CHO	0.47 ± 0.14	1.31 ± 0.29	7.43 ± 3.68	-0.37 ± 0.44	1848
PMO-2	CHO	0.55 ± 0.17	1.35 ± 0.25	6.43 ± 3.66	-0.26 ± 0.45	1281
PMO-3	CHO	0.44 ± 0.14	1.37 ± 0.31	6.93 ± 3.82	-0.48 ± 0.48	1183
PMO-1	CHNO	0.49 ± 0.15	1.2 ± 0.26	9.44 ± 3.09	-0.50 ± 0.3	1120
PMO-2	CHNO	0.59 ± 0.14	1.25 ± 0.19	8.20 ± 2.19	-0.38 ± 0.29	561
PMO-3	CHNO	0.49 ± 0.14	1.23 ± 0.21	9.25 ± 2.41	-0.52 ± 0.25	608
PMO-1	CHOS	0.48 ± 0.14	1.78 ± 0.35	2.87 ± 3.28	-1.20 ± 0.42	200
PMO-2	CHOS	0.74 ± 0.34	1.57 ± 0.23	4.05 ± 2.45	-0.54 ± 0.51	274
PMO-3	CHOS	0.40 ± 14	1.90 ± 0.47	1.60 ± 4.29	-1.50 ± 0.20	29

Formatted ... [9]
Formatted ... [10]
Formatted ... [14]
Formatted ... [11]
Formatted Table ... [12]
Formatted ... [13]
Formatted ... [15]
Formatted ... [16]
Formatted ... [17]
Formatted ... [18]
Formatted Table ... [19]
Formatted ... [20]
Formatted ... [21]
Formatted ... [22]
Formatted ... [23]
Formatted ... [24]
Formatted ... [25]
Formatted ... [26]
Formatted ... [27]
Formatted ... [28]
Formatted ... [29]
Formatted ... [30]
Formatted ... [32]
Formatted ... [31]
Formatted ... [33]
Formatted ... [34]
Formatted ... [35]
Formatted ... [36]
Formatted ... [38]
Formatted ... [37]
Formatted ... [39]
Formatted ... [40]
Formatted ... [41]
Formatted ... [42]
Formatted ... [43]
Formatted ... [44]
Formatted ... [45]
Formatted ... [46]
Formatted ... [47]
Formatted ... [48]
Formatted ... [49]
Formatted ... [50]
Formatted ... [51]
Formatted ... [52]
Formatted ... [53]
Formatted ... [54]
Formatted ... [55]
Formatted ... [56]
Formatted ... [57]
Formatted ... [58]
Formatted ... [59]
Formatted ... [60]
Formatted ... [61]
Formatted ... [62]
Formatted ... [63]
Formatted ... [64]
Formatted ... [65]
Formatted ... [66]
Formatted ... [67]
Formatted ... [68]
Formatted ... [69]
Formatted ... [70]
Formatted ... [71]
Formatted ... [72]
Formatted ... [73]

Figures

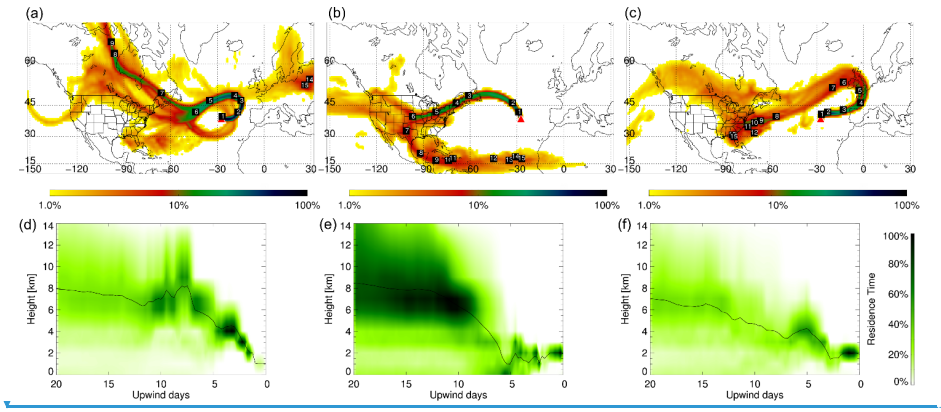

Figure 1. FLEXPART retroplumes for 28 June 2013 06:00 (PMO-1, (a, d)), 6 July 2014 03:00 (PMO-2, (b, e)), and 21 June 03:00 2015 (PMO-3, (c, f): column integrated residence time over the 20-day transport time (a-c) and vertical distribution of the retroplume residence time at given upwind times (d-f). The labels indicate the approximate locations of the center of the plume for each of the transport days. Residence time is color coded by logarithmic grades representing its ratio to the location of maximal integrated residence time (100%). The black line in d-f indicates the mean height of the plume during transport.

Formatted: Level 1

Deleted:

Deleted: 27-

Deleted: 5-

Deleted: 20-

Deleted: white

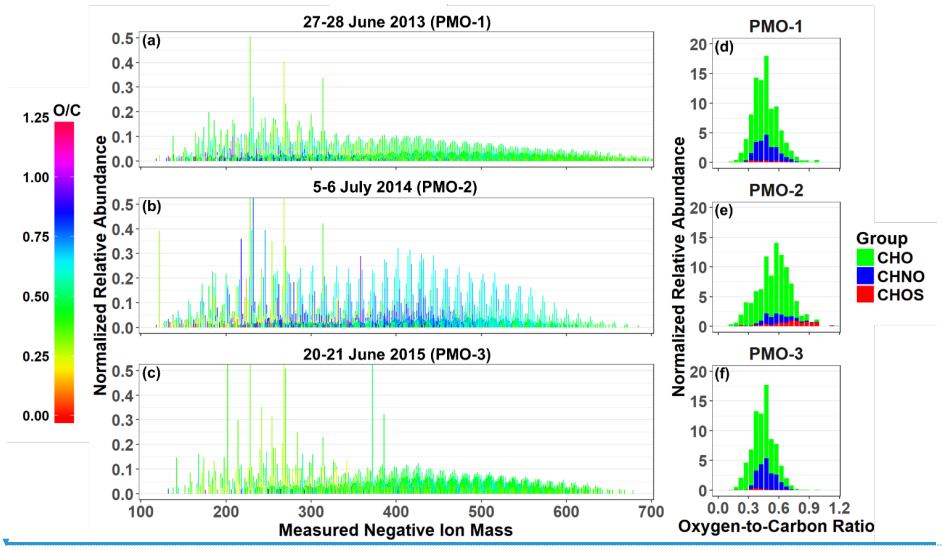

Deleted:

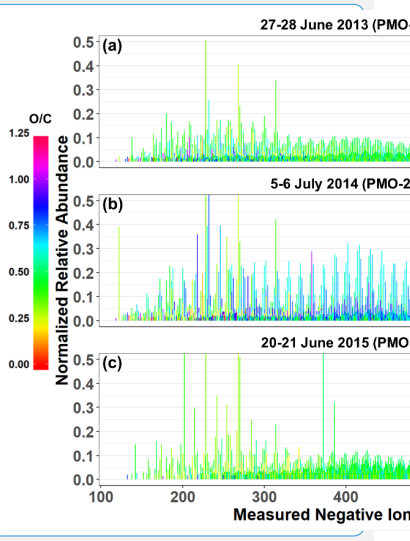

Figure 2. Reconstructed negative ion mass spectra (a-c) and O/C histograms (d-f) for the three PMO samples. The color in the mass spectra indicates the O/C value for the molecular formula it represents. The tallest peaks in the mass spectra exceed the range, this was done to improve the visibility of the lower abundance species (see also Fig. S6).

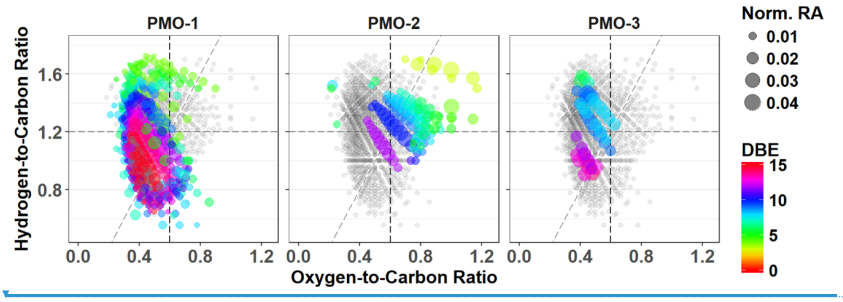

Figure 3. Van Krevelen plots for the CHNO species with all identified CHNO species (grey) and unique species (colored). The color represents the number of double bond equivalents in the corresponding molecular formula. The diagonal line is an oxidation line ($OS_C = 0$ for C, H, O elements; Tu et al., 2016), where the more oxidized formulas are on the right side and less oxidized are on the left.

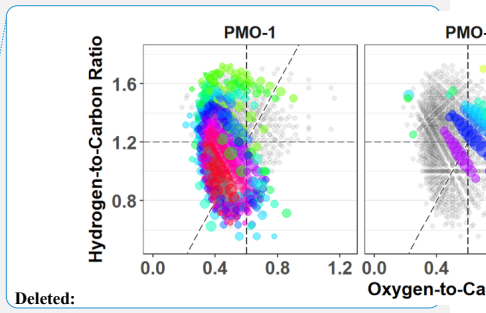

Deleted:

Deleted: both common

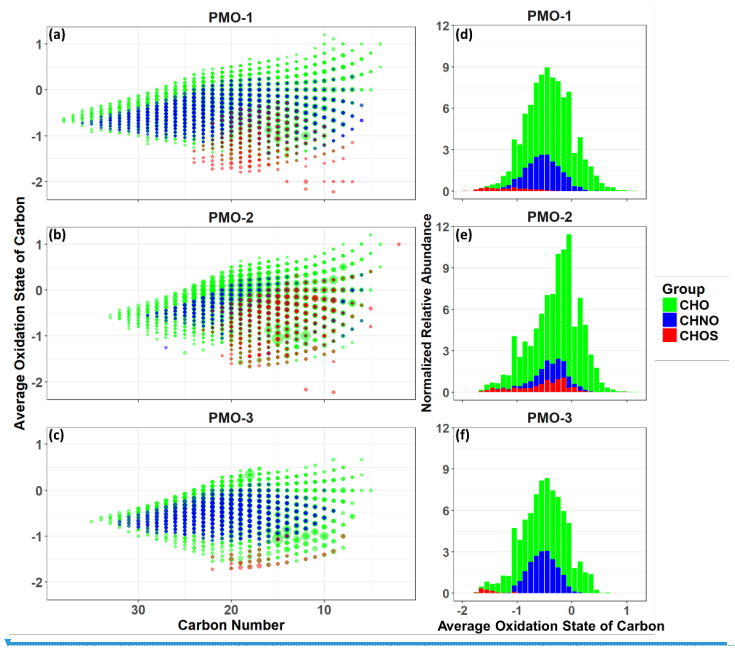

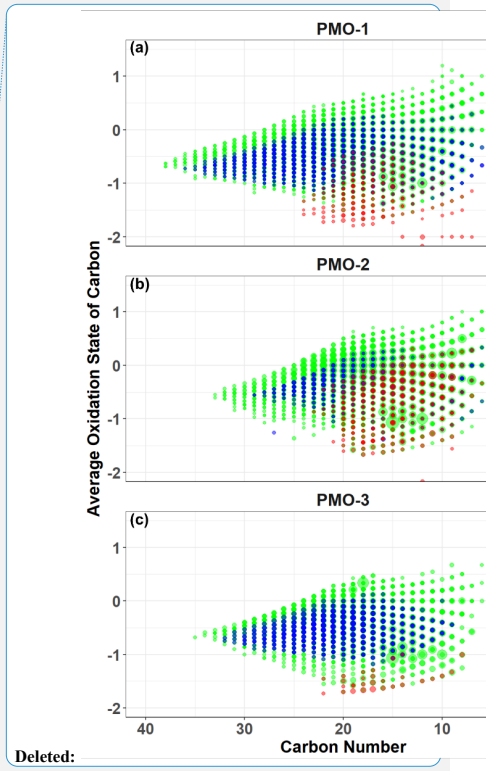

Deleted:

Figure 4. Average OS_C vs. carbon number plots for molecular formula identified in each of PMO samples (a-c). The size of the symbols is scaled to the analyte relative abundance and the color represents the elemental group: CHO (green), CHNO (blue), and CHOS (red). The right panel (d-f) contains average OS_C histograms based on the sum of normalized abundance.

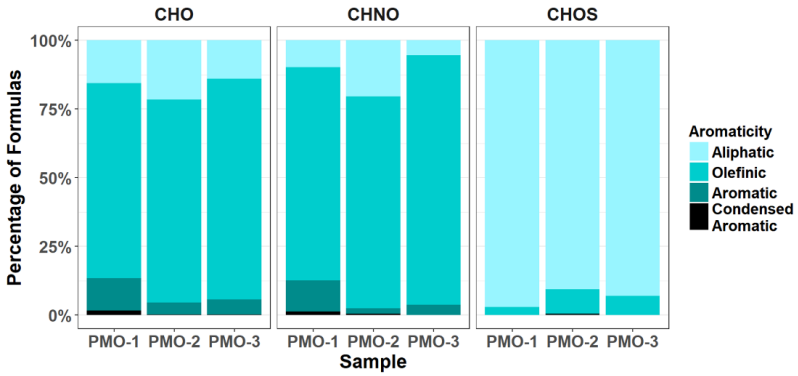

Figure 5. Normalized bar charts for the aromaticity of the three PMO samples, calculated using the Koch and Dittmar (2006; 2016) modified aromaticity index (AI_{mod}).

1525

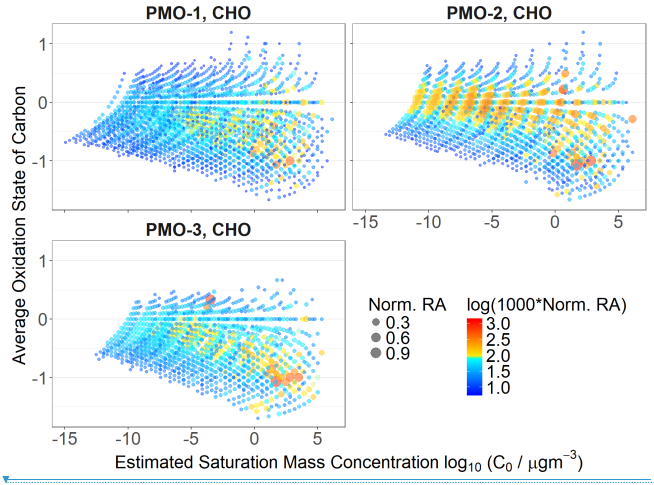

Deleted:

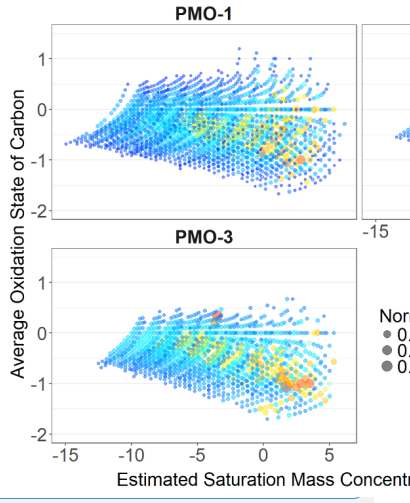

Figure 6. OS_C *vs.* volatility estimated using the Li et al. (2016) method for the CHO species in the three samples. The size is determined by the normalized relative abundance and the color is determined by the logarithm of the normalized relative abundance multiplied by 1000.

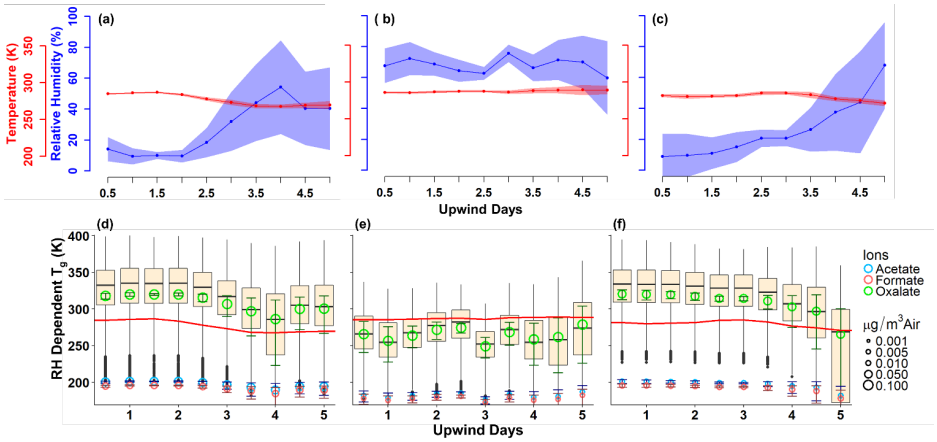

Figure 7. Panels a-c contain the ambient conditions extracted from the GFS analysis along the FLEXPART modeled path weighted by the residence time for PMO-1, PMO-2, and PMO-3, respectively. The line represents the mean value and the shading represents one standard deviation of values. Panels d-f contain the boxplot distributions of the relative humidity dependent T_g values for molecular formulas using the maximum, mean, and minimum RH for PMO-1, PMO-2, and PMO-3, respectively. The T_g values for the full composition of each sample were calculated using the maximum, mean, and minimum RH and then all three sets of data are combined and plotted as a single distribution for each time period. The open circles represent the abundance and Boyer-Kauzmann estimated T_g for the acid forms of the three most abundant low MW organic ions, the bars around the circles represent the range of possible T_g values for those compounds when the range of RH is considered. The red line demonstrates the ambient temperature at each time point, as extracted from GFS. The centerline of the boxplot represents the median, the top and bottom of the "box" represent the third and first quartiles, respectively. The "whiskers" represent Q3 + 1.5* interquartile range (IQR, Q3-Q1) (maximum), and Q1 – 1.5*(IQR) (minimum).

Deleted: ¶

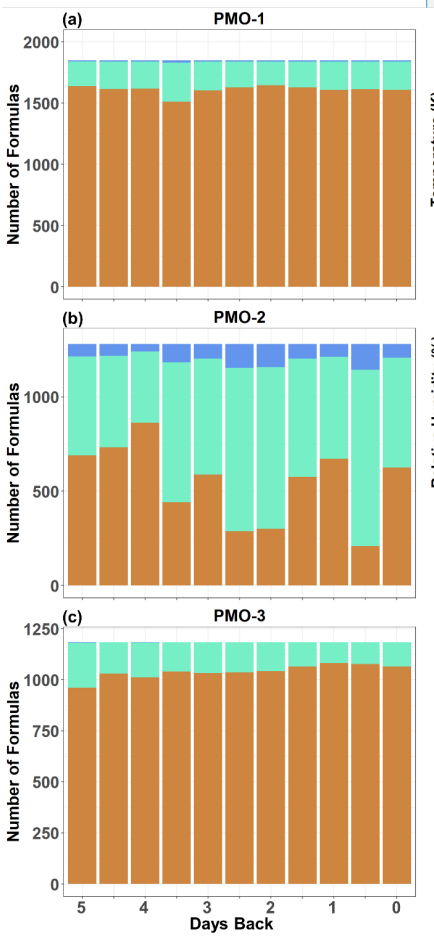

¶

Figure 7. Stacked bar charts (a-c) showing the distribution of molecular species by the phase state categories of liquid, semi-solid, and solid for the last five days of transport. Panels d and e show the atmospheric conditions extracted from GFS for the model grids along the FLEXPART simulated transport pathways. The central line is the weighted average and the shading on either side indicates the weighted standard deviation. The results are weighted by residence time.¶

Page Break

¶

¶

... [233]

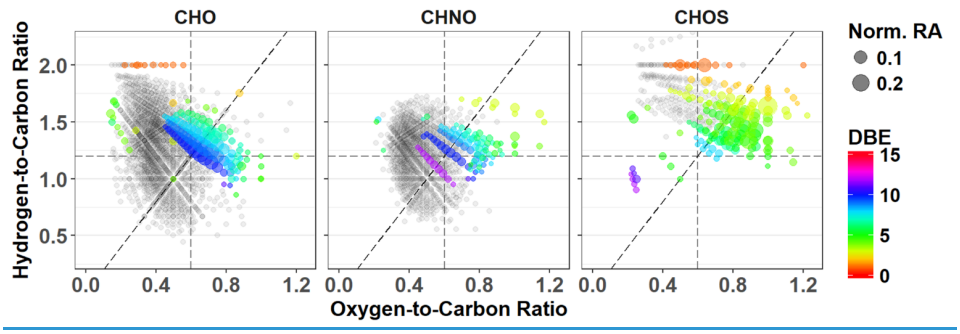

Figure 8. PMO-2 van Krevelen plots for unique molecular formulas separated by group. Symbols are scaled to indicate the normalized relative abundance. The DBE is indicated for each of unique molecular formulas using colored symbols. Formulas common with other samples are provided in grey for context.

Deleted: Common molecular formulas

Page 10: [1] Deleted **Simeon Schum** **5/29/18 10:20:00 AM**

values are increased relative to the unweighted averages in the aerosol transported in the boundary layer (PMO-2), while the aerosol transported in the free troposphere (PMO-1 and PMO-3) does not show much difference between weighted and unweighted averages. This suggests that the oxidized species may be more abundant and important to the overall chemical and physical characteristics of PMO-2 in the atmosphere and may imply higher hygroscopicity, higher cloud condensation nucleation ability (Massoli et al., 2010) and lower volatility (Ng et al. 2011) relative to PMO-1 and PMO-3. The observation of low

Page 11: [2] Deleted **Simeon Schum** **5/29/18 10:20:00 AM**

The aerosol phase state during transport was estimated using the Gordon-Taylor equation (Eqs. S6 - S7) with the calculated glass transition temperatures of the identified CHO molecular species and extracted ambient temperature and relative humidity from GFS analysis along the transport pathways using FLEXPART backward simulations. The number fraction of CHO molecular formulas predicted to be liquid, semi-solid, or solid for each sample over the last 5 days of transport is shown in Fig. 7. The prediction was only taken back 5 days due to the increased

Page 12: [3] Deleted **Simeon Schum** **5/29/18 10:20:00 AM**

observed species in each of the PMO samples in this study, we saw that most of the species observed uniquely in

Page 12: [4] Deleted **Simeon Schum** **5/29/18 10:20:00 AM**

S13). Since, these highly oxidized species were not observed in either PMO-1 or PMO-3, we hypothesize that their presence indicates aqueous phase oxidation. As mentioned previously

Page 12: [5] Deleted **Simeon Schum** **5/29/18 10:20:00 AM**

or perhaps marine aerosol contributions. In addition

Page 12: [6] Deleted **Simeon Schum** **5/29/18 10:20:00 AM**

oxalate concentration was observed, especially considering

Page 12: [7] Deleted **Simeon Schum** **5/29/18 10:20:00 AM**

to the overall organic mass. The organic mass concentration

Page 12: [8] Deleted **Simeon Schum** **5/29/18 10:20:00 AM**

respectively. Oxalate is also a potential marker of cloud processing (Sorooshian et al., 2007).

Page 20: [9] Formatted **Simeon Schum** **5/29/18 10:20:00 AM**

Level 1

Page 20: [10] Formatted **Simeon Schum** **5/29/18 10:20:00 AM**

Font: Times New Roman

Page 20: [11] Formatted **Simeon Schum** **5/29/18 10:20:00 AM**

Font Alignment: Auto

Page 20: [12] Formatted Table **Simeon Schum** **5/29/18 10:20:00 AM**

Formatted Table

Page 20: [13] Formatted **Simeon Schum** **5/29/18 10:20:00 AM**

Font: Times New Roman, Bold, Font color: Black

Page 20: [14] Formatted	**Simeon Schum**	**5/29/18 10:20:00 AM**

Font: Times New Roman

Page 20: [14] Formatted	**Simeon Schum**	**5/29/18 10:20:00 AM**

Font: Times New Roman

Page 20: [15] Formatted	**Simeon Schum**	**5/29/18 10:20:00 AM**

Font: Times New Roman

Page 20: [15] Formatted	**Simeon Schum**	**5/29/18 10:20:00 AM**

Font: Times New Roman

Page 20: [16] Formatted	**Simeon Schum**	**5/29/18 10:20:00 AM**

Font: Times New Roman

Page 20: [16] Formatted	**Simeon Schum**	**5/29/18 10:20:00 AM**

Font: Times New Roman

Page 20: [17] Formatted	**Simeon Schum**	**5/29/18 10:20:00 AM**

Font: Times New Roman

Page 20: [18] Formatted	**Simeon Schum**	**5/29/18 10:20:00 AM**

Font Alignment: Auto

Page 20: [19] Formatted Table	**Simeon Schum**	**5/29/18 10:20:00 AM**

Formatted Table

Page 20: [20] Formatted	**Simeon Schum**	**5/29/18 10:20:00 AM**

Font: Times New Roman, Bold, Font color: Black

Page 20: [21] Formatted	**Simeon Schum**	**5/29/18 10:20:00 AM**

Font: Times New Roman

Page 20: [21] Formatted	**Simeon Schum**	**5/29/18 10:20:00 AM**

Font: Times New Roman

Page 20: [22] Formatted	**Simeon Schum**	**5/29/18 10:20:00 AM**

Font: Times New Roman

Page 20: [22] Formatted	**Simeon Schum**	**5/29/18 10:20:00 AM**

Font: Times New Roman

Page 20: [23] Formatted	**Simeon Schum**	**5/29/18 10:20:00 AM**

Font: Times New Roman

Page 20: [23] Formatted	**Simeon Schum**	**5/29/18 10:20:00 AM**

Font: Times New Roman

Page 20: [24] Formatted	**Simeon Schum**	**5/29/18 10:20:00 AM**

Font: Times New Roman

Page 20: [25] Formatted	**Simeon Schum**	**5/29/18 10:20:00 AM**

Font Alignment: Auto

Page 20: [26] Formatted	**Simeon Schum**	**5/29/18 10:20:00 AM**

Font: Times New Roman, Bold, Font color: Black

Page 20: [27] Formatted	Simeon Schum	5/29/18 10:20:00 AM

Font: Times New Roman, Font color: Black

Page 20: [27] Formatted	Simeon Schum	5/29/18 10:20:00 AM

Font: Times New Roman, Font color: Black

Page 20: [28] Formatted	Simeon Schum	5/29/18 10:20:00 AM

Font: Times New Roman

Page 20: [28] Formatted	Simeon Schum	5/29/18 10:20:00 AM

Font: Times New Roman

Page 20: [29] Formatted	Simeon Schum	5/29/18 10:20:00 AM

Font: Times New Roman

Page 20: [29] Formatted	Simeon Schum	5/29/18 10:20:00 AM

Font: Times New Roman

Page 20: [30] Formatted	Simeon Schum	5/29/18 10:20:00 AM

Font: Times New Roman

Page 20: [31] Formatted	Simeon Schum	5/29/18 10:20:00 AM

Font Alignment: Auto

Page 20: [32] Formatted	Simeon Schum	5/29/18 10:20:00 AM

Font: Times New Roman, Bold, Font color: Black

Page 20: [33] Formatted	Simeon Schum	5/29/18 10:20:00 AM

Font: Times New Roman

Page 20: [33] Formatted	Simeon Schum	5/29/18 10:20:00 AM

Font: Times New Roman

Page 20: [34] Formatted	Simeon Schum	5/29/18 10:20:00 AM

Font: Times New Roman

Page 20: [34] Formatted	Simeon Schum	5/29/18 10:20:00 AM

Font: Times New Roman

Page 20: [35] Formatted	Simeon Schum	5/29/18 10:20:00 AM

Font: Times New Roman

Page 20: [35] Formatted	Simeon Schum	5/29/18 10:20:00 AM

Font: Times New Roman

Page 20: [36] Formatted	Simeon Schum	5/29/18 10:20:00 AM

Font: Times New Roman

Page 20: [37] Formatted	Simeon Schum	5/29/18 10:20:00 AM

Font Alignment: Auto

Page 20: [38] Formatted	Simeon Schum	5/29/18 10:20:00 AM

Font: Times New Roman, Bold, Font color: Black

Page 20: [39] Formatted	Simeon Schum	5/29/18 10:20:00 AM

Font: Times New Roman

Page 20: [39] Formatted	Simeon Schum	5/29/18 10:20:00 AM

Font: Times New Roman

Page 20: [40] Formatted	**Simeon Schum**	**5/29/18 10:20:00 AM**

Font: Times New Roman

Page 20: [40] Formatted	**Simeon Schum**	**5/29/18 10:20:00 AM**

Font: Times New Roman

Page 20: [41] Formatted	**Simeon Schum**	**5/29/18 10:20:00 AM**

Font: Times New Roman

Page 20: [41] Formatted	**Simeon Schum**	**5/29/18 10:20:00 AM**

Font: Times New Roman

Page 20: [42] Formatted	**Simeon Schum**	**5/29/18 10:20:00 AM**

Font: Times New Roman

Page 20: [43] Formatted	**Simeon Schum**	**5/29/18 10:20:00 AM**

Font Alignment: Auto

Page 20: [44] Formatted	**Simeon Schum**	**5/29/18 10:20:00 AM**

Font: Times New Roman, Bold, Font color: Black

Page 20: [45] Formatted	**Simeon Schum**	**5/29/18 10:20:00 AM**

Font: Times New Roman

Page 20: [45] Formatted	**Simeon Schum**	**5/29/18 10:20:00 AM**

Font: Times New Roman

Page 20: [46] Formatted	**Simeon Schum**	**5/29/18 10:20:00 AM**

Font: Times New Roman

Page 20: [46] Formatted	**Simeon Schum**	**5/29/18 10:20:00 AM**

Font: Times New Roman

Page 20: [47] Formatted	**Simeon Schum**	**5/29/18 10:20:00 AM**

Font: Times New Roman

Page 20: [47] Formatted	**Simeon Schum**	**5/29/18 10:20:00 AM**

Font: Times New Roman

Page 20: [48] Formatted	**Simeon Schum**	**5/29/18 10:20:00 AM**

Font: Times New Roman

Page 20: [49] Formatted	**Simeon Schum**	**5/29/18 10:20:00 AM**

Font Alignment: Auto

Page 20: [50] Formatted	**Simeon Schum**	**5/29/18 10:20:00 AM**

Font: Times New Roman, Bold, Font color: Black

Page 20: [51] Formatted	**Simeon Schum**	**5/29/18 10:20:00 AM**

Font: Times New Roman

Page 20: [51] Formatted	**Simeon Schum**	**5/29/18 10:20:00 AM**

Font: Times New Roman

Page 20: [52] Formatted	**Simeon Schum**	**5/29/18 10:20:00 AM**

Font: Times New Roman

Page 20: [52] Formatted	Simeon Schum	5/29/18 10:20:00 AM

Font: Times New Roman

Page 20: [53] Formatted	Simeon Schum	5/29/18 10:20:00 AM

Font: Times New Roman

Page 20: [53] Formatted	Simeon Schum	5/29/18 10:20:00 AM

Font: Times New Roman

Page 20: [54] Formatted	Simeon Schum	5/29/18 10:20:00 AM

Font: Times New Roman

Page 20: [55] Formatted	Simeon Schum	5/29/18 10:20:00 AM

Font Alignment: Auto

Page 20: [56] Formatted	Simeon Schum	5/29/18 10:20:00 AM

Font: Times New Roman, Bold, Font color: Black

Page 20: [57] Formatted	Simeon Schum	5/29/18 10:20:00 AM

Font: Times New Roman

Page 20: [57] Formatted	Simeon Schum	5/29/18 10:20:00 AM

Font: Times New Roman

Page 20: [58] Formatted	Simeon Schum	5/29/18 10:20:00 AM

Font: Times New Roman

Page 20: [58] Formatted	Simeon Schum	5/29/18 10:20:00 AM

Font: Times New Roman

Page 20: [59] Formatted	Simeon Schum	5/29/18 10:20:00 AM

Font: Times New Roman

Page 20: [59] Formatted	Simeon Schum	5/29/18 10:20:00 AM

Font: Times New Roman

Page 20: [60] Formatted	Simeon Schum	5/29/18 10:20:00 AM

Font: Times New Roman

Page 20: [61] Formatted	Simeon Schum	5/29/18 10:20:00 AM

Font Alignment: Auto

Page 20: [62] Formatted	Simeon Schum	5/29/18 10:20:00 AM

Font: Times New Roman, Bold, Font color: Black

Page 20: [63] Formatted	Simeon Schum	5/29/18 10:20:00 AM

Font: Times New Roman

Page 20: [63] Formatted	Simeon Schum	5/29/18 10:20:00 AM

Font: Times New Roman

Page 20: [64] Formatted	Simeon Schum	5/29/18 10:20:00 AM

Font: Times New Roman

Page 20: [64] Formatted	Simeon Schum	5/29/18 10:20:00 AM

Font: Times New Roman

Page 20: [65] Formatted	Simeon Schum	5/29/18 10:20:00 AM

Font: Times New Roman

Page 20: [65] Formatted	**Simeon Schum**	**5/29/18 10:20:00 AM**

Font: Times New Roman

Page 20: [66] Formatted	**Simeon Schum**	**5/29/18 10:20:00 AM**

Font: Times New Roman

Page 20: [67] Formatted	**Simeon Schum**	**5/29/18 10:20:00 AM**

Font Alignment: Auto

Page 20: [68] Formatted	**Simeon Schum**	**5/29/18 10:20:00 AM**

Font: Times New Roman, Bold, Font color: Black

Page 20: [69] Formatted	**Simeon Schum**	**5/29/18 10:20:00 AM**

Font: Times New Roman

Page 20: [69] Formatted	**Simeon Schum**	**5/29/18 10:20:00 AM**

Font: Times New Roman

Page 20: [70] Formatted	**Simeon Schum**	**5/29/18 10:20:00 AM**

Font: Times New Roman

Page 20: [70] Formatted	**Simeon Schum**	**5/29/18 10:20:00 AM**

Font: Times New Roman

Page 20: [71] Formatted	**Simeon Schum**	**5/29/18 10:20:00 AM**

Font: Times New Roman

Page 20: [71] Formatted	**Simeon Schum**	**5/29/18 10:20:00 AM**

Font: Times New Roman

Page 20: [72] Formatted	**Simeon Schum**	**5/29/18 10:20:00 AM**

Font: Times New Roman

Page 20: [73] Formatted	**Simeon Schum**	**5/29/18 10:20:00 AM**

Font Alignment: Auto

Page 20: [74] Formatted	**Simeon Schum**	**5/29/18 10:20:00 AM**

Font: Times New Roman, Bold, Font color: Black

Page 20: [75] Formatted	**Simeon Schum**	**5/29/18 10:20:00 AM**

Font: Times New Roman

Page 20: [75] Formatted	**Simeon Schum**	**5/29/18 10:20:00 AM**

Font: Times New Roman

Page 20: [76] Formatted	**Simeon Schum**	**5/29/18 10:20:00 AM**

Font: Times New Roman

Page 20: [76] Formatted	**Simeon Schum**	**5/29/18 10:20:00 AM**

Font: Times New Roman

Page 20: [77] Formatted	**Simeon Schum**	**5/29/18 10:20:00 AM**

Font: Times New Roman

Page 20: [77] Formatted	**Simeon Schum**	**5/29/18 10:20:00 AM**

Font: Times New Roman

Page 20: [78] Formatted	Simeon Schum	5/29/18 10:20:00 AM

Level 1

Page 20: [79] Formatted	Simeon Schum	5/29/18 10:20:00 AM

Font: Times New Roman

Page 20: [80] Formatted	Simeon Schum	5/29/18 10:20:00 AM

Font Alignment: Auto

Page 20: [81] Formatted	Simeon Schum	5/29/18 10:20:00 AM

Font: Times New Roman, Bold, Font color: Black

Page 20: [82] Formatted	Simeon Schum	5/29/18 10:20:00 AM

Font: Times New Roman

Page 20: [82] Formatted	Simeon Schum	5/29/18 10:20:00 AM

Font: Times New Roman

Page 20: [83] Formatted	Simeon Schum	5/29/18 10:20:00 AM

Font: Times New Roman

Page 20: [84] Formatted	Simeon Schum	5/29/18 10:20:00 AM

Font: Times New Roman, Bold, Font color: Black

Page 20: [85] Formatted	Simeon Schum	5/29/18 10:20:00 AM

Font: Times New Roman

Page 20: [86] Formatted	Simeon Schum	5/29/18 10:20:00 AM

Font: Times New Roman, Bold, Font color: Black

Page 20: [87] Formatted	Simeon Schum	5/29/18 10:20:00 AM

Font: Times New Roman, Bold, Font color: Black

Page 20: [88] Formatted	Simeon Schum	5/29/18 10:20:00 AM

Font: 9 pt, Bold, Font color: Black

Page 20: [89] Formatted	Simeon Schum	5/29/18 10:20:00 AM

Font: Times New Roman, Bold, Font color: Black

Page 20: [90] Formatted	Simeon Schum	5/29/18 10:20:00 AM

Font: Times New Roman

Page 20: [90] Formatted	Simeon Schum	5/29/18 10:20:00 AM

Font: Times New Roman

Page 20: [91] Formatted	Simeon Schum	5/29/18 10:20:00 AM

Font: Times New Roman

Page 20: [92] Formatted	Simeon Schum	5/29/18 10:20:00 AM

Font Alignment: Auto

Page 20: [93] Formatted	Simeon Schum	5/29/18 10:20:00 AM

Font: Times New Roman, Bold, Font color: Black

Page 20: [94] Formatted	Simeon Schum	5/29/18 10:20:00 AM

Font: Times New Roman, Font color: Black

Page 20: [95] Formatted	Simeon Schum	5/29/18 10:20:00 AM

Font: Times New Roman

Page 20: [96] Formatted	Simeon Schum	5/29/18 10:20:00 AM

Font: Times New Roman

Page 20: [97] Formatted	Simeon Schum	5/29/18 10:20:00 AM

Font: Times New Roman, Font color: Black

Page 20: [98] Formatted	Simeon Schum	5/29/18 10:20:00 AM

Font: Times New Roman

Page 20: [99] Formatted	Simeon Schum	5/29/18 10:20:00 AM

Font: Times New Roman

Page 20: [100] Formatted	Simeon Schum	5/29/18 10:20:00 AM

Font: Times New Roman, Font color: Black

Page 20: [101] Formatted	Simeon Schum	5/29/18 10:20:00 AM

Font: Times New Roman

Page 20: [102] Formatted	Simeon Schum	5/29/18 10:20:00 AM

Font: Times New Roman, Font color: Black

Page 20: [103] Formatted	Simeon Schum	5/29/18 10:20:00 AM

Font: Times New Roman

Page 20: [104] Formatted	Simeon Schum	5/29/18 10:20:00 AM

Font: Times New Roman

Page 20: [105] Formatted	Simeon Schum	5/29/18 10:20:00 AM

Font: Times New Roman, Font color: Black

Page 20: [106] Formatted	Simeon Schum	5/29/18 10:20:00 AM

Font: Times New Roman

Page 20: [106] Formatted	Simeon Schum	5/29/18 10:20:00 AM

Font: Times New Roman

Page 20: [107] Formatted	Simeon Schum	5/29/18 10:20:00 AM

Font: Times New Roman

Page 20: [108] Formatted	Simeon Schum	5/29/18 10:20:00 AM

Font Alignment: Auto

Page 20: [109] Formatted	Simeon Schum	5/29/18 10:20:00 AM

Font: Times New Roman, Bold, Font color: Black

Page 20: [110] Formatted	Simeon Schum	5/29/18 10:20:00 AM

Font: Times New Roman, Font color: Black

Page 20: [111] Formatted	Simeon Schum	5/29/18 10:20:00 AM

Font: Times New Roman

Page 20: [112] Formatted	Simeon Schum	5/29/18 10:20:00 AM

Font: Times New Roman

Page 20: [113] Formatted	Simeon Schum	5/29/18 10:20:00 AM

Font: Times New Roman, Font color: Black

Page 20: [114] Formatted	Simeon Schum	5/29/18 10:20:00 AM

Font: Times New Roman

Page 20: [115] Formatted	Simeon Schum	5/29/18 10:20:00 AM

Font: Times New Roman

Page 20: [116] Formatted	Simeon Schum	5/29/18 10:20:00 AM

Font: Times New Roman, Font color: Black

Page 20: [117] Formatted	Simeon Schum	5/29/18 10:20:00 AM

Font: Times New Roman

Page 20: [118] Formatted	Simeon Schum	5/29/18 10:20:00 AM

Font: Times New Roman

Page 20: [119] Formatted	Simeon Schum	5/29/18 10:20:00 AM

Font: Times New Roman, Font color: Black

Page 20: [120] Formatted	Simeon Schum	5/29/18 10:20:00 AM

Font: Times New Roman

Page 20: [121] Formatted	Simeon Schum	5/29/18 10:20:00 AM

Font: Times New Roman

Page 20: [122] Formatted	Simeon Schum	5/29/18 10:20:00 AM

Font: Times New Roman, Font color: Black

Page 20: [123] Formatted	Simeon Schum	5/29/18 10:20:00 AM

Font: Times New Roman, Font color: Black

Page 20: [124] Formatted	Simeon Schum	5/29/18 10:20:00 AM

Font: Times New Roman

Page 20: [125] Formatted	Simeon Schum	5/29/18 10:20:00 AM

Font Alignment: Auto

Page 20: [126] Formatted	Simeon Schum	5/29/18 10:20:00 AM

Font: Times New Roman, Bold, Font color: Black

Page 20: [127] Formatted	Simeon Schum	5/29/18 10:20:00 AM

Font: Times New Roman, Font color: Black

Page 20: [128] Formatted	Simeon Schum	5/29/18 10:20:00 AM

Font: Times New Roman

Page 20: [129] Formatted	Simeon Schum	5/29/18 10:20:00 AM

Font: Times New Roman, Font color: Black

Page 20: [130] Formatted	Simeon Schum	5/29/18 10:20:00 AM

Font: Times New Roman

Page 20: [131] Formatted	Simeon Schum	5/29/18 10:20:00 AM

Font: Times New Roman

Page 20: [132] Formatted	Simeon Schum	5/29/18 10:20:00 AM

Font: Times New Roman, Font color: Black

Page 20: [133] Formatted	Simeon Schum	5/29/18 10:20:00 AM

Font: Times New Roman

Page 20: [134] Formatted	Simeon Schum	5/29/18 10:20:00 AM

Font: Times New Roman

Page 20: [135] Formatted	Simeon Schum	5/29/18 10:20:00 AM

Font: Times New Roman, Font color: Black

Page 20: [136] Formatted	Simeon Schum	5/29/18 10:20:00 AM

Font: Times New Roman

Page 20: [137] Formatted	Simeon Schum	5/29/18 10:20:00 AM

Font: Times New Roman

Page 20: [138] Formatted	Simeon Schum	5/29/18 10:20:00 AM

Font: Times New Roman, Font color: Black

Page 20: [139] Formatted	Simeon Schum	5/29/18 10:20:00 AM

Font: Times New Roman, Font color: Black

Page 20: [140] Formatted	Simeon Schum	5/29/18 10:20:00 AM

Font: Times New Roman

Page 20: [141] Formatted	Simeon Schum	5/29/18 10:20:00 AM

Font Alignment: Auto

Page 20: [142] Formatted	Simeon Schum	5/29/18 10:20:00 AM

Font: Times New Roman, Bold, Font color: Black

Page 20: [143] Formatted	Simeon Schum	5/29/18 10:20:00 AM

Font: Times New Roman, Font color: Black

Page 20: [144] Formatted	Simeon Schum	5/29/18 10:20:00 AM

Font: Times New Roman

Page 20: [145] Formatted	Simeon Schum	5/29/18 10:20:00 AM

Font: Times New Roman

Page 20: [146] Formatted	Simeon Schum	5/29/18 10:20:00 AM

Font: Times New Roman, Font color: Black

Page 20: [147] Formatted	Simeon Schum	5/29/18 10:20:00 AM

Font: Times New Roman

Page 20: [148] Formatted	Simeon Schum	5/29/18 10:20:00 AM

Font: Times New Roman

Page 20: [149] Formatted	Simeon Schum	5/29/18 10:20:00 AM

Font: Times New Roman, Font color: Black

Page 20: [150] Formatted	Simeon Schum	5/29/18 10:20:00 AM

Font: Times New Roman

Page 20: [151] Formatted	Simeon Schum	5/29/18 10:20:00 AM

Font: Times New Roman, Font color: Black

Page 20: [152] Formatted	Simeon Schum	5/29/18 10:20:00 AM

Font: Times New Roman

Page 20: [153] Formatted	Simeon Schum	5/29/18 10:20:00 AM

Font: Times New Roman

Page 20: [154] Formatted	Simeon Schum	5/29/18 10:20:00 AM

Font: Times New Roman, Font color: Black

Page 20: [155] Formatted	Simeon Schum	5/29/18 10:20:00 AM

Font: Times New Roman

Page 20: [156] Formatted	Simeon Schum	5/29/18 10:20:00 AM

Font: Times New Roman, Font color: Black

Page 20: [157] Formatted	Simeon Schum	5/29/18 10:20:00 AM

Font: Times New Roman

Page 20: [158] Formatted	Simeon Schum	5/29/18 10:20:00 AM

Font Alignment: Auto

Page 20: [159] Formatted	Simeon Schum	5/29/18 10:20:00 AM

Font: Times New Roman, Bold, Font color: Black

Page 20: [160] Formatted	Simeon Schum	5/29/18 10:20:00 AM

Font: Times New Roman

Page 20: [160] Formatted	Simeon Schum	5/29/18 10:20:00 AM

Font: Times New Roman

Page 20: [161] Formatted	Simeon Schum	5/29/18 10:20:00 AM

Font: Times New Roman

Page 20: [162] Formatted	Simeon Schum	5/29/18 10:20:00 AM

Font: Times New Roman

Page 20: [162] Formatted	Simeon Schum	5/29/18 10:20:00 AM

Font: Times New Roman

Page 20: [163] Formatted	Simeon Schum	5/29/18 10:20:00 AM

Font: Times New Roman

Page 20: [164] Formatted	Simeon Schum	5/29/18 10:20:00 AM

Font: Times New Roman

Page 20: [165] Formatted	Simeon Schum	5/29/18 10:20:00 AM

Font: Times New Roman, Font color: Black

Page 20: [166] Formatted	Simeon Schum	5/29/18 10:20:00 AM

Font: Times New Roman, Font color: Black

Page 20: [167] Formatted	Simeon Schum	5/29/18 10:20:00 AM

Font: Times New Roman

Page 20: [168] Formatted	Simeon Schum	5/29/18 10:20:00 AM

Font: Times New Roman

Page 20: [169] Formatted	Simeon Schum	5/29/18 10:20:00 AM

Font: Times New Roman, Font color: Black

Page 20: [170] Formatted	Simeon Schum	5/29/18 10:20:00 AM

Font: Times New Roman

Page 20: [171] Formatted	**Simeon Schum**	**5/29/18 10:20:00 AM**

Font: Times New Roman, Font color: Black

Page 20: [172] Formatted	**Simeon Schum**	**5/29/18 10:20:00 AM**

Font: Times New Roman

Page 20: [173] Formatted	**Simeon Schum**	**5/29/18 10:20:00 AM**

Font Alignment: Auto

Page 20: [174] Formatted	**Simeon Schum**	**5/29/18 10:20:00 AM**

Font: Times New Roman, Bold, Font color: Black

Page 20: [175] Formatted	**Simeon Schum**	**5/29/18 10:20:00 AM**

Font: Times New Roman

Page 20: [175] Formatted	**Simeon Schum**	**5/29/18 10:20:00 AM**

Font: Times New Roman

Page 20: [176] Formatted	**Simeon Schum**	**5/29/18 10:20:00 AM**

Font: Times New Roman

Page 20: [177] Formatted	**Simeon Schum**	**5/29/18 10:20:00 AM**

Font: Times New Roman

Page 20: [178] Formatted	**Simeon Schum**	**5/29/18 10:20:00 AM**

Font: Times New Roman, Font color: Black

Page 20: [179] Formatted	**Simeon Schum**	**5/29/18 10:20:00 AM**

Font: Times New Roman

Page 20: [180] Formatted	**Simeon Schum**	**5/29/18 10:20:00 AM**

Font: Times New Roman

Page 20: [180] Formatted	**Simeon Schum**	**5/29/18 10:20:00 AM**

Font: Times New Roman

Page 20: [181] Formatted	**Simeon Schum**	**5/29/18 10:20:00 AM**

Font: Times New Roman

Page 20: [182] Formatted	**Simeon Schum**	**5/29/18 10:20:00 AM**

Font: Times New Roman, Font color: Black

Page 20: [183] Formatted	**Simeon Schum**	**5/29/18 10:20:00 AM**

Font: Times New Roman

Page 20: [184] Formatted	**Simeon Schum**	**5/29/18 10:20:00 AM**

Font: Times New Roman

Page 20: [184] Formatted	**Simeon Schum**	**5/29/18 10:20:00 AM**

Font: Times New Roman

Page 20: [185] Formatted	**Simeon Schum**	**5/29/18 10:20:00 AM**

Font: Times New Roman, Font color: Black

Page 20: [186] Formatted	**Simeon Schum**	**5/29/18 10:20:00 AM**

Font: Times New Roman

Page 20: [187] Formatted	Simeon Schum	5/29/18 10:20:00 AM

Font Alignment: Auto

Page 20: [188] Formatted	Simeon Schum	5/29/18 10:20:00 AM

Font: Times New Roman, Bold, Font color: Black

Page 20: [189] Formatted	Simeon Schum	5/29/18 10:20:00 AM

Font: Times New Roman

Page 20: [189] Formatted	Simeon Schum	5/29/18 10:20:00 AM

Font: Times New Roman

Page 20: [190] Formatted	Simeon Schum	5/29/18 10:20:00 AM

Font: Times New Roman

Page 20: [191] Formatted	Simeon Schum	5/29/18 10:20:00 AM

Font: Times New Roman

Page 20: [191] Formatted	Simeon Schum	5/29/18 10:20:00 AM

Font: Times New Roman

Page 20: [192] Formatted	Simeon Schum	5/29/18 10:20:00 AM

Font: Times New Roman

Page 20: [193] Formatted	Simeon Schum	5/29/18 10:20:00 AM

Font: Times New Roman

Page 20: [194] Formatted	Simeon Schum	5/29/18 10:20:00 AM

Font: Times New Roman, Font color: Black

Page 20: [195] Formatted	Simeon Schum	5/29/18 10:20:00 AM

Font: Times New Roman

Page 20: [196] Formatted	Simeon Schum	5/29/18 10:20:00 AM

Font: Times New Roman, Font color: Black

Page 20: [197] Formatted	Simeon Schum	5/29/18 10:20:00 AM

Font: Times New Roman

Page 20: [197] Formatted	Simeon Schum	5/29/18 10:20:00 AM

Font: Times New Roman

Page 20: [198] Formatted	Simeon Schum	5/29/18 10:20:00 AM

Font: Times New Roman, Font color: Black

Page 20: [199] Formatted	Simeon Schum	5/29/18 10:20:00 AM

Font: Times New Roman

Page 20: [199] Formatted	Simeon Schum	5/29/18 10:20:00 AM

Font: Times New Roman

Page 20: [200] Formatted	Simeon Schum	5/29/18 10:20:00 AM

Font: Times New Roman

Page 20: [201] Formatted	Simeon Schum	5/29/18 10:20:00 AM

Font Alignment: Auto

Page 20: [202] Formatted	Simeon Schum	5/29/18 10:20:00 AM

Font: Times New Roman, Bold, Font color: Black

Page 20: [203] Formatted	**Simeon Schum**	**5/29/18 10:20:00 AM**

Font: Times New Roman

Page 20: [203] Formatted	**Simeon Schum**	**5/29/18 10:20:00 AM**

Font: Times New Roman

Page 20: [204] Formatted	**Simeon Schum**	**5/29/18 10:20:00 AM**

Font: Times New Roman

Page 20: [205] Formatted	**Simeon Schum**	**5/29/18 10:20:00 AM**

Font: Times New Roman

Page 20: [206] Formatted	**Simeon Schum**	**5/29/18 10:20:00 AM**

Font: Times New Roman, Font color: Black

Page 20: [207] Formatted	**Simeon Schum**	**5/29/18 10:20:00 AM**

Font: Times New Roman

Page 20: [208] Formatted	**Simeon Schum**	**5/29/18 10:20:00 AM**

Font: Times New Roman

Page 20: [209] Formatted	**Simeon Schum**	**5/29/18 10:20:00 AM**

Font: Times New Roman, Font color: Black

Page 20: [210] Formatted	**Simeon Schum**	**5/29/18 10:20:00 AM**

Font: Times New Roman

Page 20: [211] Formatted	**Simeon Schum**	**5/29/18 10:20:00 AM**

Font: Times New Roman, Font color: Black

Page 20: [212] Formatted	**Simeon Schum**	**5/29/18 10:20:00 AM**

Font: Times New Roman

Page 20: [213] Formatted	**Simeon Schum**	**5/29/18 10:20:00 AM**

Font: Times New Roman

Page 20: [214] Formatted	**Simeon Schum**	**5/29/18 10:20:00 AM**

Font: Times New Roman, Font color: Black

Page 20: [215] Formatted	**Simeon Schum**	**5/29/18 10:20:00 AM**

Font: Times New Roman

Page 20: [215] Formatted	**Simeon Schum**	**5/29/18 10:20:00 AM**

Font: Times New Roman

Page 20: [216] Formatted	**Simeon Schum**	**5/29/18 10:20:00 AM**

Font: Times New Roman

Page 20: [217] Formatted	**Simeon Schum**	**5/29/18 10:20:00 AM**

Font Alignment: Auto

Page 20: [218] Formatted	**Simeon Schum**	**5/29/18 10:20:00 AM**

Font: Times New Roman, Bold, Font color: Black

Page 20: [219] Formatted	**Simeon Schum**	**5/29/18 10:20:00 AM**

Font: Times New Roman

Page 20: [219] Formatted	**Simeon Schum**	**5/29/18 10:20:00 AM**

Font: Times New Roman

Page 20: [220] Formatted	**Simeon Schum**	**5/29/18 10:20:00 AM**

Font: Times New Roman

Page 20: [221] Formatted	**Simeon Schum**	**5/29/18 10:20:00 AM**

Font: Times New Roman, Font color: Black

Page 20: [222] Formatted	**Simeon Schum**	**5/29/18 10:20:00 AM**

Centered, Font Alignment: Auto

Page 20: [223] Formatted	**Simeon Schum**	**5/29/18 10:20:00 AM**

Font: Times New Roman

Page 20: [224] Formatted	**Simeon Schum**	**5/29/18 10:20:00 AM**

Font: Times New Roman, Font color: Black

Page 20: [225] Formatted	**Simeon Schum**	**5/29/18 10:20:00 AM**

Font: Times New Roman

Page 20: [226] Formatted	**Simeon Schum**	**5/29/18 10:20:00 AM**

Font Alignment: Auto

Page 20: [227] Formatted	**Simeon Schum**	**5/29/18 10:20:00 AM**

Font: Times New Roman, Font color: Black

Page 20: [228] Formatted	**Simeon Schum**	**5/29/18 10:20:00 AM**

Font: Times New Roman

Page 20: [229] Formatted	**Simeon Schum**	**5/29/18 10:20:00 AM**

Font: Times New Roman

Page 20: [230] Formatted	**Simeon Schum**	**5/29/18 10:20:00 AM**

Font: Times New Roman, Font color: Black

Page 20: [231] Formatted	**Simeon Schum**	**5/29/18 10:20:00 AM**

Font: Times New Roman

Page 20: [231] Formatted	**Simeon Schum**	**5/29/18 10:20:00 AM**

Font: Times New Roman

Page 20: [232] Formatted	**Simeon Schum**	**5/29/18 10:20:00 AM**

Centered

Page 27: [233] Deleted	**Simeon Schum**	**5/29/18 10:20:00 AM**

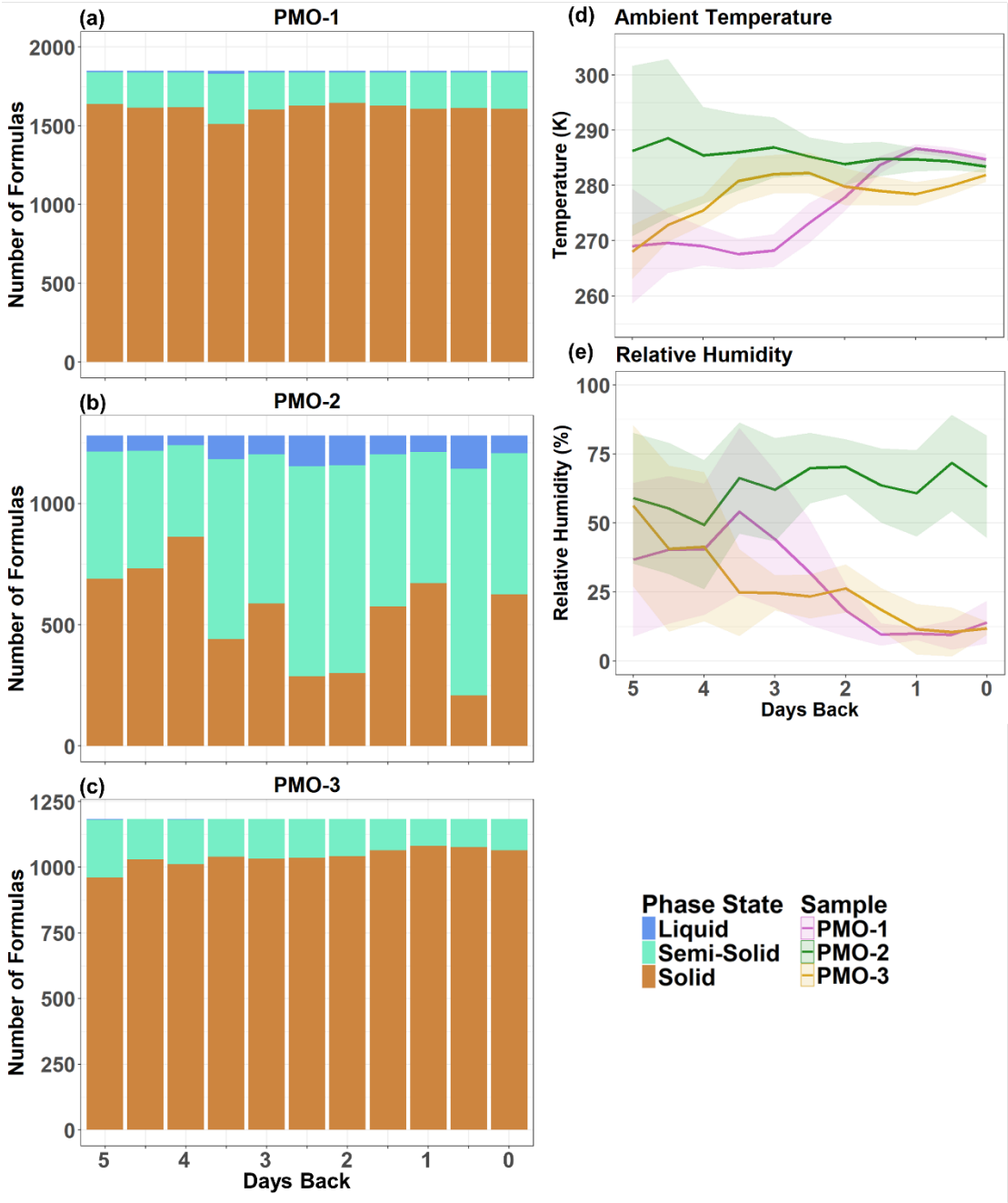

Figure 7. Stacked bar charts (a-c) showing the distribution of molecular species by the phase state categories of liquid, semi-solid, and solid for the last five days of transport. Panels d and e show the atmospheric conditions extracted from GFS for the model grids along the FLEXPART simulated transport pathways. The central line is the weighted average and the shading on either side indicates the weighted standard deviation. The results are weighted by residence time.

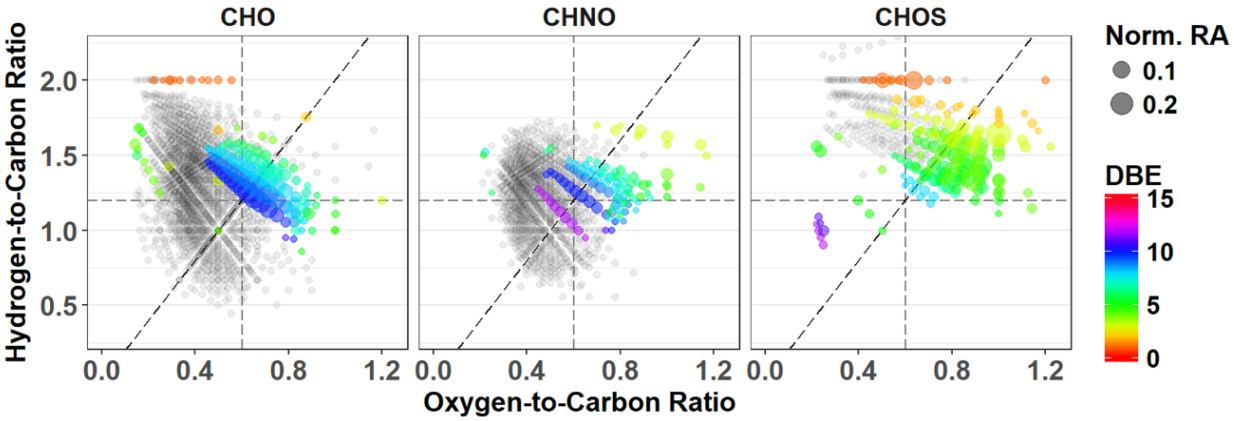
CHO
CHNO
CHOS
Hydrogen-to-Carbon Ratio
2.0
1.5
1.0
0.5
0.0
0.4
0.8
1.2
Oxygen-to-Carbon Ratio
Norm. RA
0.1
0.2
DBE
15
10
5
0